Dawei Mao

Analysis of Rock Support Performance for Tunnelling in Weakness Zones Containing Swelling Clay

Thesis for the degree of Philosophiae Doctor

Trondheim, January 2012

Norwegian University of Science and Technology
Faculty of Engineering Science and Technology
Department of Geology and Mineral Resources Engineering

NTNU – Trondheim
Norwegian University of
Science and Technology

NTNU
Norwegian University of Science and Technology

Thesis for the degree of Philosophiae Doctor

Faculty of Engineering Science and Technology
Department of Geology and Mineral Resources Engineering

ISBN 978-82-471-3284-5 (printed ver.)
ISBN 978-82-471-3285-2 (electronic ver.)
ISSN 1503-8181

Doctoral theses at NTNU, 2012:12

Printed by NTNU-trykk

Abstract

Weakness zones or faults containing swelling clay represent a challenging situation in hard rock tunnelling. When excavating in such zones, failures have occurred occasionally even though particular precautions have been taken. Instability has been encountered during tunnel excavation and sometimes also long after tunnel completion. One of the most recent cases of failure, the rock fall at the Hanekleiv road tunnel in southeast Norway, occurred ten years after tunnel completion. The rock fall was in a fault zone where swelling clay had been identified, about 1.1 km from the northern tunnel entrance of the southbound tube. Cracks had been detected in the applied shotcrete at the fault zone during tunnel excavation. In one major weakness zone containing swelling clay at the Finnfast subsea tunnel, monitoring was carried out by the Norwegian Geotechnical Institute (NGI). Strain gauges and load cells were installed in the reinforced shotcrete rib near the crown and at springlines of the tunnel.

The rock mass quality was estimated for the weakness zones of the two cases based on the Q classification system. However, it is hardly possible to characterize the complex conditions of weakness zones containing swelling clay with an empirical classification system. Except the important feature of the size (thickness) of zones, effects of swelling clay in weakness zones can not be fully accounted for in the system.

Gouge materials were collected from the zones and mineral composition identified with X-ray diffraction analysis. Laboratory testing based on measuring the swelling pressure of remoulded specimens, and free swelling test were used to quantify the swelling potential.

Numerical modelling is a powerful tool in rock engineering planning and design, particularly when difficulties and uncertainties are expected in the underground excavation. A three-dimensional program is normally preferred for the complicated

engineering mechanical computation of tunnelling through weakness zones/faults. Inappropriate use of two-dimensional modelling may induce a large deviation in simulation results. The extent of deviation is illustrated with numerical simulation and comparison based on the two-dimensional finite element program Phase^2 and the three-dimensional finite difference program FLAC^{3D}.

The instrumented weakness zone at the Finnfast subsea tunnel provides the opportunity to quantitatively evaluate the loading effects on reinforced shotcrete ribs. FLAC^{3D} was used for this modelling, where the pore pressure distribution around the tunnel periphery after each blasting round was determined by using the ground water flow analysis. The full rock support (spiling bolts, shotcrete, radial bolts, face bolts, reinforced shotcrete ribs) applied during tunnel excavation was included in the model. The weakness zone, side rock and the rock support of sprayed concrete were simulated with the Mohr-Coulomb model. The spiling bolts, radial bots, face bolts and steel bars in the reinforced ribs of shotcrete were simulated with various built-in structural elements according to the loading characteristics. Different swelling pressures were applied on the rock support during simulation, ranging from zero to 0.20 MPa at an interval of 0.04 MPa. Though swelling pressure considerably increases the loading on rock support, all instrumentation data and simulation results show that the loading on the sprayed concrete is far less than its compressive strength. The loading on rock support was found to be much higher close to the excavation face, and this area is more critical in terms of tunnel stability.

It was concluded that the rock fall at the Hanekleiv road tunnel was caused by a combination of swelling and gravitational collapse due to the very low internal friction. The swelling process most likely was caused by both the water from joints and accumulation of moisture behind the water/frost shielding, when ventilation has had little effect after tunnel completion. The strength of the rock mass was also reduced with absorption of water during the swelling process. Swelling and strength reduction gradually developed till the collapse suddenly took place. In the numerical simulation with FLAC^{3D}, the fault zone and side rock were simulated based on the Mohr-Coulomb model. The strain softening model was used for shotcrete in order to simulate its post-

failure behaviour in consideration of the cracks detected during tunnel excavation. Three stages of mechanical states have been focused in the analysis. The first stage represented tunnel excavation and detection of cracks in the shotcrete. The swelling pressure on the rock support of shotcrete was considered at the second stage. Combined effects of strength reduction of the fault zone and swelling were simulated at the last stage. Simulation results verify both the detected cracks during tunnel excavation and the tunnel collapse. The swelling pressure, according to the analysis, had a limited influence on the shotcrete, while the strength reduction played an important role in the development of instability.

Based on the analysis of swelling effects on rock support of the two cases, a flow chart of practical procedures for rock support estimation in weakness zones/faults containing swelling clay is recommended, in which the site investigation, laboratory testing and numerical simulation are integrated. Instrumentation and regular inspection for signs of instability are important for the stability control and back analysis. Further research on this issue is recommended to enrich the knowledge on tunnelling through such ground.

Acknowledgements

The work presented in this thesis has been carried out at the Department of Geology and Mineral Resources Engineering, Norwegian University of Science and Technology (NTNU) in Trondheim, Norway.

I am particularly thankful to my supervisor Professor Bjørn Nilsen, for his valuable guidance, encouragement and support throughout the study. He read all the manuscripts and provided me with important comments. He has been always available for discussions to answer my questions and give advices, and I have greatly profited from his vast experiences in geological engineering. Professor Charilie Chunlin Li has been my co-supervisor. I am deeply grateful for his inspiring discussions and valuable comments and suggestions.

I feel gratitude towards Professor Ming Lu, who gave me tremendous help during the study. His expertise and experience on numerical modelling have been invaluable and the many discussions with him have been of great value to me.

I would like to express my special thanks to Professor Einar Broch, the supervisor of my master study. His encouragement was an important motivation for me to pursue the academic study.

The experimental work has been an important part of this study. I greatly appreciate the technical staff in the laboratories at NTNU and SINTEF for their great assistance during the experiment work, Filip Dahl, Torill Sørløkk, Torkjell Breivik and Simon Alexander Hagen.

I wish to express thanks to my PhD colleagues, present and former, for the interesting discussions and pleasant working environment and the secretaries at the department for facilitating practical matters.

I would like to thank my wife, Yixuan for her moral and practical support and my son, Tingyu, for being the source of joy and inspiration during my study.

Finally, I want to thank my parents for their encouragements and support through many years.

This thesis has been mainly financed by the scholarship and teaching assistance at the Norwegian University of Science and Technology, NTNU. The Norwegian Public Road Authority has also contributed to the financing of the work.

Trondheim, Norway, November 2011

Note on contributions

Paper I. Laboratory Testing of Swelling Gouge from Weakness Zone - Principle and Recent Update

Authors: Dawei Mao, Bjørn Nilsen, Filip Dahl

The candidate wrote this paper and carried out the analysis. Bjørn Nilsen contributed to the discussion and reviewed the manuscript. The manuscript was also reviewed by Filip Dahl. Some suggestions were provided by Filip Dahl, Torkjell Breivik and Simon Alexander Hagen.

The paper was published in Proceedings of the 45th US Rock Mechanics/Geomechanics Symposium, San Francisco, United Sates, 2011.

Paper II. Numerical Analysis of Effects of Weakness Zones on Tunnel Stability - 2D versus 3D

Authors: Dawei Mao, Bjørn Nilsen

The candidate wrote this paper and did all the analysis. Bjørn Nilsen suggested the analysis and reviewed the manuscript. Charlie Chunlin Li provided several comments to the modelling.

The paper was submitted to the 13th World Conference of the Associated Research Centers for the Urban Underground Space (November 2011).

Paper III. Analysis of Loading Effects on Reinforced Shotcrete Ribs Caused by Weakness Zone Containing Swelling Clay

Authors: Dawei Mao, Bjørn Nilsen, Ming Lu

The candidate wrote the paper and carried out the laboratory tests and the analysis. Bjørn Nilsen guided the candidate during the field work and reviewed various draft versions of the paper. Ming Lu helped during the numerical modelling and reviewed the manuscript. The instrumentation data were provided by Eystein Grimstad. Stephen Lippard contributed to the improvement of the language.

The paper was published in Tunnelling and Underground Space Technology (2011), Vol. 26, p. 472–480, doi:10.1016/j.tust.2011.01.004.

Paper IV. Numerical Analysis of Rock Fall at Hanekleiv Road Tunnel

Authors: Dawei Mao, Bjørn Nilsen, Ming Lu

The candidate wrote this paper and did all the analysis. Bjørn Nilsen reviewed various draft versions of the paper and provided comments and suggestions. Ming Lu gave suggestions on the numerical modelling and reviewed the manuscript. Stephen Lippard improved the language of the paper.

The paper was accepted by Bulletin of Engineering Geology and the Environment in October 2011.

Contents

1. Introduction

1.1 Background

Major weakness zones or faults containing heavily crushed and altered rock mixed with gouge material represent one of the most difficult conditions in Norwegian hard rock tunnels. Particularly serious is when the gouge material from faults or weakness zones contains swelling clay.

ISRM (1983) defines 'Swelling' as a physico-chemical reaction involving water and stress relief. The physico-chemical reaction with water is usually the major contribution but swelling can only take place simultaneously with, or following, stress relief. The swelling is caused by volume increase with absorption of water, and has been often associated with argillaceous soil or rocks, and rocks containing anhydrite (Einstein and Bischoff, 1975; Einstein, 1996; Gysel, 1987; Kovari et al., 1988; Barla, 1999).

Swelling may cause large excavation problems and in extreme cases has caused tunnel collapses resulting in considerable additional costs and delays for the project. ISRM (1989, 1999) has recommended test methods to quantify the swelling potential by determination of the maximum axial swelling stress, the axial and radial free swelling strain, and the axial swelling stress as a function of axial swelling strain. Recent laboratory studies on swelling have mainly been focused on the use of triaxial tests (Bellwald, 1990; Aristorenas, 1992; Barla, 2007). These tests are mainly for argillaceous swelling rocks and anhydrite. Different constitutive models have been developed, e.g. models based on swelling law (e.g. Einstein et al., 1972; Wittke and Rissler, 1976; Gysel, 1987), rheological models (e.g. Lo et al., 1978; Lombardi, 1984; Sun et al., 1984; Nguyen et al., 1984) and mechanical models (e.g. Carter and Broker, 1982; Detournay and Cheng, 1988; Carter, 1988; Aristorenas, 1992; Barla, 1999, 2008). These models are discussed and summarized in Barla (1999). Despite significant efforts made by many researchers,

the swelling process at the tunnel periphery is still not fully understood and there are no general guidelines or recommendations for optimum design of tunnels in swelling ground.

Even more challenging are the weakness zones or faults containing swelling clay. For such zones, the stability problem is not only dependent upon the characteristics of the gouge and swelling minerals, it also depends on the width of the weakness zone, its orientation, its compaction, the access of water, the frequency of occurrences, the competence of the side rock and the dimension of the tunnel. All these factors must be taken into account when considering the stability problems and the necessary support measures. In many cases evaluation of rock support requirement is based mainly on experience since there are no clearly defined rules for design of tunnels in such zones. Rock mass classification may be used for empirical estimating of support requirement, and in many tunnelling projects is applied as the practical basis for rock support design. Weakness zones containing swelling clay are however not fully covered in any of the most commonly used classification systems, e.g. the Q-system, rock mass rating classification (RMR) and the new Austrian tunneling method (NATM). Palmstrøm and Broch (2006) recommended that in such ground special investigations and measurements should be performed and special analyses conducted to evaluate the results with respect to excavation and rock support.

Difficulties are often connected to quantification of the swelling capacity of the gouge as well as prediction of the response on tunnel excavation and support loading. It is very difficult to obtain usable undisturbed samples of gouge material from a weakness zone for laboratory testing, because the gouge is normally highly disturbed when a mixture of clay and rock fragments of various sizes is collected. In Norway, a laboratory test method based on measuring the swelling pressure of remoulded specimens has been extensively used since it was introduced several decades ago at NTNU (Brekke, 1965). The principle of the NTNU test is almost equivalent to the method for determining the maximum axial swelling stress for swelling rocks as suggested by ISRM (1989, 1999). Instead of having the same density and water content in the specimen as in-situ material, as described for the ISRM method, the NTNU method is however based on remoulded

specimens. Though this represents a uniform and reproducible way for preparing test samples of gouge materials from weakness zones, the in-situ structure and compaction of gouges are damaged as a result of the sampling and preparation.

For weakness zones or faults containing swelling clay, description of failure cases and discussion of possible causes have been of main focus in early literature (Brekke and Selmer-Olsen, 1965; Selmer-Olsen et al., 1989) as well as in more recent papers (Nilsen and Dahlø, 1994; Blindheim and Nilsen, 2001; Blindheim et al., 2005; Richards and Nilsen, 2007; Nilsen and Palmstrøm, 2009). The relative frequency of failure cases under such conditions in Norwegian tunnels is small, but on the rare occasions when a cave-in occurs it can be quite dramatic and cause considerable problems. During the last few years some new cases of cave-in have occurred, despite all the precautions based on experiences obtained from early accidents that have been taken.

1.2 Problem statement

The recent cases of cave-in illustrate that tunnel instabilities are not incidents that belong to the past only. Further knowledge on design of rock support in weakness zones or faults containing swelling clay therefore is required. Quantitative analysis on the effects of swelling clay in weakness zones on rock support is important for efficient and reliable tunnel design. Since the NTNU swelling pressure test has been extensively used in Norway for quantification of swelling potential for several decades, the relevance of the laboratory test results for analyzing the potential instability and application of the results on evaluation of rock support are of considerable interest for the Norwegian tunneling industry.

1.3 Thesis scope and objectives

The scope of this thesis is to improve the knowledge of the effects of swelling clay in weakness zones on rock support based on NTNU swelling pressure testing and numerical modelling. The main goal has been to establish easy to follow practical procedures for estimating rock support in weakness zones/faults containing swelling clay, and for this the following tasks have been undertaken:

- Evaluation and discussion of the relevancy of the NTNU laboratory tests for quantification of swelling capacity of gouges;
- Study of the applicability/reliability of two-dimensional numerical modelling for tunnel support design in weakness zones;
- Quantification of in-situ swelling effects on rock support in weakness zones containing swelling clay;
- Analysis of combined effects of swelling and strength reduction of rock mass on tunnel stability in weakness zones containing swelling clay.

1.4 Organization of thesis

The thesis is divided into three sections: the first section consisting of six chapters, the second section consisting of the attached main papers, and the last section consisting of appendices. The six chapters of the first section are as follows:

Chapter 1, the present chapter**,** is intended to provide an overview to the problem and the work carried out.

Chapter 2 describes several weakness zones containing swelling clay, including the weakness zones encountered in the Finnfast subsea tunnel and Hanekleiv tunnel which have been used as case studies in the thesis.

Chapter 3 discusses the rock classification systems, particularly the Q-system and its applicability on weakness zones containing swelling clay.

Chapter 4 describes the laboratory test used for characterizing swelling gouge materials.

Chapter 5 discusses the numerical simulation with the focus on selection of appropriate constitutive models and structural elements.

Chapter 6 gives comments on papers prepared for publication.

Chapter 7 contains the main conclusions and recommendations.

Main Papers:

The following papers I - IV are included in full length:

Paper I. Laboratory Testing of Swelling Gouge from Weakness Zone - Principle and Recent Update

Authors: Dawei Mao, Bjørn Nilsen, Filip Dahl

The paper was published in Proceedings of the 45th US Rock Mechanics/Geomechanics Symposium, San Francisco, United Sates, 2011.

Paper II. Numerical Analysis of Effects of Weakness Zones on Tunnel Stability - 2D versus 3D

Authors: Dawei Mao, Bjørn Nilsen

The paper was submitted to the 13th World Conference of the Associated Research Centers for the Urban Underground Space (November 2011).

Paper III. Analysis of Loading Effects on Reinforced Shotcrete Ribs Caused by Weakness Zone Containing Swelling Clay

Authors: Dawei Mao, Bjørn Nilsen, Ming Lu

The paper was published in Tunnelling and Underground Space Technology (2011), Vol. 26, p. 472–480, doi:10.1016/j.tust.2011.01.004.

Paper IV. Numerical Analysis of Rock Fall at Hanekleiv Road Tunnel

Authors: Dawei Mao, Bjørn Nilsen, Ming Lu

The paper was accepted by Bulletin of Engineering Geology and the Environment in October 2011.

Appendices

The appendices of this thesis are:

Appendix A Orignial XRD test results

Appendix B FLAC^{3D} code

2. Recent Cases of Weakness Zones Containing Swelling Clay

2.1 Introduction

Weakness zones or faults containing swelling clay have been registered in all the main rock type regions in Norway, and failure cases under such conditions have often resulted in considerable costs and delays in Norwegian tunnels (Brekke and Selmer-Olsen, 1965; Selmer-Olsen et al., 1989, Nilsen and Dahlø, 1994). Methodologies concerning investigation, excavation and rock support have been improved based on the experiences from these cases. Nevertheless, within the last few years some new cases of instability (Oslofjord tunnel, Hanekleiv tunnel, Atlanterhav tunnel) have still occurred despite the particular caution in tunnelling made in such zones as described by Nilsen (2010, 2011). These new cases, illustrating that instability when tunneling through such zones is not confined to incidents belonging to the past only and that more knowledge is required, are briefly described in this chapter. To improve the basis of support evaluation for such weakness zones, the Norwegian Geotechnical Institute (NGI) installed instrumentation in one typical such weakness zone at the Finnfast subsea tunnel, which is also described here. In this thesis, the weakness zones at the Finnfast subsea tunnel and the Hanekleiv road tunnel have been selected as cases for further study. Detailed description of these two cases can be found in Paper III and Paper IV.

2.2 Recent cases of instability

2.2.1 Oslofjord tunnel

The Oslofjord tunnel is a 7.2 km long three-lane subsea road tunnel with cross section about 79 m^2 and with its deepest part 134 m below sea level (Figure 2.1). The bedrock in the area consists of Precambrian granitic gneisses. For leakage control, considerable grouting was carried out. Shotcrete and rock bolts were applied according to the rock conditions. Faults/weakness zones were encountered during excavation, several of them containing swelling clay (smectite). Concrete lining was used for the main fault zones,

which represent approximately 1.7% of the total tunnel length. For the final frost and water shielding, concrete walls and PE-foam/shotcrete ceiling were installed. Although this shielding may cope with minor fragments of falling rock, it is not designed to withstand major rock falls.

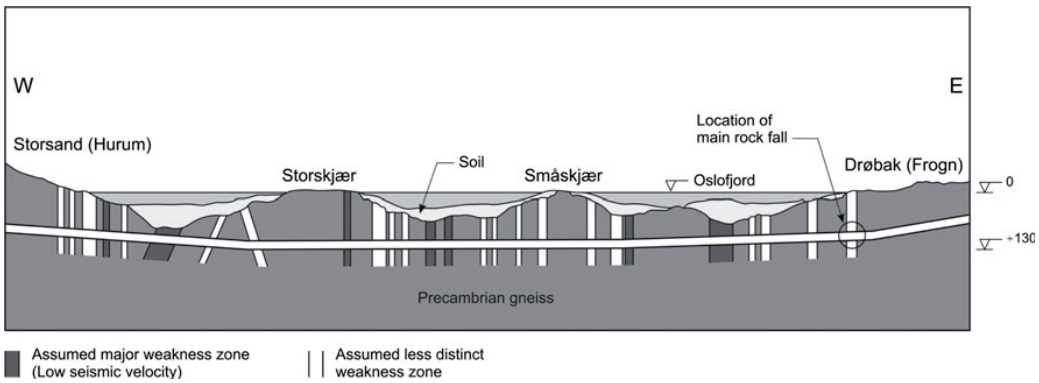

Figure 2.1 Longitudinal profile of central part of the Oslofjord subsea tunnel (Nilsen, 2011)

After 3.5 years of tunnel operation, a rock fall suddenly occurred and went through the frost and water shielding at the location indicated in Figure 2.1. The total volume of the rock fall was estimated to 40 m^3, of which about 4 m^3 went through the lining. The clay gouge in the unstable areas was tested and found to be highly active in terms of swelling potential.

The cave-in was caused by the presence of a steep 0.5 m-1 m wide clay zone. The rock support in this area was obviously insufficient. Inspection showed that only 4 – 6 cm thick shotcrete was used in the roof, and there was no support in the lower part of the wall (Kvåle et al., 2004). Two other rock falls of similar character were identified behind the shielding during inspection of the tunnel after the cave-in.

2.2.2 Hanekleiv tunnel

The 1765 m long Hanekleiv road tunnel is located in southeast Norway. It has two tubes, each with a theoretical cross section of excavation of about 65 m^2 (Norwegian Public Roads Administration, 2004). The bedrock along the northern part of the tunnel is Silurian sandstone which underlies Permian basalt and a layer of Carboniferous shale and conglomerate. The southern part of the tunnel is in Permian syenite. Topography and geology along the tunnel alignment is shown in Figure 2.2.

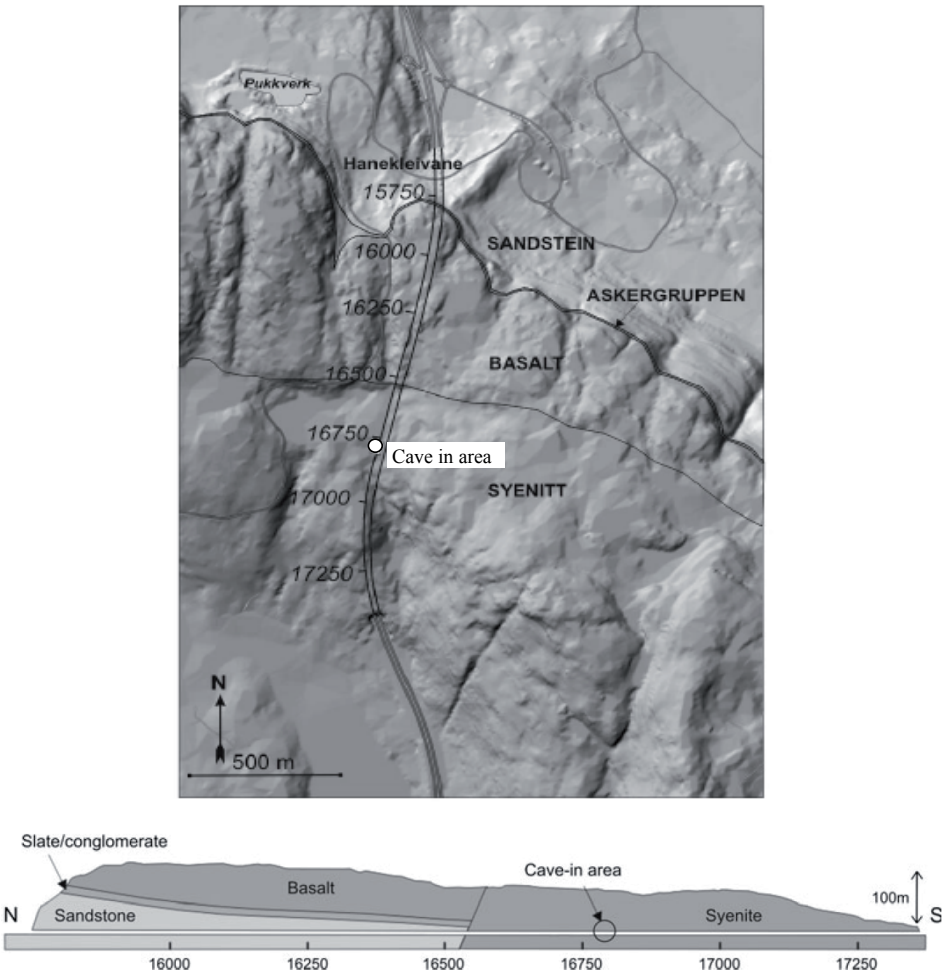

Figure 2.2. Topography and geology along the tunnel alignment, top: plan view, below: longitudinal cross section (Based on Bollingmo et al., 2007).

The rock fall at the Hanekleiv occurred, ten years after the tunnel was completed (Bollingmo et al., 2007; Reynolds, 2007; Nilsen, 2011), approximately 1.1 km from the northern tunnel entrance of the southbound tube. The total volume of caved in material was estimated to 250 m^3. Although one large block of syenite weighing several tons was found at the site, most of the material was a mixture of small blocks, gravel, and fragments of altered syenite. A fault zone (thickness < 4m) was identified here in the syenite during excavation. This zone was sealed with 15 cm thick steel fibre reinforced shotcrete. During later inspection cracks in the shotcrete were detected and 10 cm extra shotcrete was applied after tunnel break through.

The fault zone causing the cave-in intersected the tunnel at a small angle (10 – 15°), and was bounded by two parallel joints striking approximately 030 - 040° and dipping 70 - 80° to the southeast. The joints were filled with clay gouge with a thickness of 5 to10 cm (Bollingmo et al., 2007). The fault zone consisted of altered syenite and clay seams/filled joints. The rock mass quality of the fault zone based on site inspection after the rock fall was estimated to be extremely poor (Q = 0.013) (Nilsen, per. comm.). Swelling clay was found in the altered syentie as well as in the clay seams, and the swelling mineral smectite was identified (Bollingmo et al., 2007).

Based on thorough investigation it was concluded that, in addition to the effect of the swelling process, gravitational collapse due to the very low internal friction probably played an important role in the development of instability in this case (Bollingmo et al., 2007; Nilsen, 2011). The strength of the rock mass in the fault zone is believed to have been reduced with absorption of water during the swelling process (Mao et al., 2011).

2.2.3 Atlanterhav tunnel

The Atlanterhav tunnel is a 5.7 km long subsea road tunnel, located near Kristiansund in western Norway. It has a theoretical cross section of excavation of about 85 m^2 close to the shorelines and 62 m^2 in the central part where instability developed. Figure 2.3 shows the longitudinal profile along the tunnel axis.

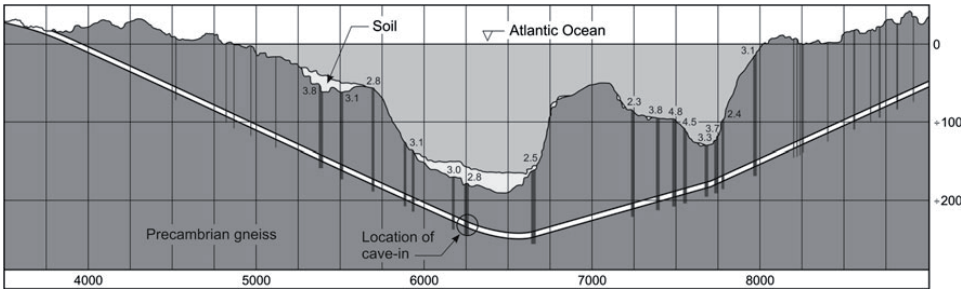

Figure 2.3 Longitudinal profile of the Atlanterhav subsea road tunnel. Assumed weakness zones/seismic low velocity zones (with velocity in km/s) are indicated. Spacing between vertical lines is 250 m and between horizontal lines 100 m (Nilsen, 2011)

The bedrock in the area consists of Precambrian granitic gneisses. Near the lowest level of the planned tunnel where the cave-in occurred, a weakness zone with seismic velocities as low as 2.8 km had been identified during pre-investigations (Figure 2.3). The rock mass quality of the zone was very poor with crushed rock and clay gouge, and minor water leakage was observed. Excavation after grouting was carried out with reduced round length (3 m), shotcreting, systematic radial bolting and installation of spiling bolts (Karlsson, 2008).

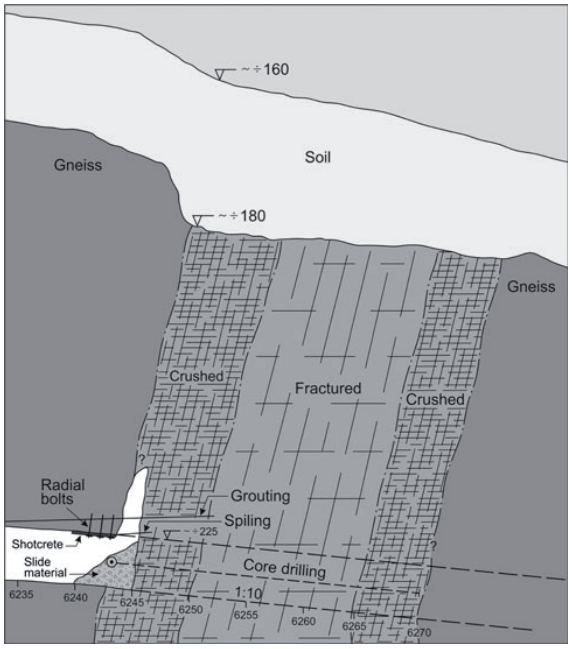

Figure 2.4 Cave-in situation approx. 225 m below sea level in the Atlanterhav tunnel (Nilsen, 2011)

When excavation of the weakness zone was started, there was a tendency for small rock fragments to drizzle/fall down between the spiling bolts. Attempts to stop this by applying shotcrete were unsuccessful, and after a few hours a 5–6 m high cave-in of the roof had developed, covering the full tunnel width and the 3 m round length. Based on holes drilled later it was found likely that the collapse extended about 10 m above the tunnel roof as illustrated in Figure 2.4.

In order to stabilize the tunnel, excavated material was placed against the face, the area between the tunnel contour and the fill material was sealed with shotcrete, and concrete was pumped into the slide scar. Additional rock support was installed behind the unstable section and a concrete plug longer than 10 m was placed to seal the tunnel. Probe drilling indicated considerable water leakage, and extensive grouting of the backfill material and the rock beyond the slide scar was required. Core drilling through the weakness zone was carried out (Figure 2.4) and showed that the zone was more than 25 m wide and had considerable water leakage.

2.2.4 Overall evaluation

The different cases discussed above are in many ways similar. At both the Oslofjord tunnel and the Hanekleiv tunnel, the stability occurred long after completion of the project, while at the Atlanterhav tunnel it occurred during excavation. These zones where instability occurred are all quite steep, although the thickness ranges from less than 1 m to more than 25 m. In all cases swelling clay was found. Table 2.1 shows the key data of the instability cases. Laboratory test results for gouge materials from the zones vary considerably. The test methods are discussed in Chapter 4.

Table 2.1 Key data of instability cases

Project	Oslofjord tunnel	Hanekleiv tunnel	Atlanterhav tunnel
Standup time	3.5 years	10 years	few hours
Slide volume (m^3)	40	250	-
Thickness of zone (m)	0.5 - 1	< 4	> 25
% material < 20μm	34	14	5
Free Swelling (%)	167	150	135
Swelling Pressure (MPa)	0.55	0.18	0.10

2.3 Case of instrumented weakness zone - Finnfast subsea tunnel

The Finnfast Subsea Tunnel is located close to Stavanger in southwest Norway. The length of the main tunnel, linking the two islands Rennesøy and Finnøy, is 5.76 km, while the branch tunnel to the smaller island Talgje in the middle of the fjord is 1.45 km. The excavation span of the tunnel is 12 m. The bedrock in the region is Precambrian with granitic gneiss as predominant rock type. The instrumented weakness zone is about 10 m wide, and has strike direction almost perpendicular to the tunnel alignment and a dip angle about 70^{o} towards east. The tunnel intersects the zone at 140 m below sea level (50 m of water, 10 m of soil and 80 m of rock overburden).

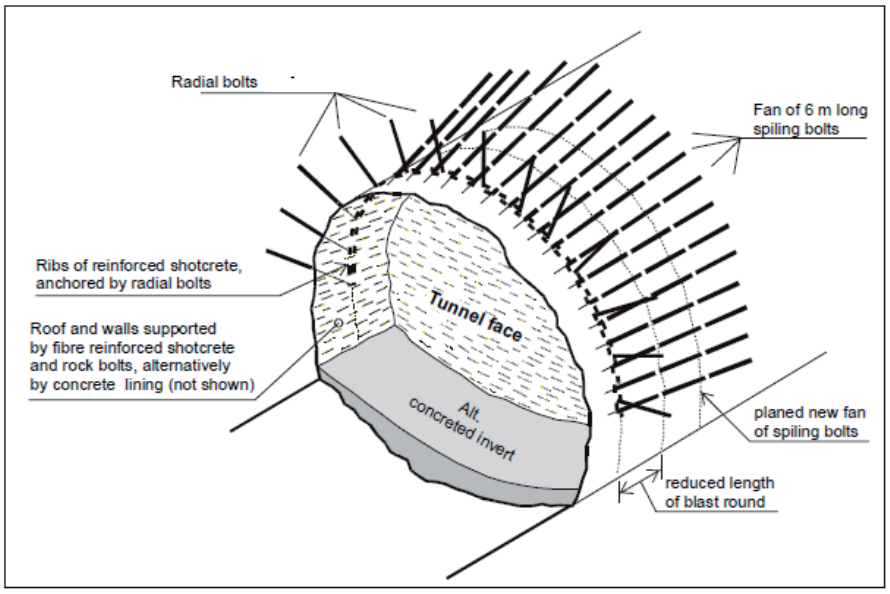

Figure 2.5 Rock support in weakness zone (Nilsen and Palmstrøm, 2001)

The material of the zone is highly crushed and the rock mass quality according to the Q-system, is exceptionally poor to extremely poor (Q=0.01-0.02) (Mao et al., 2011). Montmorillonite has been identified as the most important swelling mineral in the gouge material of the zone. Extensive engineering measures were taken when the tunnel was excavated through the zone, including spraying of 15cm fiber reinforced shotcrete after blasting; installation of 3m long radial rock bolts; installation of 4m long horizontal rock bolts at the tunnel face; installation of reinforced shotcrete ribs; installation of 6m long

spiling bolts and reduction of the length of the blasting round to 3 m (Grimstad et al., 2008; Mao et al., 2011). A principle sketch of this kind of rock support system is shown in Figure 2.5.

Figure 2.6. Spraying of the instrumented rib (Grimstad et al., 2008).

Three sets of instrumentation, including strain gauges and load cells, were installed in a shotcrete rib at the springlines and the crown when the tunnel was excavated in the middle of the major zone (Grimstad et al., 2008). The instruments were completely embedded in sprayed concrete, except the load cell for monitoring the load from rock mass, which was fixed to the tunnel periphery on an even basis. Spraying of the instrumented rib is illustrated in Figure 2.6. The readings were reset after spraying the concrete on the reinforced rib and the next round of blasting was carried out four days after instrument installation. Monitoring was conducted by the Norwegian Geotechnical Institute (NGI) (Grimstad et al., 2008), which provides a good basis for quantitative analysis of swelling effects.

3. Relevance of Rock Mass Classification

3.1 Introduction

Rock mass classification is to arrange and combine different features of a rock mass into groups or classes based on a specific system or principle. There are a large number of rock mass classification systems developed for general purposes and specific applications, and among these the commonly used ones are RQD, Q, RMR, NATM, RMi, etc. Development of rock mass classification systems and characteristics of each system is out of scope of this chapter, and for details it can be referred to Hoek et al. (1995), Palmstrøm (1995), Edelbro (2003), etc.

The classification approach often serves as the only practical basis for design of underground structures. In Norwegian tunneling practice, the Q-system (Barton et al., 1974; Grimstad and Barton, 1993; Barton, 2002; Grimstad et al., 2002) is the most commonly used rock mass classification system, which incorporates estimation of the rock mass quality, support pressure and required rock support. It has been used in this thesis for both zones at the Finnfast subsea tunnel and the Hanekleiv road tunnel and therefore is focused on in the following.

3.2 Q-system

The Q-system was first introduced by Barton et al. in 1974, based on an analysis of 212 case records, among these 180 were supported excavations and the rest were permanently unsupported. More than 90 cases of the database for developing the Q-system were provided by Cecil (1970). The numerical value of the rock mass quality index Q is defined by:

$$Q = \frac{RQD}{J_n} \times \frac{J_r}{J_a} \times \frac{J_w}{SRF} \quad \text{(Barton et al., 1974)}$$

RQD is the Rock Quality Designation (indicating the fracturing degree); J_n is the joint set number (accounting for the number of joint sets); J_r is the joint roughness number (accounting for the joint surface roughness); J_a is the joint alteration number (indicating the degree of weathering, alteration and filling); J_w is the joint water reduction factor (rating for the water inflow and pressure effects); and *SRF* is the stress reduction factor (indicating the influence of in-situ stress). The rating of individual parameters has been updated several times, with the most recent update in 2002 (Barton, 2002).

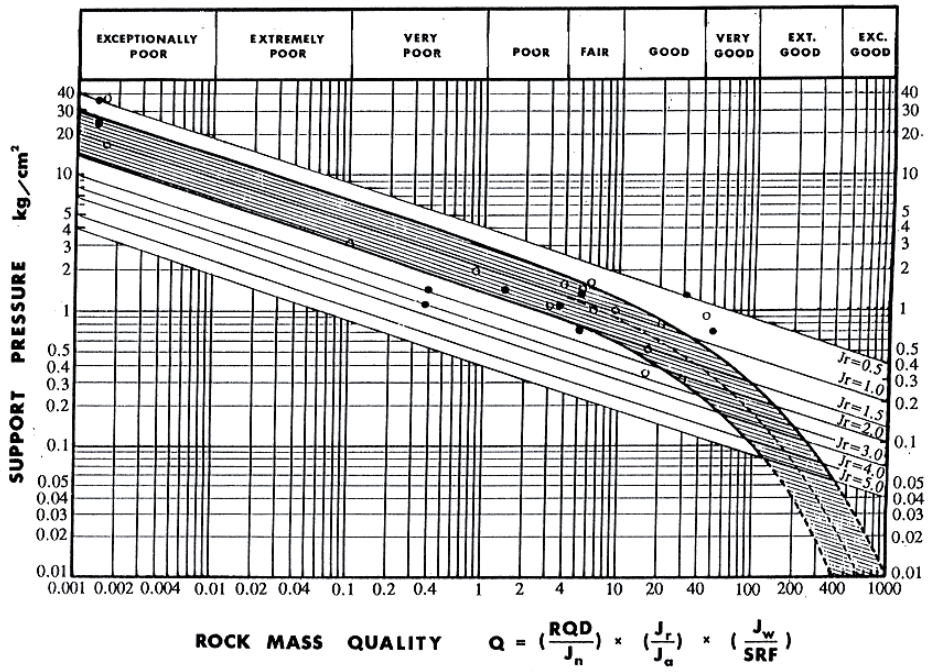

Figure 3.1 Empirical method for estimating the support pressure. Plotted points refer to case records describing measured or designed roof support pressures. (Barton et al., 1974)

With the value of the index Q, the support pressure can be estimated from the empirical diagram in Figure 3.1, which was based on the available case records of measured or designed roof support pressures (Barton et al., 1974). An equation relating the arch roof support pressure (P_{arch}) and rock mass quality Q, fitting available case records quite well, was found to be:

$$P_{arch} = \frac{2 \times J_n^{\frac{1}{2}} \times Q^{-\frac{1}{3}}}{3 \times J_r} \quad \text{(Barton et al., 1974)}$$

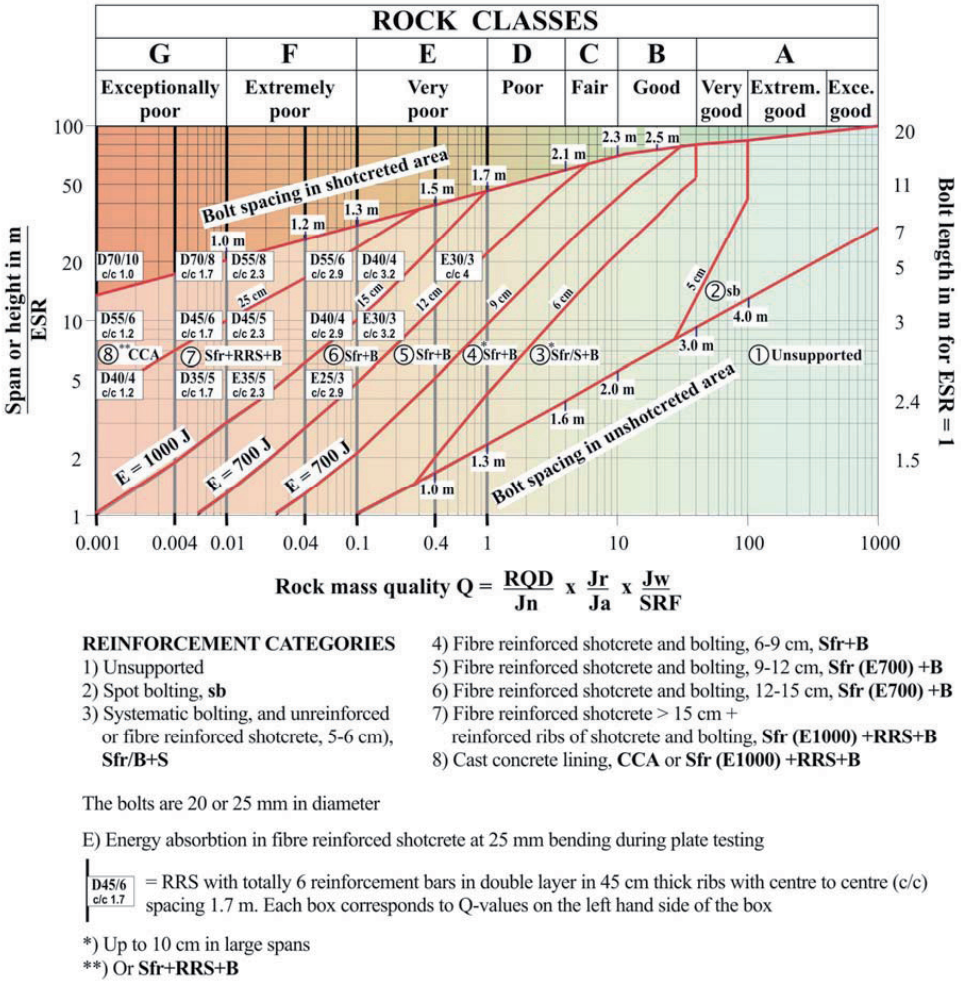

REINFORCEMENT CATEGORIES

1) Unsupported
2) Spot bolting, **sb**
3) Systematic bolting, and unreinforced or fibre reinforced shotcrete, 5-6 cm), **Sfr/B+S**
4) Fibre reinforced shotcrete and bolting, 6-9 cm, **Sfr+B**
5) Fibre reinforced shotcrete and bolting, 9-12 cm, **Sfr (E700) +B**
6) Fibre reinforced shotcrete and bolting, 12-15 cm, **Sfr (E700) +B**
7) Fibre reinforced shotcrete > 15 cm + reinforced ribs of shotcrete and bolting, **Sfr (E1000) +RRS+B**
8) Cast concrete lining, **CCA** or **Sfr (E1000) +RRS+B**

The bolts are 20 or 25 mm in diameter

E) Energy absorbtion in fibre reinforced shotcrete at 25 mm bending during plate testing

D45/6 c/c 1.7 = RRS with totally 6 reinforcement bars in double layer in 45 cm thick ribs with centre to centre (c/c) spacing 1.7 m. Each box corresponds to Q-values on the left hand side of the box

*) Up to 10 cm in large spans
) Or **Sfr+RRS+B

Figure 3.2 Q support chart with wide application of reinforced rib of shotcrete (RRS). (Grimstad et al., 2002)

In relating the value of the index Q to the stability and support requirements of underground excavations, an additional parameter called the equivalent dimension (D_e) was defined. This equivalent dimension (D_e) is obtained by dividing the span, diameter or wall height of the excavation by the excavation support ratio, *ESR* (Barton, 1976). The chart, where equivalent dimension, D_e is plotted against the value of Q, is used to define a number of support categories. In 1993, Grimstad and Barton updated the Q-system based on 1050 case records. The updated chart for rock support design reflects the increasing

use of steel fibre reinforced shotcrete in underground excavation support. The new Q-value correlations published by Barton (2002), mainly focused on the applicability of the Q-system in site characterisation and tunnel design. The experience of the wide application of the reinforced ribs of sprayed concrete (RRS) was taken into account by Grimstad et al. (2002), who specified RRS in the updated Q support chart (Figure 3.2) based on numerical analysis and deformation measurements in tunnels.

3.3 Estimation of rock support based on Q-system

The rock mass quality for the selected cases of weakness zones at the Finnfast subsea tunnel and at the Hanekleiv road tunnel has been estimated based on the Q-system. Rated individual parameters of the Q-system of these two zones are given in Table 3.1. The rock mass in the weakness zone at the Finnfast subsea tunnel is classified as exceptionally poor to extremely poor, with Q-value between 0.01 and 0.02. The estimated Q-value for the fault zone at the Haneleiv tunnel based on the site inspection after the rock fall was found to be 0.013, indicating extremely poor rock mass.

Based on the estimated Q-values and the tunnel dimension, heavy rock support like reinforced shotcrete rib or cast-in-place concrete lining should have been considered for both zones according to the rock support chart of Q-system.

Table 3.1 Rated input parameters of Q-system (based on Nilsen (per. Comm.), and Mao et al., 2011)

Parameter	A*	B*
Rock quality designation (RQD)	10	10
Joint set number (J_n)	20	20
Joint roughness number (J_r)	1.5	1
Joint alteration number (J_a)	15	15
Joint water reduction factor (J_w)	1	1
Stress reduction factor (SRF)	5	2.5

A*: Worst-case condition of the Finnfast weakness zone

B*: Hanekleiv fault zone

3.4 Limitation of Q- system for weakness zones containing swelling clay

Though there are options of rating the joint alteration number J_a and the stress reduction factor *SRF* with consideration of swelling in the Q-system, the effects of swelling clay in weakness zones have not been satisfactory included. How to rate the value of J_a according to the 'percent of swelling-clay particles' is not clearly defined (Table 3.2). Furthermore, a very important factor of the size (thickness) of zones is not considered, although several features of weakness zones have been included in the Q-system when rating the *SRF* parameter for zones in competent rocks (Barton, 2002; Palmstrøm and Broch, 2006):

- How the zone occurs; either as single zone, or as frequent occurrences of two or more zones.
- Content of clay materials or chemical alteration/weathering in the zone.
- At which depth the zone is located (in competent rocks) with a division between zones deeper or shallower than 50 m.
- The conditions of the adjacent rock mass – given for single zones only.
- Various types of zones, such as unconsolidated, open joints/heavily jointed zones, sugar cube rock.

Table 3.2 Rating of J_a (Barton, 2002)

Joint alteration number		**ϕ_r, approx. (deg)**	**J_a**
(a) *Rock-wall contact (no mineral fillings, only coatings)*			
A	Tightly healed, hard, non-softening, impermeable filling, i.e., quartz or epidote	—	0.75
B	Unaltered joint walls, surface staining only	25–35	1.0
C	Slightly altered joint walls, non-softening mineral coatings, sandy particles, clay-free disintegrated rock, etc.	25–30	2.0
D	Silty- or sandy-clay coatings, small clay fraction (non-softening)	20–25	3.0
E	Softening or low friction clay mineral coatings, i.e., kaolinite or mica. Also chlorite, talc, gypsum, graphite, etc., and small quantities of swelling clays	8–16	4.0
(b) *Rock-wall contact before 10 cm shear (thin mineral fillings)*			
F	Sandy particles, clay-free disintegrated rock, etc.	25–30	4.0
G	Strongly over-consolidated non-softening clay mineral fillings (continuous, but <5 mm thickness)	16–24	6.0
H	Medium or low over-consolidation, softening, clay mineral fillings (continuous, but <5 mm thickness)	12–16	8.0
J	Swelling-clay fillings, i.e., montmorillonite (continuous, but <5 mm thickness). Value of J_a depends on per cent of swelling clay-size particles, and access to water, etc.	6–12	8–12
(c) *No rock-wall contact when sheared (thick mineral fillings)*			
KLM	Zones or bands of disintegrated or crushed rock and clay (see G, H, J for description of clay condition)	6–24	6, 8, or 8–12
N	Zones or bands of silty- or sandy-clay, small clay fraction (non-softening)	—	5.0
OPR	Thick, continuous zones or bands of clay (see G, H, J for description of clay condition)	6–24	10, 13, or 13–20

As shown in Table 3.3, even for argillaceous swelling rock and rock containing anhydrite corresponding to 'group D', swelling effects are only roughly classified without indicating the limit between 'mild swelling pressure' and 'heavy swelling pressure'.

Table 3.3 Rating of *SRF* (Barton, 2002)

Stress reduction factor		**SRF**		
(a) *Weakness zones intersecting excavation, which may cause loosening of rock mass when tunnel is excavated*				
A	Multiple occurrences of weakness zones containing clay or chemically disintegrated rock, very loose surrounding rock (any depth)	10		
B	Single weakness zones containing clay or chemically disintegrated rock (depth of excavation $\leqslant 50$ m)	5		
C	Single weakness zones containing clay or chemically disintegrated rock (depth of excavation > 50 m)	2.5		
D	Multiple shear zones in competent rock (clay-free), loose surrounding rock (any depth)	7.5		
E	Single shear zones in competent rock (clay-free), (depth of excavation $\leqslant 50$ m)	5.0		
F	Single shear zones in competent rock (clay-free), (depth of excavation > 50 m)	2.5		
G	Loose, open joints, heavily jointed or 'sugar cube', etc. (any depth)	5.0		
		σ_c/σ_1	σ_θ/σ_c	SRF
(b) *Competent rock, rock stress problems*				
H	Low stress, near surface, open joints	> 200	< 0.01	2.5
J	Medium stress, favourable stress condition	200–10	0.01–0.3	1
K	High stress, very tight structure. Usually favourable to stability, may be unfavourable for wall stability	10–5	0.3–0.4	0.5–2
L	Moderate slabbing after >1 h in massive rock	5–3	0.5–0.65	5–50
M	Slabbing and rock burst after a few minutes in massive rock	3–2	0.65–1	50–200
N	Heavy rock burst (strain-burst) and immediate dynamic deformations in massive rock	<2	>1	200–400
		σ_θ/σ_c	SRF	
(c) *Squeezing rock: plastic flow of incompetent rock under the influence of high rock pressure*				
O	Mild squeezing rock pressure	1–5	5–10	
P	Heavy squeezing rock pressure	>5	10–20	
		SRF		
(d) *Swelling rock: chemical swelling activity depending on presence of water*				
R	Mild swelling rock pressure	5–10		
S	Heavy swelling rock pressure	10–15		

Notes: (i) Reduce these values of SRF by 25–50% if the relevant shear zones only influence but do not intersect the excavation. This will also be relevant for characterisation. (ii) For strongly anisotropic virgin stress field (if measured): When $5 \leqslant \sigma_1/\sigma_3 \leqslant 10$, reduce σ_c to $0.75\sigma_c$. When $\sigma_1/\sigma_3 > 10$, reduce σ_c to $0.5\sigma_c$, where σ_c is the unconfined compression strength, σ_1 and σ_3 are the major and minor principal stresses, and σ_θ the maximum tangential stress (estimated from elastic theory). (iii) Few case records available where depth of crown below surface is less than span width, suggest an SRF increase from 2.5 to 5 for such cases (see H). (iv) Cases L, M, and N are usually most relevant for support design of deep tunnel excavations in hard massive rock masses, with RQD/J_n ratios from about 50–200. (v) For general characterisation of rock masses distant from excavation influences, the use of SRF = 5, 2.5, 1.0, and 0.5 is recommended as depth increases from say 0–5, 5–25, 25–250 to >250 m. This will help to adjust Q for some of the effective stress effects, in combination with appropriate characterisation values of J_w. Correlations with depth-dependent static deformation modulus and seismic velocity will then follow the practice used when these were developed. (vi) Cases of squeezing rock may occur for depth $H > 350Q^{1/3}$ according to Singh [34]. Rock mass compression strength can be estimated from $SIGMA_{cm} \approx 5\gamma Q_c^{1/3}$ (MPa) where γ is the rock density in t/m^3, and $Q_c = Q \times \sigma_c/100$, Barton [29].

The support pressure caused by swelling in weakness zones/faults containing swelling clay can be substantial, but this type of ground is too complicated to define. The swelling pressure in such cases can not be considered with the empirical diagram published by Barton et al. (1974), and has been included neither in later revisions of Q-system (i.e. Grimstad and Barton, 1993; Barton, 2002) nor in research on support pressure (Sheorey, 1985; Singh Bhawani et al., 1992; Goel, 1994; Goel et al., 1996; Singh Bhawani et al.,

1997). The ground reaction curve (Brown et al., 1983; Duncan Fama, 1993; Hoek et al., 1995; Carranza-Torres, 2004) is used here to conceptually illustrate the support pressure due to swelling (Figure 3.3). Resulting swelling pressure on rock support is influenced by the time of rock support installation and the support stiffness, and can be considerably reduced with tunnel deformation.

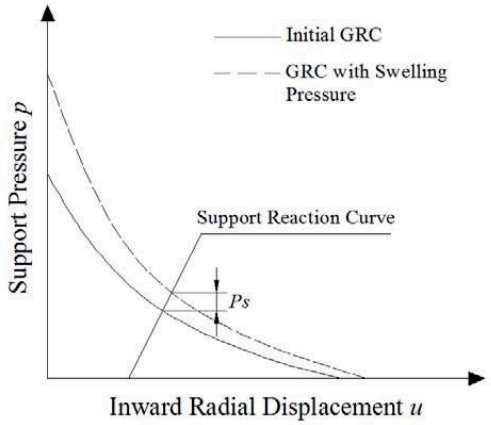

Figure 3.3 Ground reaction curve (GRC) considering swelling pressure (*Ps*: pressure on rock support caused by swelling)

If rock support pressure for the Finnfast weakness zone is estimated based on the empirical diagram in Figure 3.1, the value would be surprisingly higher than the monitored load from rock mass. To a great extent, this may be due to the fact that the location of instrumentation is not very close to the excavation face, which is the most critical area in terms of rock support and tunnel stability.

It should also be noted that the strength reduction of the rock mass with water absorption can not be accounted for by any parameter in the Q-system. This is of particular significance for the fault where cave-in occurred at the Hanekleiv road tunnel.

The Q-system is more relevant for ground conditions within the bounds of dominant case histories. As illustrated by Figure 3.1, very few cases of registered support pressure

are within the area corresponding to the Q value range of 0.002 – 0.2, which represents rated rock mass quality of the majority of weakness zones.

Thus, it is hardly possible to characterize the complex conditions of weakness zones containing swelling clay with an empirical classification system, where very few such extreme cases have been included in the database. In such complex ground special methods for analysis should therefore be used to evaluate the results with respect to tunnel stability and required rock support.

4. Laboratory Testing of Swelling Clay

4.1 Introduction

The gouge material from faults or weakness zones usually consists of a mixture of clay and rock fragments of various sizes. Swelling minerals in gouge material can be identified by X-ray diffraction analysis (XRD) or differential thermal analysis (DTA). For quantification of swelling potential, a laboratory test method based on measuring the swelling pressure of remoulded specimens and the so called free swelling test have been extensively used in Norway. X-ray diffraction analysis and the two testing methods for quantification of swelling potential have been conducted for the Finnfast and Hanekleiv samples. The gouge samples were collected from the weakness zone at the Finnfast subsea tunnel, and from the caved in material and the clay fillings of the distinct joints at the Hanekleiv road tunnel.

4.2 X-ray Diffraction Analysis

In the X-ray diffraction analysis, the sample is irradiated with x-rays of a fixed wave-length and the intensity of the reflected radiation is recorded and analyzed for the reflection angle to calculate the inter-atomic spacing. The intensity of reflection is measured to discriminate the various spacings and to identify the minerals based on possible matches (Moore and Reynolds Jr., 1997).

Figure 4.1 XRD D8 Advance

Figure 4.1 shows the test equipment used in the NTNU/SINTEF laboratory for the analysis - XRD D8 Advance (Bruker, 2010). The minerals of the collected gouge material from the instrumented weakness zone at the Finnfast subsea tunnel were identified as montmorillonite, muscovite, chlorite, clinochlore and graphite. Among these, montmorillonite is the most important swelling mineral. The mineral compositions of two tested samples show some differences (Table 4.1). Details regarding test results are shown in Appendix A. Bollingmo et al. (2007) based on X-ray diffraction identified that the minerals of tested samples of gouge material for the Hanekleiv case as alkali feldspar (53%), plagioclase (21%), smectite(6%), kaolinite(11%) and mica(9%).

Table 4.1 Mineral composition of the clay samples based on X-ray diffraction analysis – Finnfast case

Mineral	Montmorillonite	Muscovite	Chlorite	Clinochlore	Graphite
Sample 1	9.4%	27.7%	40.5%	19.9%	2.5%
Sample 2	24.4%	22.3%	31%	17.6%	4.7%

4.3 Swelling Pressure Test

The laboratory test method based on measuring the swelling pressure of remoulded specimens was introduced at NTNU several decades ago (Brekke, 1965). The procedure of the NTNU swelling pressure test has been standardized, and can generally be divided into sample preparation, compression, unloading and swelling. A principle sketch of the NTNU swelling pressure test is shown in Figure 4.2. First, the fraction of clay with grain size less than 20 μm is segregated from the gouge material and dried in an oven at 105 ^{o}C /110 ^{o}C. The dried clay is then exposed to the relative humidity of the laboratory air (40%) and laboratory temperature before it is milled into clay powder. 20 g of such clay powder is then packed in a 20 cm^2 oedometer cell and compressed at 2 MN/m^2 for a minimum of 24 hours to obtain constant volume. Thereafter, the sample is unloaded till no significant volume change is registered. Finally, water is accessed to the sample and the mobilized pressure is measured with the sample volume kept constant. Figure 4.3 shows the upgraded equipment at the NTNU/SINTEF laboratory for the test. The test apparatus, test procedure, limitation of the test, etc. are described in more detail in Paper I.

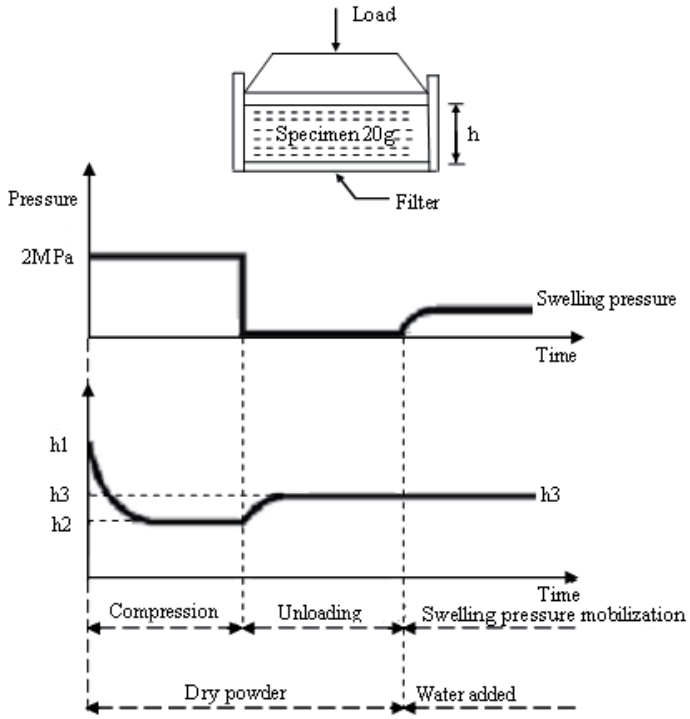

Figure 4.2. Principle sketch of the NTNU swelling pressure test (Nilsen and Broch, 2009).

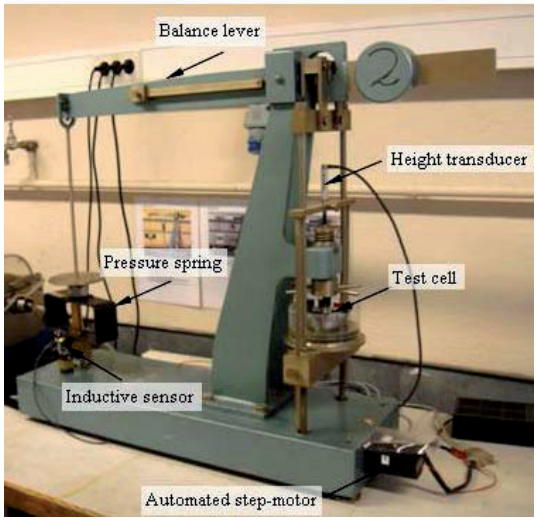

Figure 4.3 Upgraded NTNU apparatus for testing swelling pressure.

More than 500 gouge samples have been tested at the NTNU/SINTEF laboratory based on this test. The maximum value of swelling pressure that has been measured is more than 4 MPa. The Norwegian National Group of ISRM, NBG, defines swelling pressure below 0.1 MPa as low, 0.1 - 0.3 MPa as moderate, 0.3 - 0.75 MPa as high and above 0.75 MPa as very high based on this type of test (NBG, 2000). Since the water entering the weakness zone in a subsea tunnel is often saline, testing was carried out with six individual Finnfast samples using both distilled water and seawater. The fraction with grain size less than 20μm of the Finnfast samples accounted for 20.7% of the total weight. The test results based on distilled water gave swelling pressure between 0.19MPa and 0.21MPa, and based on seawater between 0.16MPa and 0.18MPa for the Finnfast samples. For the Hanekleiv samples, tested by Bollingmo et al. (2007), the fraction with grain size less than 20 μm accounted for 14% of the weight of test samples and the tested swelling pressure was 0.18 MPa.

4.4 Free Swelling Test

The so called free swelling test is another common test to quantify the relative swelling potential, in which the clay fraction with particle size less than 20 μm is also used. 10 ml of loosely packed dry clay powder is drizzled into a 50 ml measuring cylinder filled with distilled water. The volume occupied by the clay powder after sedimentation is recorded, and the free swelling is calculated as the percentage of the original powder volume.

Free swelling index number (F_S):
$F_S = V_1/V_2$
V_1 = Volume of clay after sedimentation
V_2 = Original volume of dry clay powder, 10 ml

More than 400 gouge samples have been tested at the NTNU/SINTEF laboratory based on the free swelling test. The maximum recorded value is higher than 850% while the minimum value is as low as 60%. NBG defines free swelling below 100% as low, 100% - 140% as moderate, 140% - 200% as high and above 200% as very high (NBG,

2000). Free swelling 150%- 165% in distilled water and 110%-130% in seawater were recorded for the tested samples prepared from the gouge material in the Finnfast weakness zone. For the Hanekleiv samples the free swelling was 150% (Bollingmo et al., 2007).

5. Numerical modelling

5.1 General

Numerical simulation is a powerful tool for civil and mining engineering planning and design, particularly when difficulties and uncertainties are expected in underground excavation. Generally, the numerical methods in the fields of civil and rock engineering can be categorized as below:

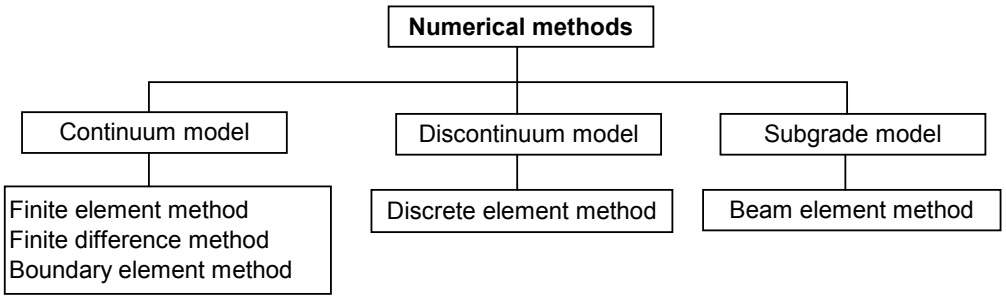

Figure 5.1 General classification of numerical methods

These numerical methods are based on different theories and assumptions, and this makes each of them suitable for particular types of problems. Details of strengths and weaknesses of each method are discussed by Pande et al. (1990) and Jing and Hudson (2002).

5.2 2D versus 3D

Due to their simplicity, two-dimensional programs have been widely used in calculating stresses and displacements around underground excavations. However, tunneling through weakness zones/faults normally can not be easily simplified into a two-dimensional problem, since the effects of the geometry of weakness zones/faults in most cases can not be considered in a two-dimensional analysis. This has been discussed in Paper II by comparison of the commonly used 2D-program Phase^2 with a powerful 3D-

program, FLAC^{3D} (Itasca, 2005). In this thesis, FLAC^{3D} (Itasca, 2005) has been used in simulating the Finnfast case and Hanekleiv case.

5.3 Phase^2

Phase^2 is a two-dimensional elasto-plastic finite element stress analysis program for underground and surface excavations in rock or soil (Rocscience, 2005). The finite element method divides the body into small elements of various shapes, e.g. triangles and rectangles. Displacements within the element are related to the displacements at the nodes through so-called shape functions. Transmission of internal forces between the edges of adjacent elements is represented by interactions at the nodes of the elements. Matrix-oriented solution schemes are common for the finite element method. An implicit method is often used for solving the equations, in which every element communicates with every other element during one solution step and several iterations are necessary before compatibility and equilibrium are obtained (Brady and Brown, 2005; Pande et al., 1990). A wide range of material models are provided in Phase^2 as shown in Figure 5.2 (Rocscience, 2005). The program also offers an extensive range of support modelling options for geotechnical applications.

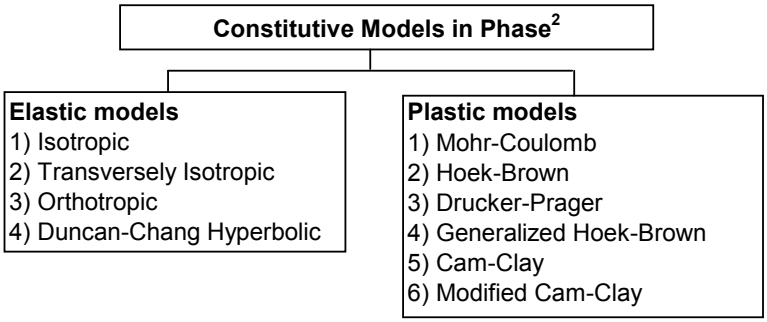

Figure 5.2 Constitutive models in Phase^2 (Rocscience, 2005)

5.4 FLAC^{3D}

FLAC^{3D} is a three-dimensional explicit finite-difference program for engineering mechanics computation. Since this is a finite difference program, it is not necessary to combine the element matrices into a large global stiffness matrix as in the finite element model. It regenerates finite equations at each step. Derivatives of governing equations are

replaced directly by algebraic expressions written in terms of field variables at discrete points in space. The finite difference method is particularly suitable for large, non-linear problems which may involve collapse or progressive failure.

The basis for FLAC^{3D} is the numerical formulation used by the two-dimensional program, FLAC (Itasca, 2005). FLAC^{3D} extends the analysis capability of FLAC (Itasca, 2005) into three dimensions. The first edition of FLAC^{3D} (FLAC^{3D} version 2.1) was issued in April 2002, the second edition (version 3.0) in September 2005, the third (version 3.1) in December 2006 and the fourth (version 4.0) in December 2009. In this thesis, FLAC^{3D} version 3.1 has been used for the Finnfast case and FLAC^{3D} version 4.0 for the Hanekleiv case. The codes of FLAC^{3D} for numerical simulation are given in Appendix B.

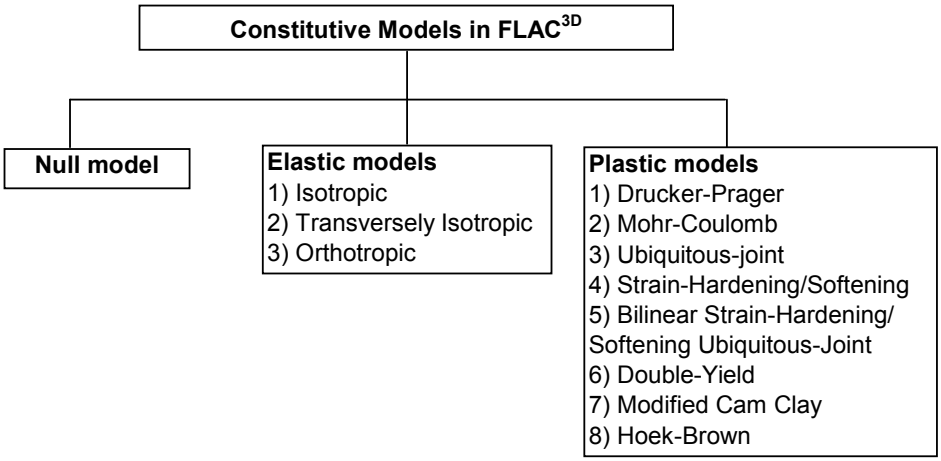

Figure 5.3 Constitutive models in FLAC^{3D}

The default calculation mode in FLAC^{3D} is for static mechanical analysis, and dynamic mechanical analysis can be performed with user-specified acceleration, velocity or stress waves as either an exterior boundary condition or an interior excitation to the model. Effects of ground water flow or heat-transfer can be considered with the coupled fluid flow–mechanical and thermal–mechanical analysis. The groundwater flow analysis or a heat-transfer analysis can also be performed independent of the mechanical

calculation. FLAC^{3D} (Itasca, 2005) has twelve basic built-in constitutive models as shown in Figure 5.3.

FLAC^{3D} also provides various structural element models for simulation of structural support including beams, cables, piles, shells, geogrids and liners.

5.5 Numerical simulation

5.5.1 Consideration of swelling effects

In numerical simulation, the effects of swelling pressure on the reinforced shotcrete rib at the Finnfast subsea tunnel as well as on the shotcrete at the Hanekleiv road tunnel are simplified from an engineering perspective as uniformly distributed load. This is realized in the model by applying the corresponding loads at the boundary between the weakness zone/fault zone and shotcrete. The swelling pressure measured in laboratory is not directly comparable with the in-situ swelling pressure. To quantify the swelling pressure on rock supports, numerical simulations have been carried out for the Finnfast case with different swelling pressures ranging from zero to 0.20MPa at an interval of 0.04MPa. For the Hanekleiv road tunnel it was concluded that, in addition to the effect of the swelling process, gravitational collapse due to the very low internal friction played an important role in the development of instability (Bollingmo et al., 2007; Nilsen, 2011). In that case, a swelling pressure of 0.09 MPa (50% of the laboratory tested value) is applied on the shotcrete superimposed on the effects of strength reduction of the fault zone.

The simulation process and analysis of simulated results have been extensively explained in the attached papers. In the following, the selection of constitutive model and support structural elements and determination of parameters are discussed.

5.5.2 Finnfast Subsea Tunnel

The Finnfast subsea tunnel is located 140 m below sea level, and the pore pressure redistribution during tunnel excavation needs to be considered in numerical analysis. Zero pore pressure is assumed within the shotcrete during tunnel excavation as all rock

support in Norwegian subsea tunnels is drained (Blindheim et al., 2005). The typical time interval between each blasting round close to the weakness zone was one day, but it was four days where the instrumentation was installed in the weakness zone. The time scale of the analysis is much larger than the characteristic time of the coupled diffusion process (estimate of time to reach steady state) and drained behavior prevails after each blasting round. Therefore, the steady-state pore pressure field can be determined using the ground water flow analysis after each blasting round before the mechanical analysis. The fully coupled hydro-mechanical analysis with FLAC^{3D} is often quite time consuming and not considered necessary for the case of Finnfast subsea tunnel.

Besides the weakness zone and side rock, rock support consisting of sprayed concrete is also simulated with the Mohr-Coulomb model (as one material layer) instead of any structural element models. Reinforced steel bars can then be installed in the sprayed concrete at the defined locations. The Mohr-Coulomb model is the conventional model used to represent shear failure in soils and rocks. Laboratory test results for concrete also match well with the Mohr-Coulomb criterion (Vermeer and de Borst, 1984). Detailed physical and mechanical properties of the weakness zone, side rock and the rock support of sprayed concrete used in the modelling are presented in Paper III.

The steel bars in the reinforced ribs of shotcrete are simulated as beam elements, the spiling bolts are simulated as pile elements (Trinh, 2006; Volkmann and Schubert, 2007), while the radial bolts and face bolts are simulated as cable elements due to different loading characteristics (Itasca, 2005). The beam element is a linearly elastic material with no failure limit, and it is used for structural support where bending and limited bending moments occur. It is possible to introduce a limiting plastic moment, or even a plastic hinge across which discontinuity in rotation may develop, between beam elements. The cable element can yield in axial tension or compression, but can not resist a bending moment. It is suitable for modelling structural-support in which tensile capacity is important, and for which axially directed frictional interaction with the rock or soil mass occurs. The pile element offers the combined features of the beam element and cable element. In addition to the structural behavior of a beam (including the ability to specify a

limiting plastic moment), both a normal-directed (perpendicular to the pile axis) and a shear-directed (parallel with the pile axis) frictional interaction between the pile and the grid can be considered.

The geometrical parameters of these structural elements are calculated from geometrical dimensions. The mechanical parameters are mostly based on general data for rock support elements. For radial bolts and face bolts, it has been discussed below how to estimate the group stiffness k_g and grout cohesive strength c_g without laboratory pull-out tests.

The grout stiffness, k_g, as discussed in the FLAC^{3D} manual (Itasca, 2005), can be measured directly in laboratory pull-out tests. Alternatively, the stiffness can be calculated from a numerical estimate for the elastic shear stress, τ_G, obtained from an equation describing the shear stress at the grout/rock interface (St. John and Van Dillen, 1983):

$$\tau_G = \frac{G}{(D/2+t)} \times \frac{\Delta u}{\ln(1+2t/D)}$$

Where Δu = relative displacement between the element and the surrounding material

G = grout shear modulus

D = reinforcing diameter

t = annulus thickness

Consequently, the grout shear stiffness, k_g, is simply given by:

$$k_g = \frac{2\pi G}{\ln(1+2t/D)}$$

In many cases, the reasonable value of k_g is about one tenth of the estimated one based on the equation accounting for the relative shear displacement that occurs between the host-zone grid-points and the borehole surface (Itasca, 2005).

The values for grout cohesive strength, c_g, can be estimated from the results of pull-out tests conducted at different confining pressures. If such results are not available, they may be obtained from (Itasca, 2005):

$$c_g = \pi(D + 2t)\tau_{peak}$$

Where τ_{peak} = peak shear strength

D = reinforcing diameter

t = annulus thickness

The peak shear strength can be estimated as one-half of the uniaxial compressive strength of the weaker of the rock and grout with perfect bonding between the grout and rock. Failure of reinforcing systems does not always occur at the grout/rock interface. Failure may occur at the reinforcing/grout interface, as is often true for cable reinforcing. In such cases, the shear stress is evaluated at this interface as:

$$c_g = \pi D \tau_{peak}$$

5.5.3 Hanekleiv Road Tunnel

In numerical simulation of the tunnel collapse at the Hanekleiv tunnel, the fault zone and side rock are also based on the Mohr-Coulomb model. Physical and mechanical properties of the original fault zone, the weakened fault zone (close to the tunnel periphery 10 years after excavation), the side rock and applied shotcrete used in the modelling have been given in Paper IV. Since the strength reduction is believed to have developed gradually inwards, there was a variation of strength reduction in the weakened fault zone. In numerical simulation, the conservative simplification has been made that the properties of the weakest material from the caved in rock mass are assumed for the whole weakened fault zone.

For simulating the thin support structure, e.g., thin shotcrete, the shell element or liner element have been introduced in FLAC^{3D}. The shell element is used to model the structural support provided by any thin-shell structure in which the displacements caused by transverse-shearing deformations can be neglected. The liner element is used to model thin liners for which both normal-directed compressive/tensile interaction and shear-

directed frictional interaction with the host medium occurs. However, both the shell element and liner element behave as linearly elastic material with no failure limit. Rotation along the edges between shell elements or liner elements is possible by introducing the plastic-hinge lines. Since cracks in the shotcrete had been detected at the fault zone during the tunnel excavation, the post-failure behaviour of shotcrete needs to be considered. This can not be achieved with either the shell element or liner element as the elastic material. The FLAC^{3D} grid based on the strain hardening/softening model is used for the rock support of shotcrete. This model is based on the Mohr-Coulomb model. The difference lies in the possibility that the cohesion, friction, dilation and tensile strength may harden or soften after the onset of plastic yield. In the Mohr-Coulomb model, these properties are assumed to remain constant.

Back-analysis shows the observed cracks in shotcrete during tunnel excavation were caused by tension. The tension failure of shotcrete is characterized by a gradual growth of cracks which join together and finally disconnect larger parts of the structure. The tensile strength of shotcrete is assumed to drop to zero when failure occurs. In numerical simulation, the shotcrete is in tensile failure when the plastic tensile strain reaches 20 μs, which is calibrated based on the grid size of model. The rate at which the tensile strength drops is controlled by the plastic tensile strain and the linear softening law for the tensile strength in FLAC^{3D} (Itasca, 2009).

6. Comments on Papers

The papers based on this PhD research are numbered I-IV and included in full length after this introductory part of the thesis. Brief comments on the papers and the main conclusions based on each paper are given in the following.

6.1 Paper I Laboratory testing of swelling gouge from weakness zone – principle and recent update

Published in Proceedings of 45th US Rock Mechanics/Geomechanics Symposium, San Francisco, USA, 2011

Paper I is discussing the two laboratory testing methods commonly used in Norway for quantifying the swelling potential of gouges: 1) testing of the swelling pressure of remoulded specimens, and 2) the so called free swelling test, measuring the volume increase of the clay powder after sedimentation in water.

The test apparatus for the swelling pressure test has been updated several times since it was introduced. However, the principle and main procedures have remained the same. The test procedure can be generally divided into stages of specimen preparation, compression, unloading and swelling. Figure 6.1 shows the test procedures belonging to each stage.

One requirement for the NTNU swelling pressure test is that the specimen volume has to be kept constant during the swelling process. If expansion of the specimen is allowed during the swelling process, the mobilized swelling pressure may significantly decrease. In the recent update of the apparatus, the specimen volume is kept constant by instantaneous compensation of the axial deformation during the swelling process, and a continuous logging of the swelling pressure is achieved. A height transducer and inductive sensor replace the dial gauges for measuring specimen height and pressure, and an automated step-motor replaces the manually operated wheel for worm gear adjustment.

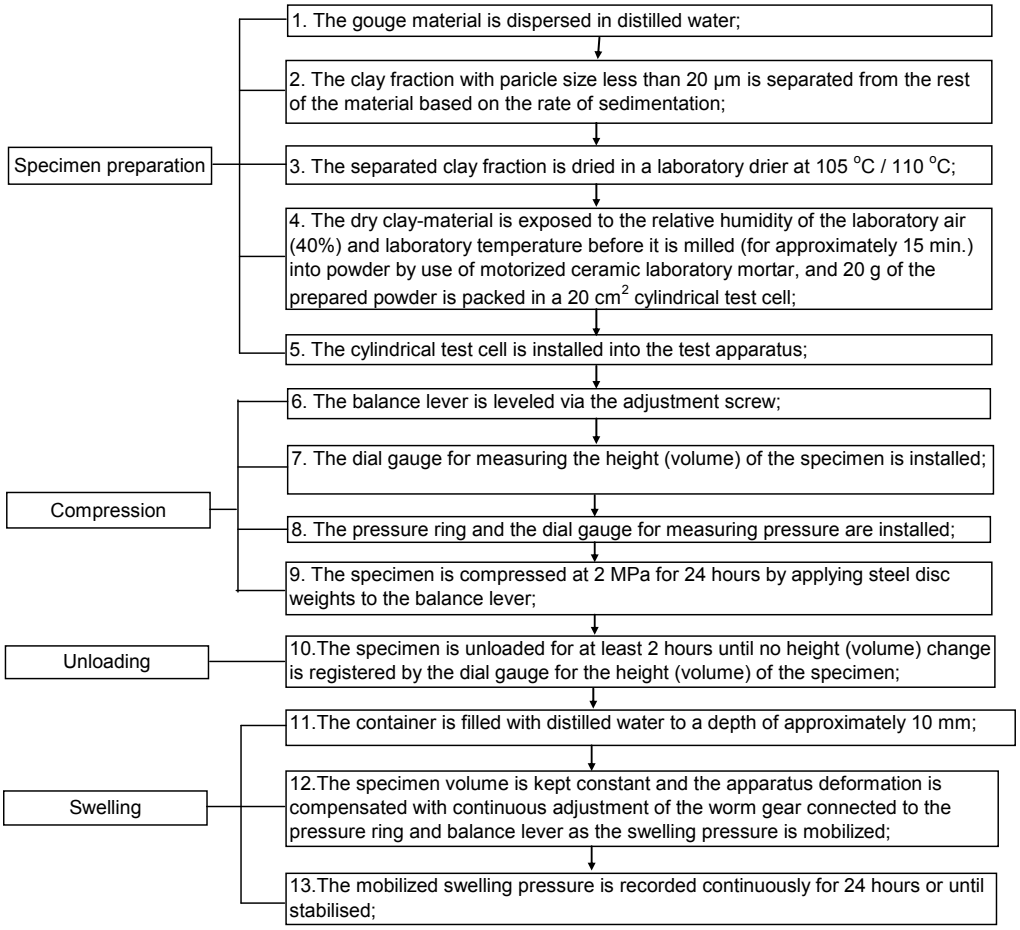

Figure 6.1. Procedure of NTNU Swelling Pressure Test.

At the NTNU/SINTEF laboratory, more than 500 swelling pressure tests and more than 400 free swelling tests have been carried out. The test results are classified based on the guidelines given by the Norwegian National Group of ISRM, NBG (NBG, 2000). The categories of low, moderate, high and very high in terms of swelling pressure for the NTNU/SINTEF testing account for 17.7%, 38.5%, 27.2% and 16.6% respectively, of all the tested samples. For the free swelling test, the categories of low, moderate, high and very high in terms of free swelling account for 8.0%, 33.6%, 34.8% and 23.6%, respectively, of all the tested samples.

Free swelling vs. swelling pressure for the tested samples is illustrated in Figure 6.2. There seems to be a positive correlation between these two parameters for swelling pressure values below 1MPa. However, there is no obvious correlation when considering the whole dataset.

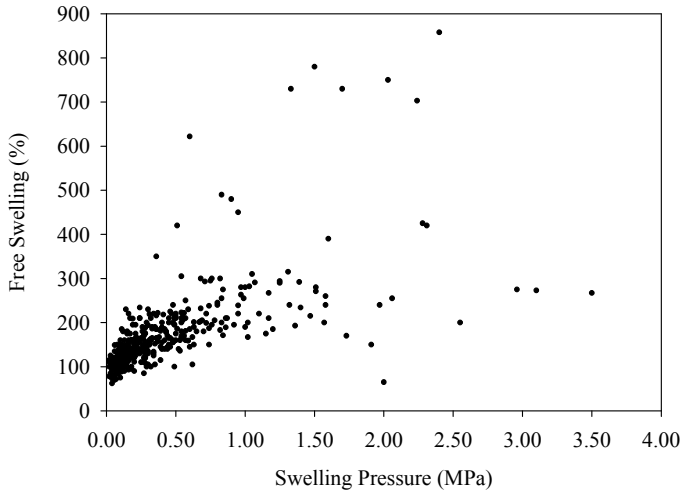

Figure 6.2. Laboratory test results – Free Swelling vs. Swelling Pressure.

It is concluded in the paper that both the swelling pressure and free swelling test methods are primarily appropriate as index tests, and that the swelling pressure measured in the laboratory is not representative of the in-situ swelling pressure on rock support. This is mainly for the following reasons:

- The laboratory test results are based on a fixed clay amount of 20g.
- The in-situ structure and compaction are damaged as a result of the sampling process and the sample preparation.
- The clay fraction used in the tests represents the most active part of the gouge material, and the dry condition represents the highest swelling potential.
- The in-situ swelling pressure on rock support to a great extent depends on the time between blasting and rock support installation, and also on the support deformation.

6.2 Paper II Numerical analysis of effects of weakness zones on tunnel stability – 2D versus 3D

Submitted to the 13th World Conference of the Associated Research Centers for the Urban Underground Space, November 2011

For modelling tunnel excavation and support through major weakness zones or faults where the geometry is complex, three-dimensional programs have been widely used. In most cases the geometry effects of tunnel and weakness zones/faults can not be considered in a two-dimensional model. Simulation results may be considerably deviating from reality if a two-dimensional program is improperly used. This is investigated based on two representative numerical programs in rock engineering, the two-dimensional finite element program, Phase^2, and the three-dimensional finite-difference program, FLAC^{3D}.

Steep weakness zones with thickness 10 -15 m are quite typical and often represent considerable challenges for tunnel stability. In numerical analysis in this paper, the weakness zone is taken as vertical and assumed to be perpendicular to the tunnel alignment. As tunnel geometry is used a traditional Norwegian road tunnel design, an arched tunnel with excavation span of 12 m and theoretical cross section of excavation of about 65 m^2 (Norwegian Public Roads Administration, 2004). The typical parameters of the weakness zone are taken as the same as for the Finnfast weakness zone (described in Grimstad, 2008). The properties of the side rock are typical for granitic gneiss, a predominant rock type in Norway.

Scenarios of different horizontal/vertial stress ratios and strengths of the weakness zone are included in the analysis. Simulation results for vertical displacements and yielded zones based on FLAC^{3D} and Phase^2 are compared. The influences of the initial stresses and strength of the weakness zone are discussed. The loading effects on rock support are compared for one selected senario where the maximum displacement is obtained. The material softening method (Swoboda, 1979; Swoboda et al., 1994) is used for defining the amount of deformation before installation of rock support in the Phase^2 simulation (Rocscience, 2005).

It is found that for a major weakness zone with typical thickness, 2D modelling may result in a large deviation from the 3D results. The lower strength of the weakness zone, the larger the deviation will be. For Phase^2 to be realistically used for analyzing the effects of a weakness zone which is perpendicular to the tunnel alignment, the thickness of the zone has to be much wider than the tunnel span.

6.3 Paper III Analysis of loading effects on reinforced shotcrete ribs caused by weakness zone containing swelling clay

Published in Tunnelling and Underground Space Technology, 26 (2011): 472–480, doi:10.1016/j.tust.2011.01.004

In this paper, the loading effects on rock support of reinforced shotcrete ribs caused by a major weakness zone containing swelling clay is analysed based on monitoring results and numerical simulation.

Instrumentation was installed in one of the weakness zones containing swelling clay encountered during excavation of the Finnfast subsea tunnel. Comprehensive support was used when excavating through the zone (spiling bolts, shotcrete, radial bolts, face bolts and reinforced ribs of sprayed concrete) and, in addition, the length of the blast round was reduced. Instrumentation was installed at the reinforcement rib of sprayed concrete to measure the strain of reinforcement bar in the concrete rib, strain in concrete along the tunnel axis, the load from rock mass acting on the concrete rib and the ring stress in sprayed concrete. The variation of temperature due to shotcrete curing at the instrumentation location was also recorded. These data were collected by the Norwegian Geotechnical Institute (NGI) (Grimstad et al., 2008).

The laboratory test results based on distilled water gave swelling pressure between 0.19MPa and 0.21MPa, and based on seawater between 0.16MPa and 0.18MPa. Free swelling 150%- 165% in distilled water and 110%-130% in seawater were recorded.

The three-dimensional finite difference program FLAC^{3D} has been used for numerical analysis. The excavation process is explicitly simulated by changing corresponding

ground elements into null elements. Application of shotcrete is simulated by changing the corresponding layers of null elements into elements with corresponding properties of shotcrete. Rock supports of spiling rock bolts, radial bolts, face bolts and steel bars in the reinforced ribs of shotcrete are simulated with the built-in structural elements based on different loading characteristics (Itasca, 2005). Pore pressure distribution during excavation is simulated after each blasting round before the mechanical response of ground is calculated. Effects of the swelling pressure on rock supports are simplified as uniformly distributed load. This is realized in the model by applying the corresponding loads at the boundary between the weakness zone and shotcrete for staged swelling pressures varied from 0.04MPa to 0.20MPa at an interval of 0.04MPa. The flow chart of the whole modelling process is shown in Figure 6.3.

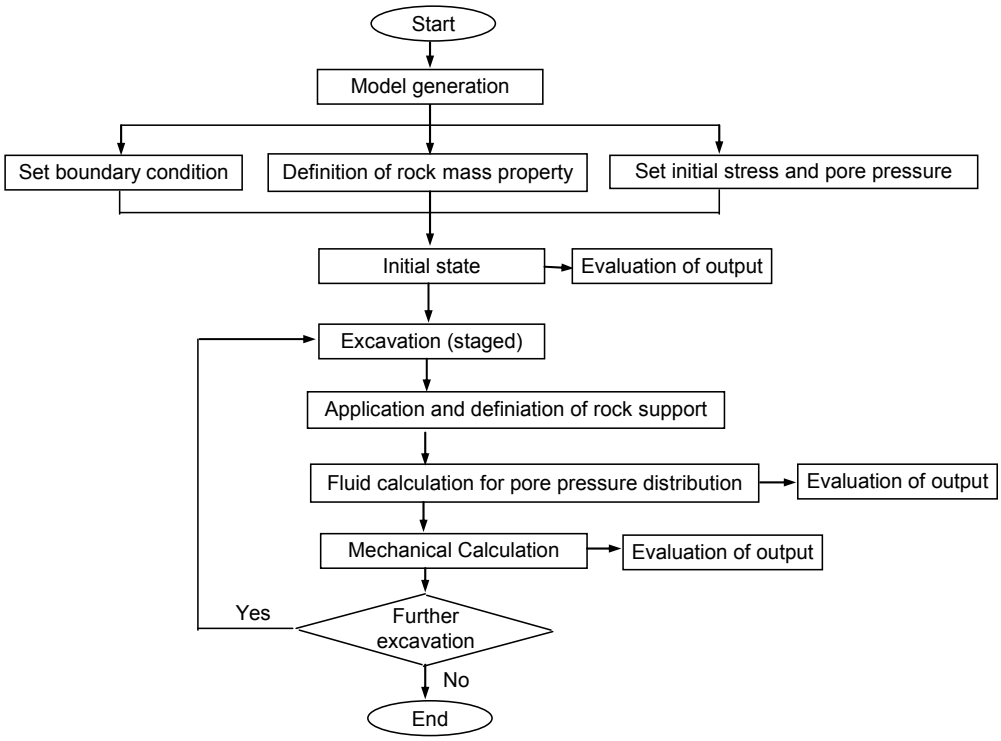

Figure 6.3. Flow chart of modelling process of the Finnfast case.

Simulation focuses on the response of the reinforced shotcrete rib at equilibrium state when the tunnel has advanced far from the weakness zone. This eliminates the influence of temperature variation due to shotcrete curing. The long term loading on rock support at this state is compared with the stabilized instrumented data. The paper concludes that swelling pressure may considerably increase the loading on rock support. For a swelling pressure on rock support at the instrumentation location of 0.16 MPa, many simulation results are comparable with the monitoring results. It is also concluded that the loading on the sprayed concrete is far less than its compressive strength, even for rock support without the reinforcement sprayed concrete rib. This suggests that such zones may be excessively supported when the swelling clay is not very active. The loading on rock supports is much higher close to the excavation face compared with the instrumented location. For reliable stability control through such zones, the instrumentation should be installed as close to the excavation face as possible.

6.4 Paper IV Numerical analysis of rock fall at Hanekleiv road tunnel

Accepted by Bulletin of Engineering Geology and the Environment, October 2011

This paper describes the numerical analysis of the rock fall at the Hanekleiv road tunnel, one of several recent failure cases in weakness zones/faults containing swelling clay.

The rock fall occurred ten years after completion of the tunnel, and the volume of caved in material was estimated to be 250 m^3. It was concluded by Bollingmo et al. (2007) and Nilsen (2011), that in addition to the effect of swelling, gravitational collapse due to the very low internal friction in this case played an important role in the development of instability.

Clay samples were collected from the caved in material as well as from the clay fillings of the distinct joints at one cross passage intersecting the fault zone. Swelling clay (smectite) was identified based on X-ray diffraction analysis. The clay fraction with grain size less than 20 μm accounted for only 14% of the weight. The swelling pressure was found to be 0.18 MPa and the free swelling 150% (Bollingmo et al., 2007; Nilsen, 2011).

The finite difference code, FLAC^{3D} (Itasca, 2009), was used for numerical simulation of the Hanekleiv case. The time for the instability to develop was 10 years, indicating a long lasting, gradual process of mobilization of swelling pressure and strength weakening of the fault zone. This process is hard to define explicitly, and it has been numerically simulated as three stages of mechanical states. The first stage represents tunnel excavation without consideration of effects of swelling and strength reduction of the fault zone. The swelling pressure on the rock support of shotcrete is considered at the second stage. Combined effects of strength reduction of the fault zone and swelling are simulated at the last stage. Alternative supports of shotcrete rib and concrete lining are simulated for estimating rock support requirements of this zone. The flow chart of the modelling of the Hanekleiv case is shown in Figure 6.4.

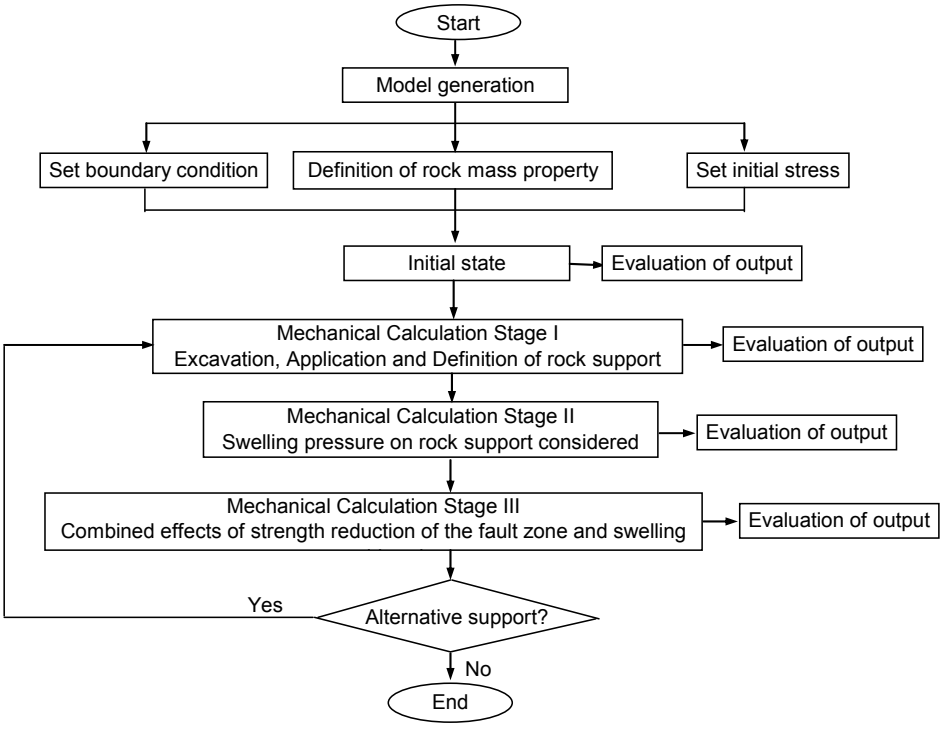

Figure 6.4. Flow chart of modelling process of the Hanekleiv case.

Both the detected cracks during tunnel excavation and the tunnel collapse are verified with numerical simulation. The swelling pressure has been found to have had a limited influence on the shotcrete, while the strength reduction played an important role in the development of instability. According to the numerical analysis, rock support with reinforced shotcrete ribs could not have fully prevented tunnel instability. It could have prevented the rock fall, but cracks between the shotcrete ribs indicate potential instability. A 25 cm thick concrete lining, in addition to the concrete, would have reduced the cracked area considerably. It is concluded that special consideration is required for rock support under the combined effects of swelling and strength reduction of rock mass.

7. Conclusions and Recommendations

The main research of this thesis is represented by the scientific papers in section 2. Important aspects of each paper have been discussed in Chapter 6. In the following, the main conclusions and recommendations based on these papers are given.

7.1 Conclusions

- It is hardly possible to characterize the complex condition of a weakness zone containing swelling clay based on an empirical classification system (e.g. Q-system). In such challenging ground special analyses should be performed to evaluate the situation with respect to tunnel stability and required rock support.
- For characterizing the swelling potential of gouge materials from weakness zones/faults, the NTNU swelling pressure and free swelling laboratory tests have been extensively used, and the resulting data represent a large database. There is however no obvious correlation between swelling pressure and free swelling in terms of the whole dataset.
- The laboratory results of swelling pressure and free swelling tests indicate the relative swelling potential, which is valuable for evaluation of potential stability problems and security measures. The two NTNU test methods are appropriate to use as index tests. The swelling pressure measured in the laboratory is not representative of the in-situ swelling pressure on rock supports.
- In numerical analysis, the geometry effects of tunnel and weakness zones/faults in most cases can not be realistically considered in a two-dimensional model. A three-dimensional model should normally be used for such complicated engineering mechanical computation.
- For a two-dimensional program, e.g. Phase^2, to be realistically used for analyzing the effects of a weakness zone which is perpendicular to the tunnel alignment, the thickness of the zone has to be much wider than the tunnel span. This is quite unusual for the road tunnels with a typical excavation span of 10 - 12 m.

- The loading on the sprayed concrete in Finnfast weakness zone has been found to be far less than its compressive strength, even for rock support without sprayed concrete rib. This suggests that such zones may often be excessively supported when the swelling clay is not very active.
- In the simulation of the Finnfast case it is found that the loading on rock support is much higher close to the excavation face, which is the area more critical in terms of tunnel stability, than the instrumented location further behind. For reliable stability control of excavation through weakness zones/faults, the instrumentation should be installed as close to the excavation face as possible.
- The Finnfast case illustrates that uncertainties may exist in the instrumentation results for weakness zones due to undulations or depressions of the excavated tunnel profile, local flaws in the sprayed concrete attaching to instrumentation equipments and voids created when spraying through reinforcement steel bars.
- Numerical simulation of the Hanekleiv case shows that the strength reduction played an important role in the development of instability, while the swelling pressure was found to have a limited influence on the rock support.
- Numerical analysis at the Hanekleiv fault zone indicates that rock support with reinforced shotcrete ribs could not have fully prevented the instability. A 25 cm thick concrete lining, in addition to the concrete, would have however reduced the cracked area considerably.

7.2 Recommendations

For rock support estimation in weakness zones/faults containing swelling clay, it is recommended to follow the flow chart shown in Figure 7.1 as supplement to empirical design. Pure empirical design is not sufficient since swelling effects are not fully accounted for in the Q-system or other commonly used rock mass classification systems.

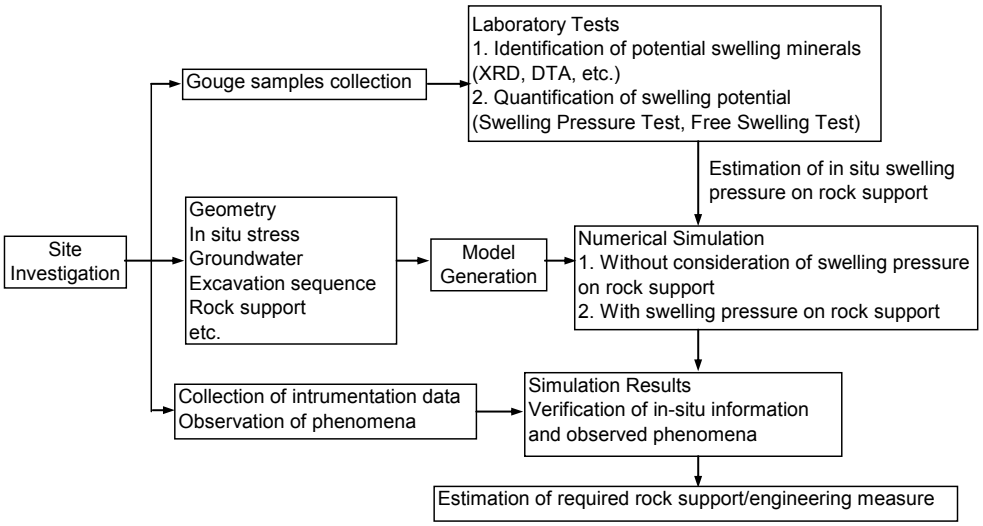

Figure 7.1 Flow chart of rock support estimation in weakness zones/faults containing swelling clay.

Site investigation, laboratory testing and numerical simulation are integrated in the recommended procedure of the flow chart in Figure 7.1. The risk of other unfavourable conditions (e.g., strength reduction, high water pressure on rock support, squeezing) should also be carefully examined and if applicable included in analysis. Due to the complexity of the swelling process, the analysis can be focused on selected equilibrium mechanical states, particularly the one representing the long term loading on rock support. Three-dimensional numerical analysis is to be used for such complicated geometry and the created model should reflect the in-situ situations.

Instrumentation should be installed for difficult zones as close as possible to the tunnel excavation face. This will also provide data for back analysis and further improve the understanding of rock support in such zones. High quality of instrument installation is essential for obtaining reliable instrumentation data. Long term, regular check of signs of instability, e.g. accelerated movement of tunnel periphery, cracks in shotcrete, is very important for stability control. Simulation results should be able to verify instrumentation results and observation of signs of instability in the tunnel contour.

Further research should be carried out for more cases of weakness zones/faults containing swelling clay. This will greatly enrich the knowledge on tunneling through such ground. In a longer perspective, swelling effects of weakness zones may be able to be accounted in rock classification systems when substantial experiences from tunneling in such zones are gained.

References

Aristorenas, G. V., 1992. Time-dependent behaviour of tunnels excavated in shale. Ph.D. Thesis. Massachusetts Institute of Technology, Boston, USA.

Barla, M., 1999. Tunnels in swelling Ground – Simulation of 3D stress paths by triaxial laboratory testing. Ph.D. Thesis. Geotechnical Engineering, Politecnico di Torino, Italy.

Barla, M., 2008. Numerical simulation of the swelling behaviour around tunnels based on special triaxial tests. Tunnelling and Underground Space Technology 23(5):508-521.

Barton, N., Lien, R., Lunde, J., 1974. Engineering classification of rock masses for the design of tunnel support. Rock Mechanics and Rock Engineering 6(4):189-236.

Barton, N., Lien, R., Lunde, J., 1974. Analysis of rock mass quality and support practice in tunneling, and a guide for estimating support requirements. Report from Norwegian Geotechnical Institute.

Barton, N., 1976. The shear strength of rock and rock joints. International Journal of Rock Mechanics and Mining Science & Geomechanics Abstracts 13(9): 255-279.

Barton, N., 2002. Some new Q-value correlations to assist in site characterization and tunnel design. International Journal of Rock Mechanics and Mining Sciences 39(2): 185-216.

Bellwald, P., 1990. A contribution to the design of tunnels in argillaceous rock. Ph.D. Thesis. Massachusetts Institute of Technology, Boston, USA.

Blindheim, O. T., Nilsen, B., 2001. Rock cover requirements for subsea road tunnels. In: Proceedings of Strait Crossings 2001, Balkema, Bergen, Norway, pp. 439–448.

Blindheim, O. L., Grøv, E, Nilsen, B., 2005. Nordic sub sea tunnel projects. Tunnelling and Underground Space Technology 20(6): 570-580.

Bollingmo, P., Nilsen, B., Nordgulen, Ø., 2007. The cave-in at the Hanekleiv tunnel - 25 December 2006. Report from investigation panel established by the Norwegian Department of Transportation. In Norwegian.

Brady, B. H. G., Brown, E. T., 2005. Rock Mechanics for Underground Mining (3rd edition). Springer.

Brekke, T. L., 1965. On the measurement of the relative potential swellability of hydrothermal montmorillonite clay from joints and faults in Precambrian and Paleozoic

rocks in Norway. International Journal of Rock Mechanics and Mining Science & Geomechanics Abstracts 2:155-165.

Brekke, T. L., Selmer-Olsen, R., 1965. Stability problems in underground constructions caused by montmorillonite-carrying joints and faults. Engineering Geology 1 (1): 3-19.

Bruker, 2010. Introductory User Manual. In: Bruker Corporation, Germany. http://www.brukeraxs.de/uploads/tx_linkselectorforpdfpool/D8_ADVANCE_A25_Introductory_User_Manual_DOC-M88-ZXX146_V4_complete.pdf.

Brown, E. T., Bray, J. W., Ladanyi, B., Hoek, E., 1983. Ground response curves for rock tunnels. Journal of Geotechnical Engineering 109(1): 15-39.

Carranza-Torres, 2004. Elasto-plastic solution of tunnel problems using the generalized form of the Hoek-Brown failure criterion. International Journal of Rock Mechanics and Mining Sciences 41(suppl. 1): 1-11.

Carter, J. P., Broker, J. R., 1982. Elastic response around a deep circular tunnel. International Journal of Solids and Structures 18:1059-1074.

Carter, J. P., 1988. A semi-analytical solution for swelling around a borehole. International Journal of Rock Mechanics and Mining Science & Geomechanics Abstracts 12:197-212.

Cecil III, O. S., 1970. Correlations of rock bolt-shotcrete support and rock quality parameters in Scandinavian tunnels. Ph.D. Thesis. Urbana, University of Illinois, USA.

Detournay E., Cheng, A. H.-D., 1988. Poroelastic response of a borehole in a non hydrostatic stress field. International Journal of Rock Mechanics and Mining Science & Geomechanics Abstracts 25(3):171-182.

Duncun Fama M. E., 1993. Numerical modeling of yield zones in weak rock. In Comprehensive Rock Engineering, (ed. Hudson J. A.) 2. Pergamon, Oxford, U.K., pp. 49-75.

Edelbro, C., 2003. Hard Rock Mass Strength - A review. Technical Report, Luleå University of Technology, Sweden.

Einstein, H. H., Bishoff, N., Hoffmann, E.,1972. Behaviour of invert slabs in swelling shale. In: Proceedings of the International Symposium On Underground Openings, Lucerne, Switzerland.

Einstein, H. H., Bischoff, N., 1975. Design of Tunnels in Swelling Rock. In: Proceedings of the 16th U.S. symposium on Rock Mechanics, Mineapolis, Minnesota, USA.

Einstein, H. H., 1996. Tunnelling in difficult ground – swelling behaviour and identification of swelling rocks. Rock Mechanics and Rock Engineering 29 (3):113-124.

Grimstad, E., Barton, N., 1993. Updating of the Q-system for NMT. In: Proceedings of the International Symposium on Sprayed Concrete - Modern Use of Wet Mix Sprayed Concrete for Underground Support, Oslo, Norway.

Grimstad, E., Kankes, K., Bhasin, R., Magnussen, A.W., Kaynia, A., 2002. Rock mass quality Q used in designing reinforced ribs of sprayed concrete and energy absorption. Report from Norwegian Geotechnical Institute.

Grimstad, E., Tunbridge, L., Bhasin, R., Aarset, A., 2008. Measurements of forces in reinforced ribs of sprayed concrete. In: Proceedings of the 5th International Symposium on Sprayed Concrete, Lillehammer, Norway, pp. 46-66.

Goel, R. K., 1994. Correlations for predicting support pressures and closures in tunnels. Ph.D. Thesis. Nagpur University, India.

Goel, R. K., Jethwa, J. L., Dhar, B. B., 1996. Effect of tunnel size on support pressure. International Journal of Rock Mechanics and Mining Science & Geomechanics Abstracts 33(7): 749-755.

Gysel, M., 1987. Design of tunnels in swelling rock. Rock Mechanics and Rock Engineering 20(4): 219-242.

Hoek, E., Kaiser, P. K., Bawden, W. F., 1995. Support of Underground Excavations in Hard Rock. Rotterdam: A.A. Balkema.

ISRM Commission on Swelling Rock, 1983. Characterisation of Swelling Rock. Pergamon, Oxford, U.K.

ISRM Commission on Swelling Rocks, 1989. Suggested methods for laboratory testing of argillaceous swelling rock. International Journal of Rock Mechanics and Mining Science & Geomechanics Abstracts 26 (5): 415-426.

ISRM Commission on Swelling Rocks, 1999. Suggested methods for laboratory testing of swelling rocks. International Journal of Rock Mechanics and Mining Science & Geomechanics Abstracts 36 (3): 291-306.

Itasca, 2005. Fast Language Analysis of continua in 3 dimensions, version 3.1, user's manual. In: Itasca Consulting Group, Minneapolis, Minnesota, USA.

Itasca, 2009. Fast Language Analysis of continua in 3 dimensions, version 4.0, user's manual. In: Itasca Consulting Group, Minneapolis, Minnesota, USA.

Jing, L., Hudson, J. A., 2002. Numerical methods in rock mechanics. International Journal of Rock Mechanics and Mining Sciences 39: 409–427.

Karlsson K., 2008. Main road 64, the Atlanterhavs tunnel - leakage zone 230 m below sea level. In: Proceedings of the Norwegian National Tunneling Conference, Oslo, Norway. In Norwegian.

Kovari, K., Amstad, C., Anagnostou, G., 1988. Design/construction methods-Tunelling in swelling rocks. In Proceedings of the 29th U.S: symposium on Rock Mechanics, Minneapolis, Minnesota, USA.

Kvåle, J., Nilsen, B., Grimstad, E., Bollingmo, P., Halvorsen, A., Iversen, E., Sorte, G., 2004. Stability evaluation and support recommendation for the Oslofjord tunnel. Report from expert panel established by the Norwegian Public Roads Administration. In Norwegian.

Lo, K.Y., Wai, R. S. C., Palmer, J. H. L., Quigley, R. M., 1978. Time dependent deformation of shaly rocks in southern Ontario. Canadian Geotechnical Journal 15(4): 537-547.

Lombardi, G., 1984. Underground openings in swelling rock. In: Proceedings of the 1st National Conference on Case Histories in Geotechnical Engineering, Lahore, Pakistan.

Mao, D., Nilsen, B., Dahl, F., 2011. Laboratory Testing of Swelling Gouge from Weakness Zone - Principle and Recent Update. In: Proceedings of the 45th US Rock Mechanics / Geomechanics Symposium, San Francisco, USA.

Mao, D., Nilsen, B., Lu, M., 2011. Analysis of loading effects on reinforced shotcrete ribs caused by weakness zone containing swelling clay. Tunnelling and Underground Space Technology 26: 472–480.

Moore, D. M., Reynolds Jr., R. C., 1997. X-Ray diffraction and the identification and analysis of clay minerals. 2nd Edition. Oxford University Press, New York.

Nguyen, M. D., Habib, P., Guerpillon, Y., Time-dependent Behaviour of a Pilot Tunnel Drive in Hard Marls. In: Proceedings of ISRM Symposium on Design and Performance of Underground Excavation, Cambridge, UK, pp. 453–459.

Nilsen, B., Dahlø, T. S., 1994. A study of cases of instability in hard rock tunnel. In: Proceedings of the 7th IAEG Congress, Lisbon, Vol. VI, Balkema, pp. 4233-4242.

Nilsen, B. , Palmstrøm, A., 2001. Stability and water leakage of hard rock subsea tunnels. In: Proceedings of the International Symposium on Modern Tunneling Science and Technology, Kyoto, Japan, pp. 497–502.

Nilsen, B., Broch, E., 2009. Engineering Geology of Rocks, Basic Level Compendium. Department of Geology and Mineral Resources, NTNU. In Norwegian.

Nilsen, B., Palmstrøm, A., 2009. Engineering geological key factors for planning and constructing hard rock subsea tunnels. In: Proceedings of the 5th Symposium on Strait Crossings, Trondheim, Norway, pp. 403-408.

Nilsen, B., 2010. Recent Cases of Instability caused by Faults/Weakness Zones in Norwegian Tunnels. In: Proceedings of the Symposium of Rock Machanics in Nordic Countries 2010, Norway, pp. 205-214.

Nilsen, B., 2011. Cases of instability caused by weakness zones in Norwegian tunnels. Bulletin of Engineering Geology and the Environment 70:7–13.

Norwegian Group for Rock Mechanics (NBG), 2000. Engineering Geology and Rock Engineering, Handbook No. 2. Oslo, Norway, p. 192.

Norwegian Public Roads Administration, 2004. Manual of Road Tunnels, Handbook No. 021. Oslo, Norway, pp. 31-38.

Palmstrøm, A., 1995. RMi - A rock mass characterization system for rock engineering purposes. Ph.D. Thesis. University of Oslo, Norway.

Palmstrøm, A., Broch, E., 2006. Use and misuse of rock mass classification systems with particular reference to the Q-system. Tunnelling and Underground Space Technology 21: 575–593.

Pande, G. N., Beer, G., Williams, J. R., 1990. Numerical Methods in Rock Mechanics. John Wiley and Sons, Ltd., West Sussex, England.

Reynolds, P., 2007. Finding fault at Hanekleiv. Tunnels and Tunnelling International, March 2007, pp 14 –16.

Richards, D. P., Nilsen, B., 2007. Geotechnical risk management for tunneling beneath open water. In: Proceedings of the 33rd ITA World Tunnel Congress, Prague, pp. 1585-1590.

Rocscience, 2005. Phase^2 User Manual (6.001 ed.), Rocscience Incorporation, Toronto.

Sakurai, S., 1983. Displacement measurements associated with the design of underground openings. In: Proceedings of International Symposium of Field Measurements in Geomechanics, Zurich 2: 1163-1178.

Selmer-Olsen, R., Palmstrøm, A., Strømme, B., 1989. Tunnel collapses in swelling clay zones. Tunnels & Tunnelling, November 1989, pp. 49-51.

Singh Bhawani, Jethwa, J. L., Dube, A. K., Singh, B., 1992. Correlation between observed support pressure and rock mass quality. Tunnelling and Underground Space Technology 7(1): 59-74.

Singh Bhawani, Goel, R. K., Jethwa, J. L., Dube, A. K., 1997. Support pressure assessment in arched underground openings through poor rock masses. Engineering Geology 48: 59-81.

Sheorey, P. R., 1985. Support Pressure Estimate in Failed Rock Conditions. Engineering Geology 22: 127-140.

St. John, C. M., Van Dillen, D. E., 1983. Rockbolts: A New Numerical Representation and Its Application in Tunnel Design. In: Proceedings of the 24th U.S. Symposium on Rock Mechanics, Texas, USA, pp. 13-25.

Sun, J., Zhang, D., Li, C., 1984. The Coupled-Creep Effect of Pressure Tunnels Interacted with Its Water-Osmotic Swelling Viscous Elasto-Plastic Surrounding Rocks. Journal of Tongji University. In Chinese.

Swoboda, G., 1979. Finite element analysis of the New Austrian Tunnelling Method (NATM). In: Proceedings of the 3rd International Conference on Numerical Methods in Geomechanics, Aachen, 2: 581–586.

Swoboda, G., Marence, M., Mader, I., 1994. Finite element modelling of tunnel excavation. International Journal of Engineering Modelling 6: 51–63.

Trinh, Q. N., 2006. Analysis of a cave-in problem in a hydropower tunnel in Vietnam. Ph.D. Thesis. NTNU, Trondheim, Norway.

Vermeer, P. A., de Borst, R., 1984. Non-Associated Plasticity for Soils, Concrete and Rock. Heron 29 (3): 11-15.

Volkmann, G. M., Schubert, W., 2007. Geotechnical Model for Pipe Roof Supports in Tunneling. In: Proceedings of the 33rd ITA-AITES World Tunneling Congress, Underground Space – the 4th Dimension of Metropolises, Prague, Czech, pp. 755-760.

Wittke W., Rissler, P., 1976. Dimensioning of the lining of underground openings in swelling rock applying the finite element method. Publications of the Institute for Foundation Engineering, Soil Mechanics, Rock mechanics and Water Ways Construction. RWTH (University) Aachen 2: 7-48.

Main papers

Paper I

Laboratory testing of swelling gouge from weakness zone - principle and recent update

Authors: Dawei Mao, Bjørn Nilsen and Filip Dahl

The paper was published at the 45th US Rock Mechanics/Geomechanics Symposium held in San Francisco, CA, June 26–29, 2011.

ARMA 11-152

Laboratory Testing of Swelling Gouge from Weakness Zone - Principle and Recent Update

Dawei Mao, Bjørn Nilsen
Norwegian University of Science and Technology, Trondheim, Norway

Filip Dahl
SINTEF Rock Engineering, Trondheim, Norway

This paper was prepared for presentation at the 45th US Rock Mechanics / Geomechanics Symposium held in San Francisco, CA, June 26–29, 2011.

ABSTRACT: Major weakness zones or faults containing heavily crushed and altered rock mixed with gouge material, particularly when the gouge contains swelling clay minerals, represent some of the most difficult conditions in hard rock tunnels. The gouge is normally highly disturbed when a mixture of clay and rock fragments of various sizes is collected, and it is therefore very difficult to obtain usable undisturbed samples of gouge material from a weakness zone for laboratory testing. In Norway, a laboratory test method based on measuring the swelling pressure of remoulded specimens has been extensively used since it was introduced several decades ago at NTNU. The details of the test apparatus and procedure, recent update, test results and significance for tunnel stability are discussed in this paper. Another test used at NTNU to quantify the relative swelling potential, the free swelling test, is also briefly discussed.

1. INTRODUCTION

Problems in tunnels and underground excavations caused by swelling have been widely recognized, as well as the need for a test to determine the swelling behavior. The ISRM Commission on Swelling Rock has recommended a series of test methods to determine the maximum axial swelling stress, the axial and radial free swelling strain, and the axial swelling stress as a function of axial swelling strain [1, 2]. Recent laboratory studies on swelling have mainly been focused on the use of triaxial tests [3, 4, 5]. These methods are however mainly for swelling rocks (argillaceous and rocks containing anhydrite). The most difficult conditions in Norwegian hard rock tunnels are related to major weakness zones or faults with heavily crushed and alterted rock mixed with gouge material containing swelling clay minerals. Some cases of tunnel instability have been encountered in hydropower tunnels in such zones [6, 7]. In several recent cases, failures occurred, even though precaution measures had been taken [8, 9]. It is very difficult to obtain usable undisturbed samples of gouge material from a weakness zone for laboratory testing, because the gouge is normally highly disturbed when a mixture of clay and rock fragments of various sizes is collected. The ISRM suggested that the remoulded specimens may be used when the sample is too weak or too broken to allow preparation of undisturbed specimens, as is usually the case with joint-filling materials [10]. In Norway, a laboratory test method based on measuring the swelling pressure of remoulded specimens [11] has been extensively used since it was introduced several decades ago at NTNU. This method and recent update of the apparatus will be discussed in detail in this paper. In addition, the free swelling test will be briefly discussed.

2. NTNU SWELLING PRESSURE TEST

2.1. Apparatus

The test apparatus used to measure swelling pressure has been updated several times, but the principle and main procedures have remained the same. The traditional apparatus is shown schematically in Figure 1.

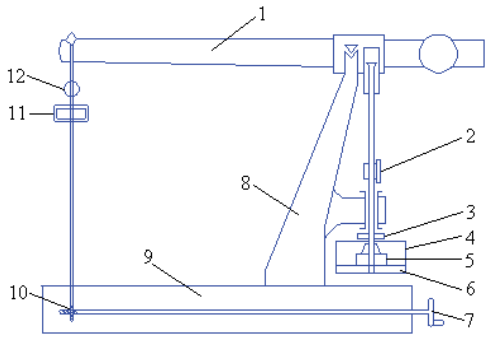

Fig. 1. Sketch of traditional NTNU apparatus for measuring swelling pressure (based on [11]).

The apparatus consists of the following components as shown in Figure 1:

1) Balance lever, with the ratio of 1:10.
2) Dial gauge with a sensitivity of 0.001 mm to measure the height (volume) of the specimen.
3) Adjustment screw.
4) Container.
5) Cylindrical test cell.
6) Steel base plate of the container.
7) Wheel.
8) Frame.
9) Base.
10) Worm gear.
11) Pressure ring .
12) Dial gauge with a sensitivity equivalent to 0.05tons/m^2 to measure the pressure.

2.2. Test procedure

The standard procedures for measuring swelling pressure are as follows [12]:

1. The gouge material is dispersed in distilled water.
2. The clay fraction with particle size less than 20 μm is separated from the rest of the material based on the rate of sedimentation (e.g., particles of 20 μm settle 25 cm in 11 minutes and 55 seconds in distilled water (20 ^oC)).
3. The separated clay fraction is dried in a laboratory drier at 105 ^oC / 110 ^oC.
4. The dry clay-material is exposed to the relative humidity of the laboratory air (40%) and laboratory temperature before it is milled (for approximately 15 min.) into powder by use of motorized ceramic laboratory mortar, and 20 g of the prepared powder is packed in a 20 cm^2 cylindrical test cell.
5. The cylindrical test cell is installed into the test apparatus;
6. The balance lever is leveled via the adjustment screw;
7. The dial gauge for measuring the height (volume) of the specimen is installed;
8. The pressure ring and the dial gauge for measuring pressure are installed;
9. The specimen is compressed at 2 MPa for 24 hours by applying steel disc weights to the balance lever;
10. The specimen is unloaded for at least 2 hours until no height (volume) change is registered by the dial gauge for the height (volume) of the specimen;
11. The container is filled with distilled water to a depth of approximately 10 mm;
12. The specimen volume is kept constant and the apparatus deformation is compensated with continuous adjustment of the worm gear connected to the pressure ring and balance lever as the swelling pressure is mobilized;
13. The mobilized swelling pressure is recorded continuously for 24 hours or until stabilised;

Generally, the NTNU swelling pressure test can be divided into specimen preparation, compression, unloading and swelling as illustrated in the principle sketch in Figure 2.

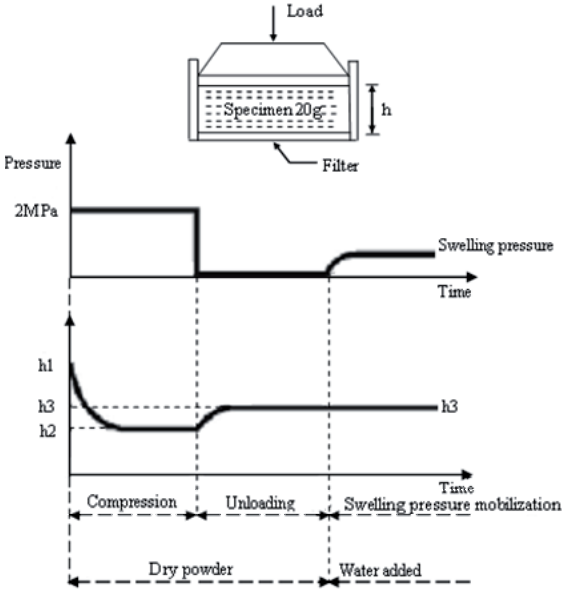

Fig. 2. Sketch of NTNU swelling pressure test principle (based on [13]).

2.3. Recent update of test apparatus

One basic requirement for the NTNU swelling pressure test is that the specimen volume has to be kept constant during the swelling process. If expansion of the specimen is allowed during the swelling process, the

mobilized swelling pressure may significantly decrease. This is illustrated in Figure 3, which shows the swelling pressure as a function of expansion for some swelling clays in Norway.

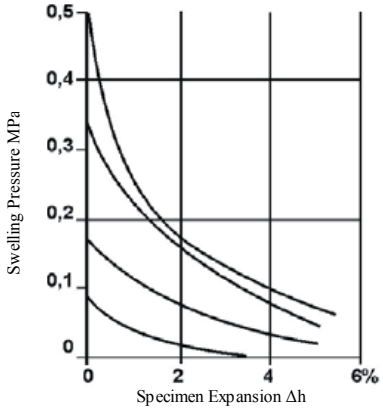

Fig. 3. Swelling pressure versus specimen expansion [14].

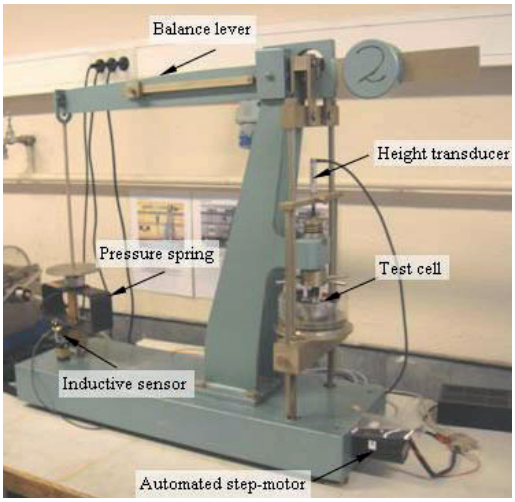

Fig. 4. Updated apparatus for testing swelling pressure.

As described previously in the traditional test procedure, the specimen volume is kept constant by continuous adjustment of the worm gear (connected to the pressure ring and balance lever) to compensate for the apparatus deformation when the swelling pressure is mobilized. In the recent update of the test apparatus, a height transducer and inductive sensor replace the dial gauges for measuring specimen height and pressure, and an automated step-motor replaces the manually operated wheel for worm gear adjustment. This update, together with the in-house developed software, makes it possible to instantaneously compensate for the deformation of the apparatus to keep the specimen volume constant, and to get an automated continuous logging of the swelling pressure. Figure 4 shows the updated apparatus at the NTNU/SINTEF laboratory.

3. NTNU FREE SWELLING TEST

The clay fraction with particle size less than 20 μm is also used in the free swelling test. 10 ml of loosely packed dry clay powder is drizzled into a 50 ml measuring cylinder filled with distilled water. The volume occupied by the clay powder after sedimentation is recorded, and the free swelling is calculated as the percentage of the original powder volume.

Free swelling index number (Fs):

$$Fs = \frac{V_1}{V_0}$$

V_1 = Volume of clay after sedimentation

V_0 = Original volume of dry clay powder, 10 ml

4. TEST RESULT

The NTNU swelling pressure test and free swelling test have been extensively used in Norway for swelling gouge materials. The principle of the NTNU swelling pressure test is almost equivalent to the method for determining maximum axial swelling stress for swelling rocks as suggested by ISRM. Instead of using the sample representative of the in situ material, the NTNU method however is based on remoulded specimens consisting of dry clay powder. The reason for this is that it is very difficult to prepare samples representative of the in situ gouge material. The use of remoulded specimens represents a uniform, reproducible way for laboratory testing of the swelling gouge.

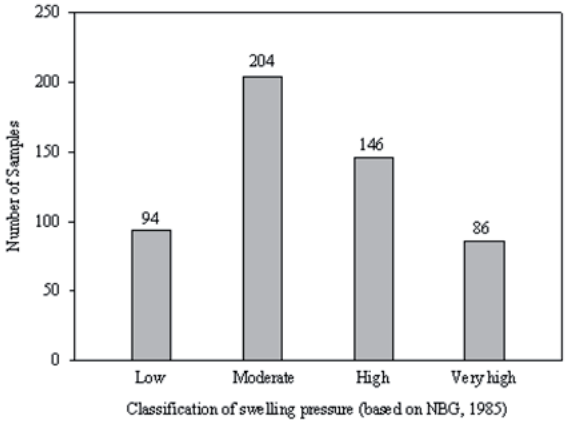

Fig. 5. Numbers of tested samples in each category of swelling pressure.

The Norwegian National Group of ISRM, NBG, defines swelling pressure below 0.1 MPa as low, 0.1 - 0.3 MPa as moderate, 0.3 - 0.75 MPa as high and above 0.75 MPa as very high based on this type of test [15, 16]. More than 500 gouge samples have so far been tested at the NTNU/SINTEF laboratory and the results are registered in a database. The maximum value of swelling pressure that has been measured is more than 4 MPa. Figure 5 shows the number of tested samples in each category of swelling pressure based on the definition by NBG. Figure 6 shows the accumulative curve of the laboratory test results of swelling pressure. The categories of low, moderate, high and very high in terms of swelling pressure account for respectively 17.7%, 38.5%, 27.2% and 16.6% of all the tested samples.

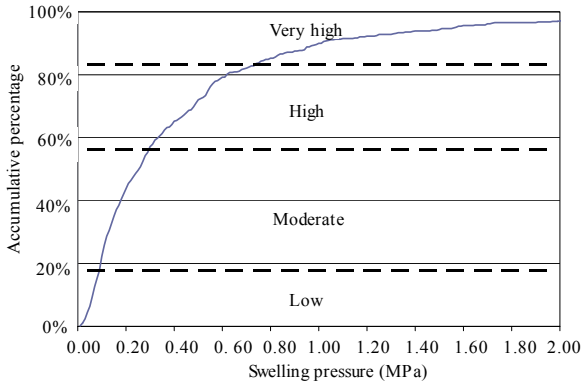

Fig. 6. Accumulative curve of laboratory test results for swelling pressure.

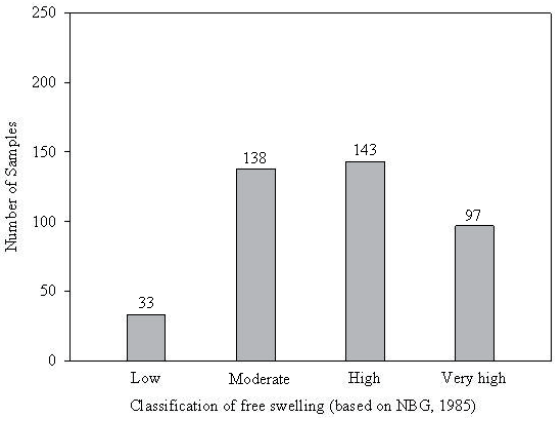

Fig. 7. Numbers of tested samples in each category of free swelling.

Compared with the swelling pressure test, the free swelling test is easier to carry out. It gives another index for relative swelling potential. NBG defines free swelling below 100% as low, 100% - 140% as moderate, 140% - 200% as high and above 200% as very high. More than 400 gouge samples have so far been tested at the NTNU/SINTEF laboratory based on this test. The maximum recorded value is higher than 850% while the minimum value is as low as 60%. Figure 7 shows the number of the tested samples in each category of free swelling based on the definition by NBG. Figure 8 shows the accumulative curve of the laboratory test results. The categories of low, moderate, high and very high in terms of free swelling account for respectively 8.0%, 33.6%, 34.8% and 23.6% of all the tested samples.

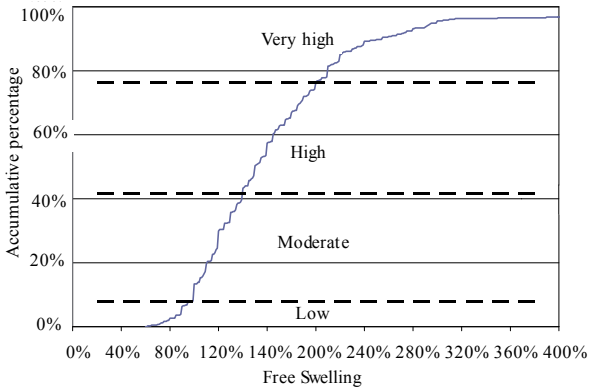

Fig. 8. Accumulative curve of laboratory test results of free swelling.

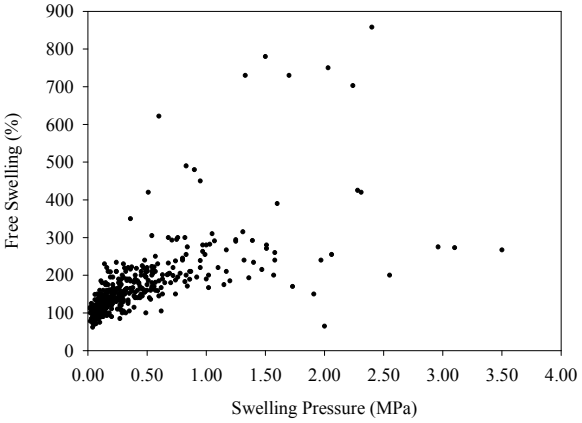

Fig. 9. Laboratory test results – Free Swelling vs. Swelling Pressure.

Figure 9 shows the laboratory test results of swelling pressure and corresponding free swelling of the tested samples. It seems to be a positive correlation between the test results of these two test methods for swelling pressure values below 1MPa. However, there is no obvious correlation when considering the whole dataset.

Since the swelling pressure and free swelling tests are based on the separated clay fraction with particle size less than 20 μm, the amount of the clay fraction in the gouge sample also needs to be considered. Figure 10 shows the amount of the clay fraction as the percentage

of the weight of the gouge material for all tested samples. There are approximately 40% and 70% of gouge samples with the clay fraction (< 20 μm) respectively less than 10% and 20%. More than 95% of the tested gouge samples have a clay fraction (< 20 μm) less than 50%.

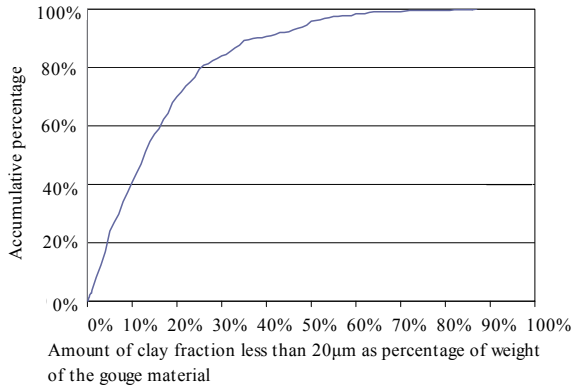

Fig. 10. Accumulative curve of amount of clay fraction (< 20 μm) as the percentage of the weight of the gouge material.

It should be emphasized that both the swelling pressure and free swelling test methods are primarily used as index tests. The swelling pressure measured in the laboratory is not representative of the in situ swelling pressure on rock supports. The main reasons for that are:

- The laboratory test results are based on a fixed clay amount of 20g.
- The in situ structure and compaction are damaged as a result of the sampling and preparation.
- The clay fraction used in the tests represents the most active part of the gouge material, and the dry condition represents the highest swelling potential.
- The in situ swelling pressure on rock supports to a great extent also depends on the time between blasting and rock support installation and the support deformation.

Previous research carried out at NTNU suggests that the swelling pressure in situ is often lower than the laboratory measured value, and in some cases only 50% [17].

5. RELEVANCY OF TEST RESULTS FOR TUNNEL STABILITY

The laboratory results of swelling pressure and free swelling tests indicate the relative swelling potential, which is valuable for evaluation of potential stability problems and security measures. This is illustrated by the following recent cases of instability:

When swelling pressure and free swelling have been measured to be low in the laboratory tests, stability problems due to swelling very seldom occurred. Stability problems and security measures should be emphasized when high values of swelling pressure and free swelling are measured, especially when the clay content (< 20 μm) is also high. The collapse in the Oslofjord tunnel in December 2003 (3.5 years after project completion) illustrates this. Total volume of the rock fall from the steep clay zone was estimated to be around 40 m^3, of which 4 m^3 went through the lining [9]. The gouge samples were laboratory tested and found to be highly active, with swelling pressure up to 0.55 MPa and free swelling up to 167%. The fraction with particle size less than 20μm constituted 34% of the gouge material.

Serious problems may occur even if the clay is classified as moderately active. However, it should be noted that swelling often is not the only cause, and sometimes even not the main cause of instability. On December 25th 2006 (10 years after project completion), rock mass estimated to 250 m^3 collapsed along a section of about 25 m in the Hanekleiv tunnel [9]. Swelling pressure of 0.16 MPa was measured. The swelling process and reduced rock strength due to weathering were concluded to be the main causes of the collapse. In the Atlanterhavs tunnel, cave-in progressed several meters above the roof during tunnel excavation in February 2008 [8, 9]. The measured swelling pressure was 0.1 MPa and the free swelling 135%. The clay content (< 20 μm) was as low as 5%. It was concluded that a combination of large water inflow at high pressure and very poor rock mass were the main causes of instability. These incidents show that moderately active clay combined with other unfavourable conditions always should be carefully evaluated.

ACKNOWLEDGEMENTS

The Norwegian Public Roads Administration is acknowledged for financing the recent update of the test apparatus. Mr. Torkjell Breivik from NTNU and Mr. Simon Alexander Hagen from SINTEF are highly acknowledged for their good suggestions on the paper.

REFERENCES

1. ISRM Commission on Swelling Rocks. 1989. Suggested methods for laboratory testing of argillaceous swelling rock. *International Journal of Rock Mechanics and Mining Science & Geomechanics Abstracts. Res*. 26 (5): 415-426.
2. ISRM Commission on Swelling Rocks. 1999. Suggested methods for laboratory testing of swelling

rocks. *International Journal of Rock Mechanics and Mining Science & Geomechanics Abstracts. Res.* 36 (3): 291-306.

3. Aristorenas, G. V. 1992. *Time-dependent behaviour of tunnels excavated in shale.* Ph.D. Thesis. Massachusettes Institute of Technology, Boston, USA.
4. Bellwald, P. 1990. *A contribution to the design of tunnels in argillaceous rock.* Ph.D. Thesis. Massachusetts Institute of Technology, Boston, USA.
5. Barla, M. 2008. Numerical simulation of the swelling behaviour around tunnels based on special triaxial tests. *Tunnelling and Underground Space Technology. Res.* 23 (5): 508-521.
6. Brekke, T. L. and R. Selmer-Olsen. 1965. Stability problems in underground constructions caused by montmorillonite-carrying joints and faults. *Engineering Geology.* 1 (1): 3-19.
7. Selmer-Olsen, R., A. Palmstrøm, and B. Strømme. 1989. Tunnel collapses in swelling clay zones. *Tunnels & Tunnelling*. 21: 49-51.
8. Nilsen, B. and A. Palmstrøm. 2009. Engineering geological key factors for planning and constructing hard rock subsea tunnels. *In Proceedings of the Fifth Symposium on Strait Crossings, Trondheim, Norway,* 403-408.
9. Nilsen, B. 2010. Recent cases of instability caused by faults/weakness zones in Norwegian tunnels. *In Proceedings of Rock Mechanics in the Nordic Countries, Kongsberg, Norway,* 205-214.
10. ISRM Commission on Standardization of Laboratory and Field Tests. 1979. Suggested methods for determining water content, porosity, density, absorption and related properties and swelling and slake-durability index properties. *International Journal of Rock Mechanics and Mining Sciences*. *Res.*16 (2): 143-156.
11. Brekke, T. L. 1965. On the measurement of the relative potential swellability of hydrothermal montmorillonite clay from joints and faults in Precambrian and Paleozoic rocks in Norway. *International Journal of Rock Mechanics and Mining Science. Res.* 2: 155-165.
12. SINTEF, Rock Engineering Group. 2005. *Test procedure for swelling pressure measurement.* Internal Report. In Norwegian.
13. Nilsen, B. and E. Broch. 2009. *Engineering Geology of Rocks, Basic Level Compendium*. Department of Geology and Mineral Resources, NTNU, 76-77. In Norwegian.
14. Nilsen, B. and A. Thidemann. 1993. *Rock Engineering, Hydropower Development Vol. 9.* Norwegian Institute of Technology (NTH), 26-27.
15. Norwegian Group for Rock Mechanics (NBG). 1985. *Handbook in Engineering Geology – Rock.* Trondheim, Norway, 140. In Norwegian.
16. Norwegian Group for Rock Mechanics (NBG). 2000. *Engineering Geology and Rock Engineering, Handbook No. 2.* Oslo, Norway, 192.
17. Tyssekvam, I. O. 1996. *Sampling and characterization of swelling material in weakness zones.* Diploma Thesis. NTNU, Trondheim, Norway. In Norwegian.

Paper II

Numerical analysis of effects of weakness zones on tunnel stability – 2D versus 3D

Authors: Dawei Mao, Bjørn Nilsen

The paper was submitted to the 13th World Conference of the Associated Research Centers for the Urban Underground Space, November 2011.

Numerical Analysis of Effects of Weakness Zones on Tunnel Stability – 2D versus 3D

Dawei Mao, Bjørn Nilsen

Norwegian University of Science and Technology, Trondheim, Norway

ABSTRACT

For tunneling through major weakness zones or faults where the geometry is complex, three-dimensional programs have been widely applied. Two-dimensional programs are fast and very convenient to use, but simulation results may considerably deviate from reality if a two-dimensional program is improperly used. This is discussed in the paper based on two representative numerical programs in rock engineering, Phase^2 and FLAC^{3D}. It is concluded that, for Phase^2 to be realistically used for analyzing the effects of a weakness zone perpendicular to the tunnel alignment, the thickness of the zone has to be much wider than the tunnel span. This is quite unusual for "normal" tunnel excavation spans. In addition, it is difficult to define the deformation before the installation of rock support when using Phase^2 for tunneling through weakness zones.

Keywords: Weakness zone; Tunnel stability; Phase^2; FLAC^{3D}; Numerical analysis

Address: Department of Geology and Mineral Resources Engineering, Norwegian University of Science and Technology, Trondheim 7491

Corresponding author: Dawei Mao

Tel.: +47 46398642

Fax: +47 73590898

E-mail address: dawei.mao@ntnu.no

1. Introduction

Numerical simulation is a powerful tool in rock engineering planning and design, particularly when difficulties and uncertainties are expected in the underground excavation of civil and mining engineering. In Norway, the tunnels are mainly located in hard, Precambrian rocks, and major weakness zones or faults represent one of the most difficult condtions (Blindheim et al., 2005; Nilsen and Palmstrøm, 2009; Nilsen, 2011). A three-dimensional program (e.g. FLAC3D, Itasca, 2005) is normally perferred for such complicated engineering mechancis computation. Two-dimensional programs (e.g. Phase^2, Rocscience Inc., 2005) have also been used sometimes (Grimstad et al., 2008, NGI; Trinh et al., 2010) for its simplicity. FLAC^{3D} (Itasca, 2005) is a three-dimensional explicit finite-difference program for engineering mechanics computation. The basis for FLAC^{3D} is the numerical formulation used by the two-dimensional program, FLAC (Itasca, 2005). FLAC^{3D} extends the analysis capability of FLAC into three dimensions. Phase^2 is a two-dimensional finite element program, and it is widely used for plane strain analysis and axis-symetric analysis.

Geometry effects of tunnel and weakness zone /fault in most cases can not be considered in a two-dimensional model. The initial state of stress at the weakness zone is normally quite anisotropic, and tunneling in weakness zones or faults should not be simplified as an axis-symmetric problem (Panet M, 1993). It can be simplified as the plane strain problem when the orientation of the weakness zone is parallel to the tunnel alignment. The approximation in other cases by application of plane strain analysis may be considerably deviated from reality. The extent of deviation/error is studied in this paper by comparison of the numerical simulation with Phase^2 and FLAC^{3D}.

2. Model Description

Based on experience from several projects, a major weakness zone in Norwegian tunnels has a typical thickness of 10 – 15m and is in most cases steep. It often represents high risk of instability. In the numerical simulation in this paper, the weakness zone is taken as vertical and perpendicular to the tunnel alignment. The thickness of the weakness zone up

to 30m has been considered. The weakness zone and side rock are simulated based on the Mohr-Coulomb model with elasto-perfectly plastic stress-strain law. Physical and mechanical properties of the weakness zone and the side rock used in the modeling are presented in Table 1. The properties of the weakness zone are taken as the same as for the weakness zone described in Grimstad (2008). The properties of the side rock are typical for granitic gneiss, one of the predominant rock types in Norway. The initial vertical stress is assumed to be caused by gravity, 2 MPa at the tunnel location, and considered as one of the principal stresses. Different sets of ratios of horizontal stresses to vertical stress are used in numerical analysis.

The analysis is based mainly on traditional Norwegian road tunnel design, an arched tunnel with excavation span of 12m and the theoretical cross section of excavation of about 65 m^2 (Norwegian Public Roads Administration, 2004). The tunnel geometry is symmetrical and half of the tunnel is considered for the FLAC^{3D} model as shown to the left of Figure 1. Except the boundary of the model representing the symmetry plane of the tunnel, the rest of boundaries are far away from the interested area. The model size is $49m \times 93m \times 150m$ ($X \times Y \times Z$), in which the longest axis represents the tunnel alignment. Though very fine mesh can hardly be achieved for a three-dimensional model in practice, the mesh near the middle cross section of the weakness zone is made denser for higher simulation accuracy. Each boundary is fixed in the direction perpendicular to it, except the top boundary where the pressure caused by the gravity of rock overburden is applied. The two-dimensional model based on Phase^2 is shown to the right of Figure 1. Half of the tunnel is generated and the boundary conditions are the same as used in the three-dimensional model. The element type is the three nodded triangle and the mesh is made very fine to minimize the mesh influence.

3. Simulation Results

3.1 Simulation results of FLAC^{3D}

Long-round drill and blast method is assumed for tunnel excavation and the tunnel portion in the model is deleted/excavated in one stage. Figure 2 shows the yielded zone in

the middle cross-section of the weakness zone of alternative widths when the maximum horizontal stress is perpendicular to the tunnel alignment (k_H = 1.5, k_h = 0.8). The depth of yielded area above the crown ranges from 4.8 m to 8.7 m, while the depth of the yielded area below the invert ranges from 7.0 m to 9.4 m. Though the estimated depth depends also on the grid dimension, this illustrates that the yielded zone is highly influenced by the width of the weakness zone. For quantitative comparison of simulation results, the displacements are focused in the further analysis.

Figures 3-5 shows the vertical displacement at the crown and at the middle of invert in the middle cross-section of weakness zone of alternative widths when the maximum horizontal stress is perpendicular to the tunnel alignment. Scenarios of alternative ratios of the horizontal stress to vertical stress (k_H = 1.5, k_h = 0.6, 0.8, 1, 1.2; k_H = 1, 1.2, 1.7, k_h = 0.8) and different reduced strength of weakness zones (Cohesion: 0.2 MPa, Friction angle = 20^o; Cohesion: 0.2 MPa, Friction angle = 25^o) have been simulated.

All simulated results show that the influence of the width of weakness zone is substantial when the width of weakness zone is in the range of 10 m - 30 m. The simulated displacements at the crown for a 10 m wide weakness zone are less than 40% of the simulated displacement for the infinite weakness zone, in some case, as low as 23%. The simulated displacements at the crown for a 20 m wide weakness zone are mainly around half of the simulated displacement for the infinite weakness zone. When the width of weakness zone is 30m, the simulated displacements at the crown are at least 30% lower than for the infinite weakness zone. Though the displacements at the invert for weakness zones of different widths are closer to the infinite weakness zone compared to displacement at the crown, the displacements are still quite different between the 10 m – 20 m wide weakness zones and the infinite weakness zone. The in-situ stress in the tunnel axis direction has much less impact on simulation results. If the strength of the weakness zone is reduced, the difference of the displacements between the weakness zones with limited width and the infinite weakness zone further increases.

For maximum horizontal stress parallel with the tunnel alignment, simulated results of the vertical displacement at the crown and at the middle of invert in the middle cross-section of weakness zone of alternative widths are as shown in Figures 6-8. The displacements are generally smaller than those simulated for the maximum horizontal stress perpendicular to the tunnel alignment. The displacements at the crown for a 10 m wide weakness zone are less than 45% of the displacement for the infinite weakness zone. The displacements at the crown for a 20 m wide weakness zone are often close to half of the simulated displacement for the infinite weakness zone. When the width of weakness zone is 30 m, the displacements at the crown in many cases are more than 30% lower than the infinite weakness zone. At the invert, the displacements for the 10 m – 30 m wide weakness zone are much closer to the simulated displacements for the infinite weakness zone compared with the early cases where the maximum horizontal stress is perpendicular to the tunnel alignment.

3.2 Simulation results of Phase^2

When the width of weakness zone is infinite, it can be simplified as a plane strain problem and the two-dimensional program Phase^2 can be used. Figure 9 shows the yielded zone above the crown and below the invert simulated by Phase^2 (maximum horizontal stress perpendicular to the tunnel alignment, k_H=1.5, k_h=0.8). The yielded depth is 8.4 m above the crown and 10.1 m below the invert, which is slightly different from the simulated results with FLAC^{3D} for the infinite weakness zone. Table 2 gives the values of simulated displacements with Phase^2 for assumed different horizontal stresses, strength of weakness zone and tunnel geometry. This is compared with the displacements at the crown and invert for the infinite weakness zone and 15 m wide weakness zone simulated by FLAC^{3D} as shown in Figures 10 and 11. The simulated vertical displacements at the crown for the infinite weakness zone based on both numerical programs are quite similar. The maximum difference is no more than 10% of the total. The displacements at the invert for infinite weakness zone from the FLAC^{3D} are however always higher, sometimes almost 1/3 higher than the results from the Phase^2. Such differences of simulation results may be mainly due to the different solution methods (and thus the different stress paths) used in these two programs. For plasticity analysis,

FLAC^{3D} checks the element state (elastic or plastic) and stresses are corrected by using the plastic flow rule in each cycling step, while in Phase^2, an elastic solution is first obtained and then the stress state in each element is checked against the yield criteria. Cai (2011) found that the simulated results may be quite different when different solution methods are used, particularly when the tensile strength is low as the case for weakness zones. The grid geometry may also induce uncertainties of simulation results, since it can hardly be finely refined for a three-dimensional model.

If the simulation results based on Phase^2 are wrongly applied for the narrow weakness zones, large errors may be the result due to the effects of the width. For the typical 15 m wide weakness zones range, the displacement at the crown can be much overestimated (2 - 3 times) compared with the one simulated with FLAC^{3D} (Figures 10 and 11). In some cases, the displacements at the invert for 15 m wide weakness zone simulated with FLAC^{3D} are however also comparable with the results based on Phase^2. This is mainly due to the different solution methods of these two numerical programs, and illustrates the unreliability of using Phase^2 for narrow weakness zones.

In the following, loading effects on rock support based on these two programs are compared for a 15 m wide weakness zone as an illustration.

3.3. Loading Effects on Rock Support

As early as 1980's, Sakurai (1983) suggested that the stability of tunnels can be assessed on the basis of the strain in the rock mass surrounding the tunnel. Hence the scenario where the maximum displacements are obtained in early simulations is selected for the analysis of loading effects on rock support (Maximum horizontal stress perpendicular to the tunnel alignment: k_H =1.5, k_h =0.8, Reduced strength of weakness zone: cohesion 0.2 MPa, friction angle 20^o). A typical width of 15 m is taken for the weakness zone and the blasting round in the weakness zone is taken as 3 m. The middle section of the 15 m weakness zone has been assumed to be representative of the middle section of one blasting round. 20 cm rapid hardening sprayed concrete (E= 20 GPa, Poisson's ratio 0.2)

is applied after each blasting round for the whole blasted section. Linearly elastic behavior is assumed for the sprayed concrete in both numerical programs.

The tunnel portion in the model of FLAC^{3D} is deleted/excavated according to the excavation sequence, and the rock support of sprayed concrete is simulated as 'shell structural element' (Itasca, 2005) installed immediately after each blasting round. The final displacement at the crown for this 15 m wide weakness zone is -2.04 cm if no rock support is applied (Figure 5 – A8). In the middle of the blasting round, the vertical displacement at the crown is -0.81 cm before the sprayed concrete is installed, which accounts for 39.7% of the final displacement without rock support. The corresponding simulated average axial stress in the sprayed concrete is 8.6 MPa. At the excavation face of the blasting round, the displacement at the crown is only -0.44 cm before the sprayed concrete is installed, which accounts 21.6% of the final displacement without rock support. The simulated axial stress is 15.0 MPa.

For rock support estimation in Phase^2, several approaches, e.g. material softening, internal pressure reduction, load splitting (Rocscience Inc., 2005) can be used. To define the amount of deformation before the installation of sprayed concrete is difficult here. There are no observed field values and developed relationships of defining the longitudinal displacement profile (e.g. Panet,1993; Carranza-Torres and Fairhurst, 2000; Vlachopoulos1 and Diederichs, 2009) are based on the assumption of uniform ground and not appropriate for this case. To make the simulation results comparable, the same percentages of the displacements before installation of sprayed concrete of the final displacements without rock support as obtained by FLAC^{3D} are assumed.

The vertical displacement at the crown without any rock support simulated with Phase^2 is -5.92 cm. Thus, the displacements at the crown before installation of rock support as described above are calculated as -2.35 cm (39.7%) and -1.28 cm (21.6%). This can be achieved in the simulation based on the material softening method (Swoboda, 1979; Swoboda et al., 1994). The elasticity modulus of the material inside the excavation is progressively reduced over a number of stages until the material is removed (Rocscience

Inc., 2005). Figure 12 shows the relationship of the modulus reduction and the tunnel displacement at the crown. For the required displacements of -1.28 cm and -2.35 cm at the crown before installation of rock support, all the softening stages should be followed until the elastic modulus reduces to 218 MPa and 82 MPa respectively. The simulated axial stress in the sprayed concrete at the crown is 10.3 MPa (with displacement of -2.35 cm occurred before installation of sprayed concrete) and 16.4 MPa (with displacement of -1.28 cm occurred before installation of sprayed concrete). For different values of displacement, the simulated axial stresses in the sprayed concrete based on these two numerical programs are however quite similar as shown in Figure 13.

Sometimes, active swelling clay occurs in the gouge of major weakness zones or faults. Effects of swelling could be considered as a swelling pressure on rock support and from an engineering perspective simplified as uniformly distributed load (Mao et al; 2011), and this can be realized with both FLAC^{3D} and Phase^{2}.

4. Concluding Remarks

Complicated geometry for tunneling in weakness zones/faults can be considered with the three-dimensional program. In this paper, weakness zones with various thicknesses have been analyzed by FLAC^{3D}. For Phase^{2} to be realistically used for analyzing the effects of a weakness zone which is perpendicular to the tunnel alignment, the thickness of the zone has to be much wider than the tunnel span. This is quite unusual for road tunnels, which have a typical excavation span of around 12 m. For a major weakness zone with typical thickness, 2D modelling may result in a large deviation from the 3D results. The lower strength of the weakness zone, the larger the deviation will be. For example, for a 15 m wide weakness zone the simulated displacements at the crown with Phase^{2} are often around two times those obtained with FLAC^{3D}. When the strength of the weakness zone is reduced, the difference of simulated displacements can be 3:1.

When using Phase^{2} for tunneling through weakness zones, it is also difficult to define the amount of deformation before the installation of rock support. Sometimes, similar loading effects on rock support as for FLAC^{3D} can be estimated based on unrealistic

simulation results from Phase^2. This could be one cause for some of the misuse of Phase^2 for inappropriate cases.

Empirical diagrams are not realistic to develop for tunnelling in a weakness zone due to several uncertain factors, such as the geometry of weakness zone and tunnel, the anisotropic stress state, the properties of weakness zone, and the influence of the side rock.

Reference

Jounal article

Blindheim, O. L., Grøv, E., Nilsen, B., 2005. Nordic sub sea tunnel projects. Tunnelling and Underground Space Technology 20 (6): 570-580.

Cai, M., 2008. Influence of stress path on tunnel excavation response – Numerical tool selection and modeling strategy. Tunnelling and Underground Space Technology 23: 618-628.

Nilsen, B., 2011. Cases of instability caused by weakness zones in Norwegian tunnels. Bulletin of Engineering Geology and the Environment 70: 7–13.

Swoboda, G., Marence, M., Mader, I., 1994. Finite element modelling of tunnel excavation. International Journal of Engineering Modelling 6: 51–63.

Vlachopoulos1, N. and Diederichs, M. S., 2009. Improved Longitudinal Displacement Profiles for Convergence Confinement Analysis of Deep Tunnels, Rock Mechanics and Rock Engineering 42: 131–146.

Conference paper

Grimstad, E., Tunbridge, L., Bhasin, R., Aarset, A., 2008. Measurements of forces in reinforced ribs of sprayed concrete. 5th International Symposium on Sprayed Concrete. Lillehammer, Norway.

Nilsen, B., Palmstrøm, A., 2009. Engineering geological key factors for planning and constructing hard rock subsea tunnels. In: Proceedings of the Fifth Symposium on Strait Crossings, Trondehim, Norway, pp 403-408.

Sakurai, S., 1983. Displacement measurements associated with the design of underground openings. Proc. Int. Symp. Field Measurements in Geomechanics, Zurich 2: 1163-1178.

Swoboda, G., 1979. Finite element analysis of the New Austrian Tunnelling Method (NATM). In: Proceedings of the 3rd International Conference on Numerical Methods in Geomechanics, Aachen, 2: 581–586.

Book

Itasca, 2005. Fast Language Analysis of continua in 3 dimensions, version 3.1, user's manual. In: Itasca, I. (Ed.), Consulting Group, Minneapolis, Minnesota, USA.

Rocscience, 2005. Phase^2 User Manual (6.001 ed.), Rocscience Inc., Toronto.

Book Chapter

Norwegian Public Roads Administration, 2004. Manual of Road Tunnels, Handbook No. 021. Oslo, Norway, pp 31-38.

Panet, M., 1993. Understanding deformations in tunnels. Comprehensive Rock Engineering, Pergamon, London, 1: 663–690.

Table 1 Properties of weakness zone and side rock

Properties	Weakness zone	Side rock
Density (kg/m^3)	2700	2700
Modulus of elasticity (E) (GPa)	2.68	43.5
Poisson's ratio (υ)	0.3	0.16
Bulk modulus[a] (*K*) (GPa)	2.23	21.3
Shear modulus[b] (G) (GPa)	1.03	18.8
Cohesion (MPa)	0.3	1.0
Friction	25^o	35^o
Dilation	-	10^o

[a] *K=E/3(1-2 υ)*
[b] *G=E/2(1+ υ)*

Table 2 Simulated displacements with Phase^2 for infinite weakness zone

No.	Displacement (cm)				Notes
	A*		B*		
	At crown	At invert	At crown	At invert	
1	-2.33	2.11	-1.35	1.10	k_H=1.5, k_h=0.8
2	-2.33	2.11	-1.39	1.15	k_H=1.5, k_h=0.6
3	-2.33	2.11	-1.48	1.25	k_H=1.5, k_h=1.0
4	-2.33	2.12	-1.76	1.56	k_H=1.5, k_h=1.2
5	-1.42	1.16	-1.27	0.96	k_H=1, k_h=0.8
6	-1.72	1.49	-1.28	1.00	k_H=1.2, k_h=0.8
7	-2.82	2.64	-1.42	1.19	k_H=1.7, k_h=0.8
8	-5.92	4.45	-3.28	1.97	Cohesion 0.2 MPa, Friction angle 20^o (k_H=1.5, k_h=0.8)
9	-3.71	3.00	-1.96	1.43	Cohesion 0.2 MPa, Friction angle 25^o (k_H=1.5, k_h=0.8)

[*] *A: the maximum horizontal stress perpendicular to the tunnel alignment*
[*] *B: the maximum horizontal stress parallel to the tunnel alignment*

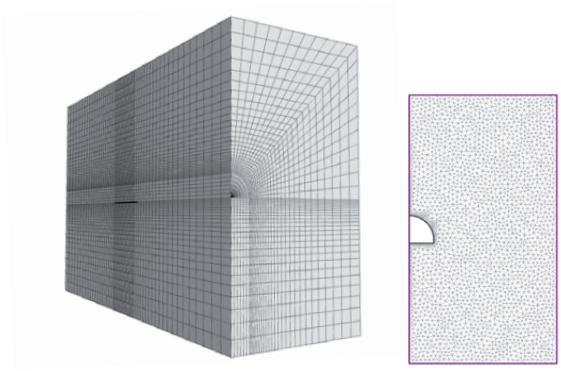

Figure 1: Generated model for arched tunnel (left: FLAC^{3D} model, Right: Phase^{2} model)

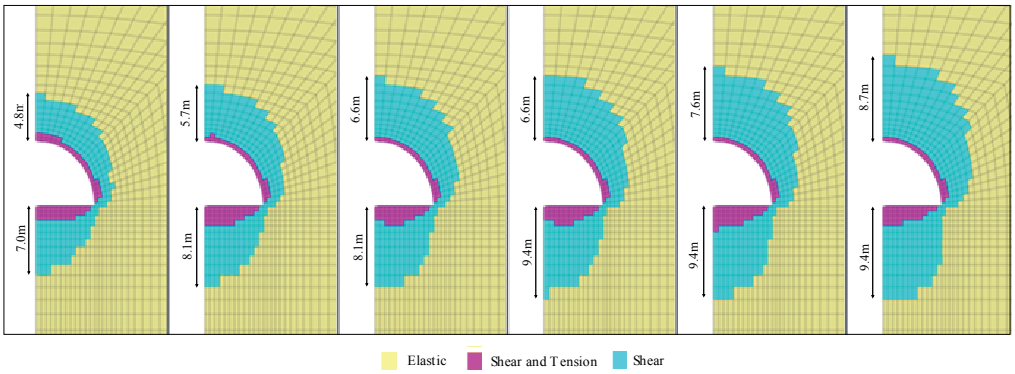

Figure 2: Yielded zone based on FLAC3D for the middle cross-section of weakness zone of alternative widths, from left: 10m, 15m, 20m, 25m, 30m, infinite (maximum horizontal stress perpendicular to the tunnel alignment, k_H=1.5, k_h=0.8)

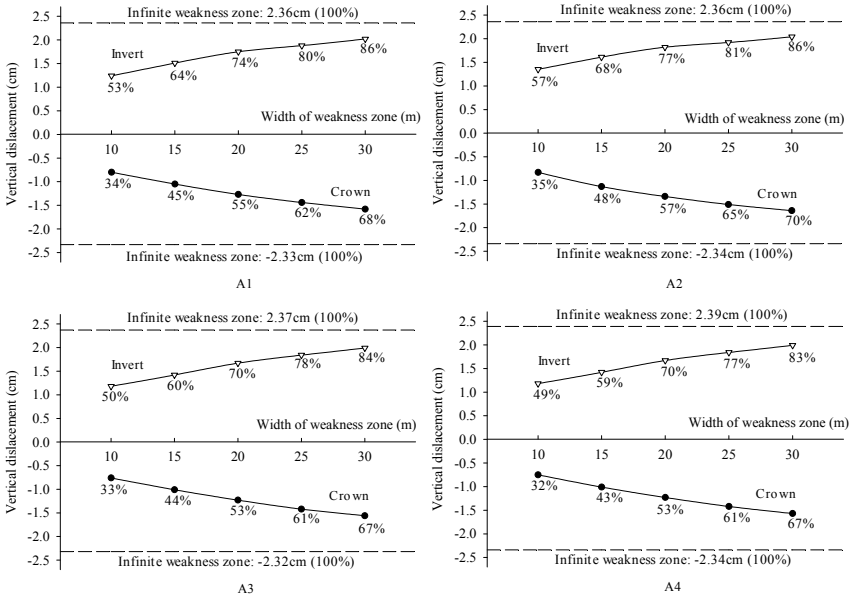

Figure 3 Vertical displacement at the crown and at the middle of invert in the middle cross-section of the weakness zone - maximum horizontal stress perpendicular to the tunnel alignment, varied minimum horizontal stress.

A1. k_H=1.5, k_h=0.8 A2. k_H=1.5, k_h=0.6 A3. k_H=1.5, k_h=1.0 A4. k_H=1.5, k_h=1.2

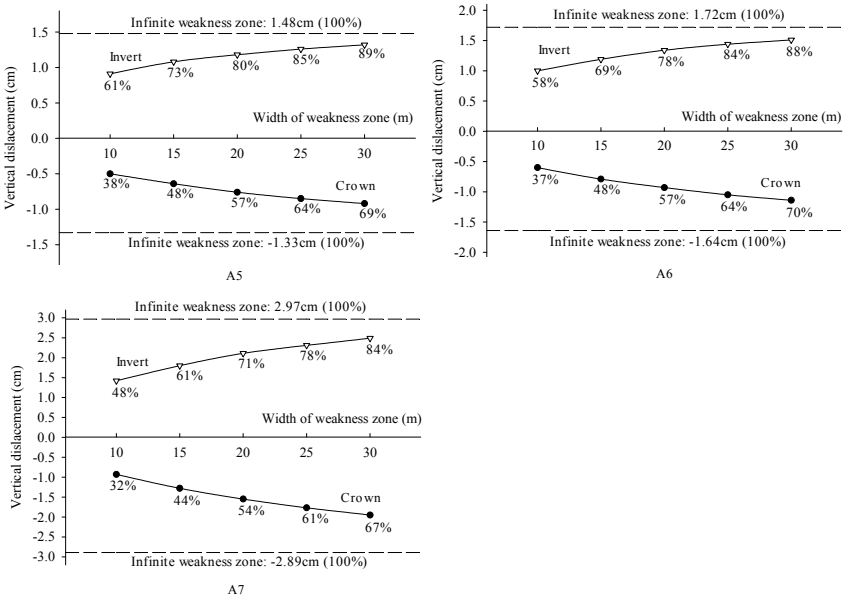

Figure 4 Vertical displacement at the crown and at the middle of invert in the middle cross-section of the weakness zone - maximum horizontal stress perpendicular to the tunnel alignment, varied maximum horizontal stress.

A5. k_H=1, k_h=0.8 A6. k_H=1.2, k_h=0.8 A7. k_H=1.7, k_h=0.8

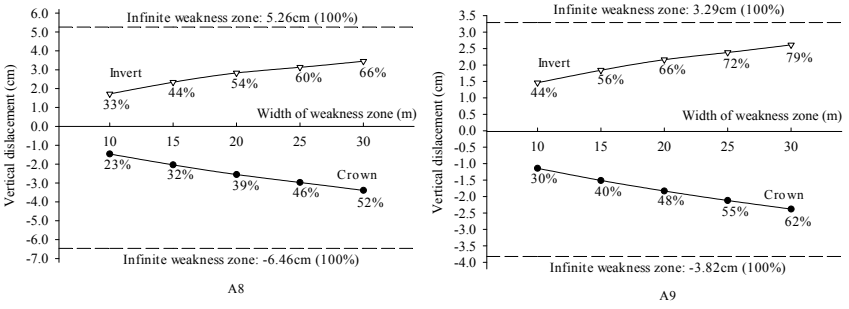

Figure 5 Vertical displacement at the crown and at the middle of invert in the middle cross-section of the weakness zone - maximum horizontal stress perpendicular to the tunnel alignment, reduced strength of weakness zone.

A8. cohesion 0.2MPa, friction angle 20° (k_H =1.5, k_h =0.8)

A9. cohesion 0.2MPa, friction angle 25° (k_H =1.5, k_h =0.8)

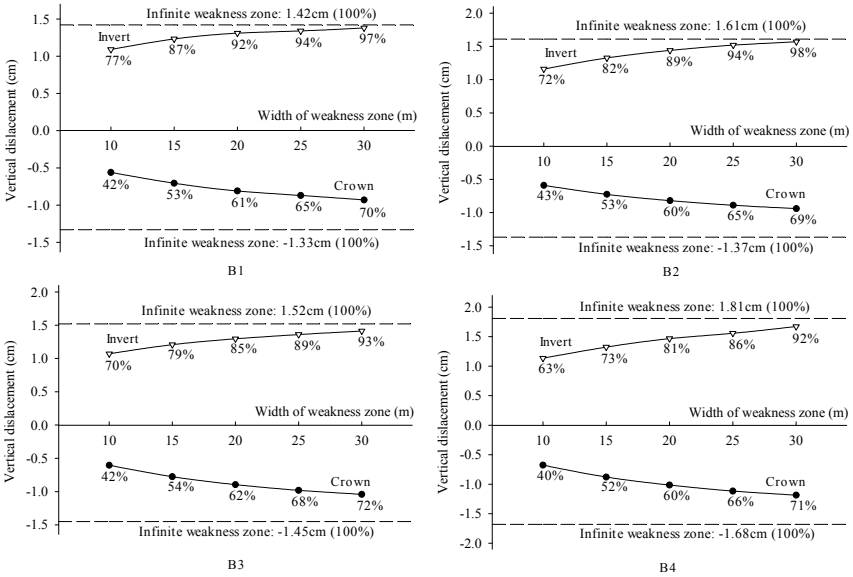

Figure 6 Vertical displacement at the crown and at the middle of invert in the middle cross-section of the weakness zone - maximum horizontal stress parallel to the tunnel alignment, varied minimum horizontal stress.

B1. k_H=1.5, k_h=0.8 B2. k_H=1.5, k_h=0.6 B3. k_H=1.5, k_h=1.0 B4. k_H=1.5, k_h=1.2

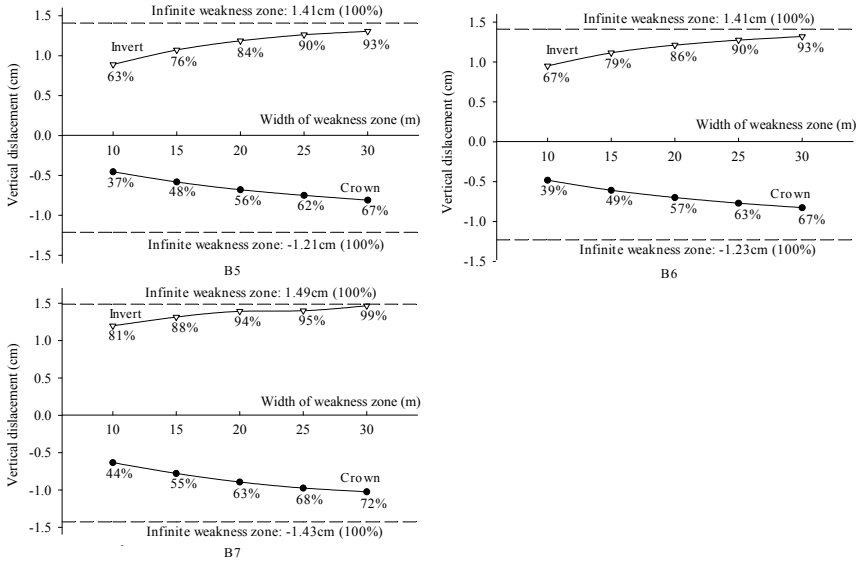

Figure 7 Vertical displacement at the crown and at the middle of invert in the middle cross-section of the weakness zone - maximum horizontal stress parallel to the tunnel alignment, varied maximum horizontal stress.

B5. k_H=1, k_h=0.8 B6. k_H=1.2, k_h=0.8 B7. k_H=1.7, k_h=0.8

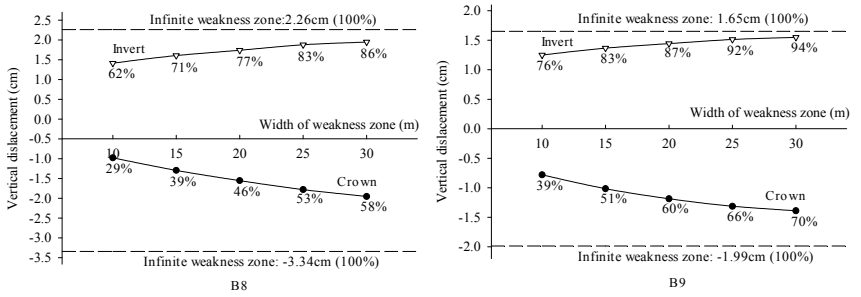

Figure 8 Vertical displacement at the crown and at the middle of invert in the middle cross-section of the weakness zone - maximum horizontal stress parallel to the tunnel alignment, reduced strength of weakness zone.

B8. cohesion 0.2MPa, friction angle 20^o (k_H =1.5, k_h =0.8)

B9. cohesion 0.2MPa, friction angle 25^o (k_H =1.5, k_h =0.8)

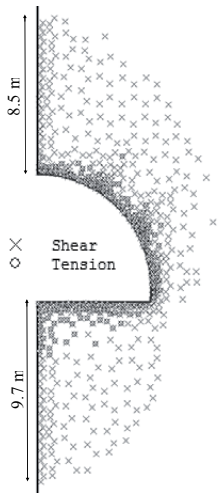

Figure 9 Yielded zones along the tunnel periphery based on Phase^2 (maximum horizontal stress perpendicular to the tunnel alignment, k_H=1.5, k_h=0.8).

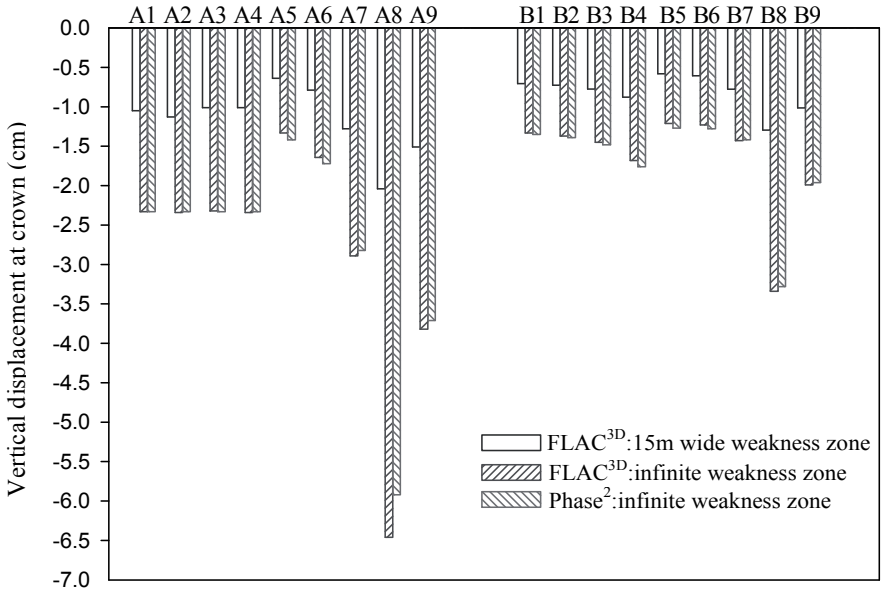

Figure 10 Vertical displacement at the crown in the middle cross-section of the weakness zone – FLAC^{3D} versus Phase^{2}.

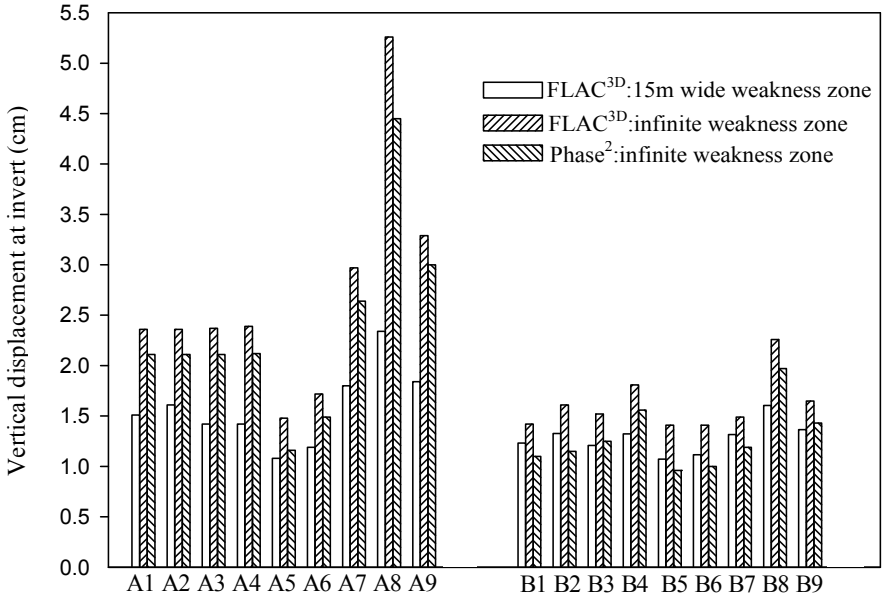

Figure 11 Vertical displacement at the middle of invert in the middle cross-section of the weakness zone – FLAC^{3D} versus Phase^{2}.

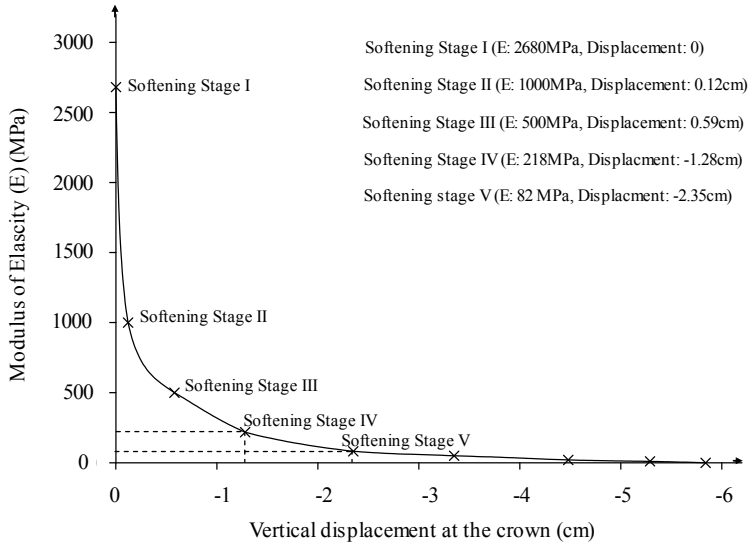

Figure 12 Vertical displacement at the crown with Modulus reduction.

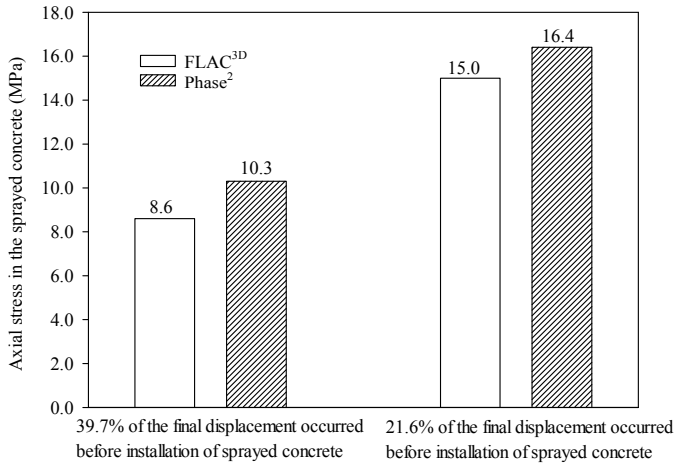

Figure 13 Axial stresses in sprayed concrete based on FLAC^{3D} and Phase^2.

Paper III

Analysis of loading effects on reinforced shotcrete ribs caused by weakness zone containing swelling clay

Authors: Dawei Mao, Bjørn Nilsen and Ming Lu

The paper was published in Tunnelling and Underground Space Technology (2011), Vol. 26, pages 472-480, doi:10.1016/j.tust.2011.01.004.

Tunnelling and Underground Space Technology 26 (2011) 472–480

Contents lists available at ScienceDirect

Tunnelling and Underground Space Technology

journal homepage: www.elsevier.com/locate/tust

Tunneling

Analysis of loading effects on reinforced shotcrete ribs caused by weakness zone containing swelling clay

Dawei Mao [a,*], Bjørn Nilsen [a], Ming Lu [b]

[a] Norwegian University of Science and Technology, Trondheim, Norway
[b] SINTEF Rock Engineering, Trondheim, Norway

ARTICLE INFO

Article history:
Received 23 September 2010
Received in revised form 7 December 2010
Accepted 30 January 2011
Available online 23 February 2011

Keywords:
Swelling clay
Tunnel
Rock support
Instrumentation
Numerical analysis

ABSTRACT

Tunneling in weakness zones containing swelling clay represents one of the most difficult conditions in hard rock tunneling. Evaluation of rock support requirements in such zones is normally empirical, i.e. mainly based on experience. In this paper, rock supports in a major weakness zone containing swelling clay is analysed based on monitoring results and numerical analysis in order to enrich the experience of support evaluation under such conditions. The Finnfast subsea road tunnel is used as a case. Laboratory tests of the gouge material from the actual zone indicate that the swelling pressure is moderate. All instrumentation data and simulation results show that the loading on the sprayed concrete is far less than its compressive strength, even for the rock support without the reinforced sprayed concrete rib. This suggests that such zones may often be excessively supported when the swelling clay is not very active. It is also found that for reliable stability control through such zones the instrumentation should be installed as close to the excavation face as possible.

1. Introduction

Major weakness zones or faults containing heavily crushed and altered rock mixed with gouge material represent the most difficult conditions in Norwegian hard rock tunnels including subsea tunnels. Description of failure cases under such conditions and discussion of possible causes have been the main focus in early literature (Brekke and Selmer-Olsen, 1965; Selmer-Olsen et al., 1989) as well as in more recent papers (Blindheim et al., 2005; Nilsen and Palmstrøm, 2009). In most cases, gouge materials with active swelling clay have been found in the failure zones.

For such weakness zones, the stability problem is not only dependent upon the characteristics of the gouge and swelling minerals. The width of the weakness zone, its orientation, the access of water, the frequency of occurrences, the competence of the side rock and the dimension of the tunnel are among the factors that must also be taken into account when considering the stability problems and the necessary support measures. In many cases evaluation of rock support requirement is based mainly on experience since there are no clearly defined rules for design of tunnels in such zones. Difficulties are often connected to quantification of the swelling capacity of the gouges as well as prediction of the response on tunnel excavation and support loading.

Laboratory testing techniques for quantifying the swelling potential have been developed as described by the Commission on Swelling Rocks of the ISRM (1989, 1999), and recent laboratory studies on swelling have mainly been focused on the use of triaxial tests (Aristorenas, 1992; Bellwald, 1990; Barla, 2008). These methods are however mainly for argillaceous swelling rocks and anhydrite. Moreover, the triaxial tests are especially laborious and stress paths are hard to define to reproduce the complicated in situ conditions.

The gouge material from faults or weakness zones usually consists of a mixture of clay and rock fragments of various sizes. For such materials, a laboratory test method based on measuring the swelling pressure of remoulded samples (Brekke, 1965) was introduced at NTNU several decades ago as described in Section 3, and is still commonly used in Norway.

During excavation of one of the most recent Norwegian subsea road tunnels, the Finnfast tunnel, several weakness zones containing swelling clay were encountered. One of these zones was instrumented, and the data on support loading has been collected by the Norwegian Geotechnical Institute (NGI) (Grimstad et al., 2008). To enrich experiences of support evaluation through such weakness zones, this instrumented zone is used as a case example and the effects of reinforced shotcrete ribs for support in this zone are studied in this paper.

2. Characteristics of case example

The Finnfast subsea tunnel is located close to Stavanger in south-western Norway, see Fig. 1. Granitic gneisses are the

* Corresponding author. Tel.: +47 46398642; fax: +47 73590898.
E-mail address: dawei.mao@ntnu.no (D. Mao).

0886-7798/$ - see front matter © 2011 Elsevier Ltd. All rights reserved.
doi:10.1016/j.tust.2011.01.004

predominant rock types in the region. The length of the main tunnel linking the two main islands (Rennesøy and Finnøy) is 5.76 km, while the branch to the third island (Talgje) in the middle of the fjord is 1.45 km. The excavation span of the tunnel is 12 m. The instrumented weakness zone intersects the tunnel at 140 m below sea level, including 50 m of water, 10 m of clay and 80 m of rock overburden. The zone is about 10 m wide, with strike direction almost perpendicular to the tunnel alignment and dip angle about 70°.

Fig. 2 shows drilled cores from the weakness zone. The rock mass quality in the zone, according to the *Q*-system, is exceptionally poor to extremely poor ($Q = 0.01–0.02$). The individual parameters of the *Q*-system for the worst-case condition of the zone are given in Table 1. When the tunnel was excavated through the zone, the blasting round was reduced from the normal 5 m to 3 m, and comprehensive support measures were taken. Spiling rock bolts and face rock bolts were installed before blasting and spraying with polypropylene fibre reinforced shotcrete was carried out combined with installation of radial rock bolts after blasting. Reinforcement with two reinforced ribs of sprayed concrete was installed before blasting of the next round. The details of the applied rock support are given in Table 2.

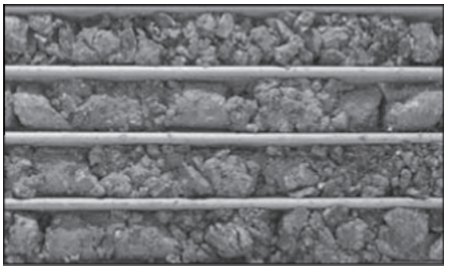

Fig. 2. Drilled cores from the weakness zone at the Finnfast tunnel.

Table 1
Input parameters of *Q*-system – estimated for the worst-case condition of the weakness zone.

Parameter	Value
Rock quality designation (RQD)	10
Joint set number (J_n)	20
Joint roughness number (J_r)	1.5
Joint alteration number (J_a)	15
Joint water reduction factor (J_w)	1
Stress reduction factor (SRF)	5

3. Laboratory test of gouge material

Based on X-ray diffraction analysis, the minerals of the gouge material from the weakness zone were identified as montmorillonite, muscovite, chlorite, clinochlore and graphite. Among these, montmorillonite is the most important swelling mineral. The mineral compositions of two tested samples show some differences, as shown in Table 3. The NTNU swelling pressure test was then conducted based on the standardized procedure involving sample preparation, compression, unloading and swelling (Brekke, 1965). First, the fraction of clay with grain size less than 20 μm was segregated from the gouge material and dried in the oven at 110 °C. The dried clay was then exposed to the relative humidity of the laboratory air (40%) and laboratory temperature before it was milled into clay powder. 20 g of the clay powder was then packed in a 20 cm^2 oedometer cell and compressed at 2 MN/m^2 for a minimum of 24 h to obtain constant volume. Thereafter, the sample was unloaded until no volume change was registered. Finally, water was accessed to the sample and the mobilized pressure measured with the sample volume kept constant. A principle sketch of the NTNU swelling pressure test is shown in Fig. 3. Fig. 4 shows the updated NTNU laboratory set-up for testing swelling pressure. The use of height transducer at the oedometer cell and inductive sensor at the steel spring makes it possible to compensate instantaneously for the axial strain of the oedometer cell to keep the sample volume constant.

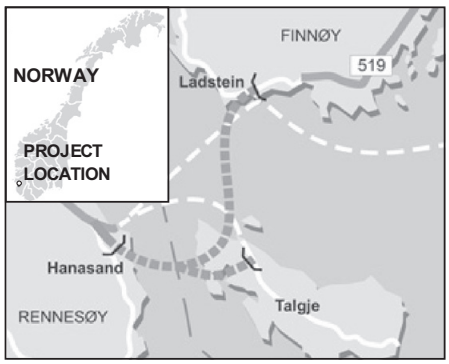

Fig. 1. Location of the Finnfast subsea road tunnel.

The principle of the NTNU test is almost equivalent to the method for determining the maximum axial swelling stress for swelling rocks as suggested by ISRM (1989, 1999). Instead of having the same density and water content in the specimen as in situ material, as described for the ISRM method, the NTNU method is based on remoulded specimens consisting of dried clay powder since it is very difficult to collect and prepare samples representative of the in situ gouge material. The gouge sample is always highly disturbed when a mixture of clay and rock fragments of various sizes is collected. The use of dried clay powder represents a uniform, reproducible way of preparing specimens of gouge materials from weakness zones.

The clay fraction with grain size less than 20 μm accounts for 20.7% of the weight of gouge material. Since the water entering the weakness zone in a subsea tunnel is often saline, testing was carried out using both distilled water and seawater. Fig. 5 shows swelling pressure versus time after water was accessed to specimens prepared from gouge material of the weakness zone at Finnfast. As shown, the swelling pressure increases quickly when the specimen gets access to water. After the maximum value has been reached, the swelling pressure drops temporarily. This may be due to the structural failure caused by high pressure. The swelling pressure then increases again until a second maximum value is reached, and the process repeats several times although less distinctively until the pressure is stabilized. The first peak value represents the maximum value of swelling pressure. The swelling pressures with sea water are generally a little lower than those with distilled water, and the peaks of the curves for sea water are not as distinct as for the curves with distilled water. The tests based on distilled water gave swelling pressure between 0.19 MPa and 0.21 MPa, while the tests with seawater gave swelling pressure of 0.16 MPa to 0.18 MPa. The Norwegian Group for Rock Mechanics, NBG defines the swelling pressure below 0.1 MPa as low, 0.15–0.3 MPa as moderate, 0.3–0.75 MPa as high and above 0.75 MPa as very high with this type of test (NBG, 2000). Based on this definition, the swelling pressure for clay from the gouge material of the instrumented weakness zone is moderate.

Table 2
Rock support used in the weakness zone at the Finnfast subsea tunnel.

Type of rock support	Support description
Fiber reinforced shotcrete	Thickness: 15 cm
Radial rock bolt	Length: 3 m, diameter: 20 mm Installation pattern: 1.5 m × 2 m, pretensioning: 30 kN
Spiling rock bolt	Length: 6 m, diameter: 25 mm, installation pattern: along the periphery of the excavation face at spacing 0.5 m and angle 15° relatively to the tunnel axis
Face rock bolt	Length: 4 m, diameter: 20 mm Installation pattern: around 25 bolts at the tunnel face
Reinforced rib of shotcrete	Thickness of reinforced rib of shotcrete: 30 cm Rib spacing: approximately 1.5 m, number of reinforcement steel bars in each rib: 6 Diameter of steel bar: 16 mm, spacing between bars: around 8 cm Distance from the steel bar to rib surface: 10 cm

Table 3
Mineral composition of the gouge material based on X-ray diffraction analysis.

Mineral	Sample 1 (%)	Sample 2 (%)
Montmorillonite	9.4	24.4
Muscovite	27.7	22.3
Chlorite	40.5	31
Clinochlore	19.9	17.6
Graphite	2.5	4.7

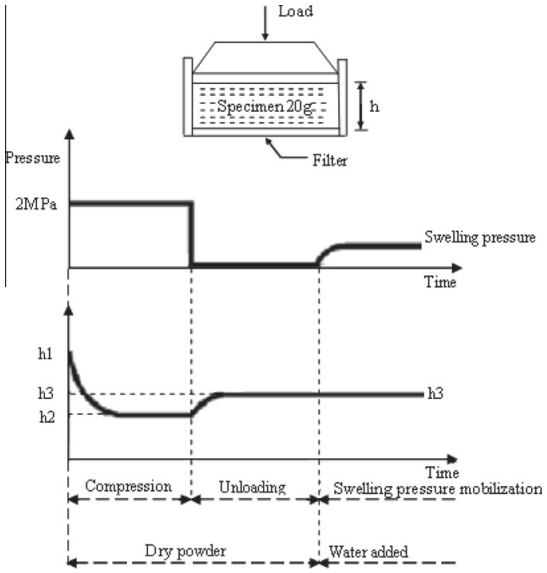

Fig. 3. Principle sketch of the NTNU swelling pressure test (based on Nilsen and Broch (2009)).

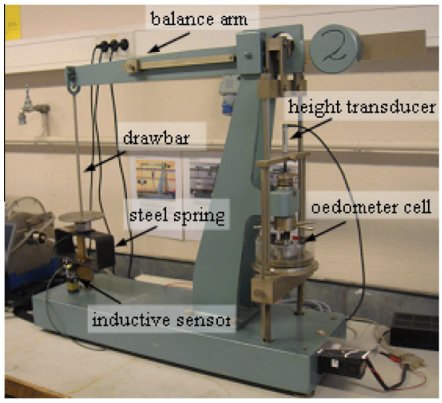

Fig. 4. NTNU laboratory set-up for testing swelling pressure.

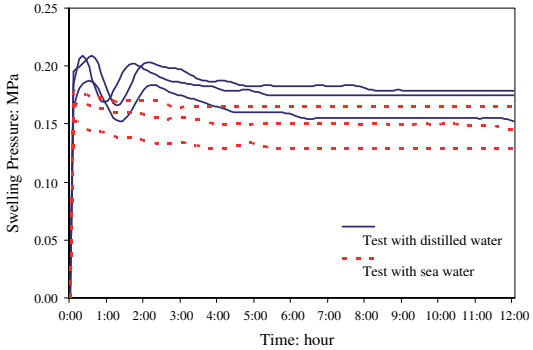

Fig. 5. Swelling pressure recorded for six individual samples of gouge material from the Finnfast weakness zone.

It should be emphasized that the swelling pressure measured in laboratory is primarily used as an index number, and that this value is not representative of the in situ swelling pressure on rock supports. The laboratory test results are based on the fixed clay amount of 20 g. The in situ structure and compaction are damaged as a result of the sampling process. The clay fraction used in the tests represents the most active part of the gouge material and that the dried condition represents the highest swelling potential. Moreover, the in situ swelling pressure on rock supports depends on the time between blasting and rock support installation and the support deformation. Previous research carried out at NTNU suggests that the in situ swelling pressure is often lower than the laboratory value, in some cases only 50% (Tyssekvam, 1996).

4. Instrumentation in the tunnel

The instrumentation of rock support was conducted at the second reinforcement rib of sprayed concrete counted from the excavation face when the tunnel was excavated in the middle of the weakness zone on January 18th, 2008 (Grimstad et al., 2008). Fig. 6 illustrates the blasting rounds in the weakness zone and

the location of the reinforced shotcrete ribs. Three similar sets of equipment, including strain gauges and load cells, were installed near the crown and at the springlines of the tunnel. The next round was excavated four days after instrument installation. The location of two of the three sets of instrumentation is shown in Fig. 7. The third set was installed at the left springline. Fig. 8 shows the lay-out of one set of equipment. Details regarding the instrumentation are given in Table 4 (Geokon, 2008).

The strain was measured for the second bar of the second rib from the tunnel face, while the ring stress in shotcrete was measured above the fourth steel bar. The load from the rock mass was measured above the fifth bar, and the strain in the shotcrete along the tunnel axis was measured between the fourth and fifth steel bars. The instruments were completely embedded in sprayed concrete except the load cell for monitoring load from the rock mass, which was fixed to the tunnel periphery on an even basis. The readings were reset after spraying the concrete on the reinforced rib. Due to the hydration heat from shotcrete curing, the temperature at the instrumented location once reached a maximum of 38 °C. It gradually dropped to 15–20° when the next round was excavated, and decreased to 12–13° when the excavation advanced further.

Monitoring results are shown in Figs. 9–11 and will be briefly discussed below. Near the crown, both the load from the rock and the ring stress in the shotcrete rib were close to zero during the monitoring period. At the right springline, the load from the rockmass fluctuated between 0.1 MPa and 0.25 MPa until it stabilized at 0.2 MPa. The ring stress in the shotcrete rib increased gradually to more than 1.5 MPa and then dropped to around 0.8 MPa. At the left springline, the load from the rockmass stabilized also at 0.2 MPa, but the ring stress in the shotcrete rib kept on increasing to more than 2.1 MPa. The recorded strain in the reinforcement bar steadily reached −160 μs and −280 μs at the right and left springlines respectively, indicating significant compression. The strain at the crown stabilized around −100 μs. In the longitudinal tunnel direction compression occurred in sprayed concrete near the crown, while tension was recorded at the right and left springlines.

The monitored ring stress in sprayed concrete near the crown is surprisingly low. This may be caused by voids created when spraying through reinforcement steel bars. Undulations or depressions of the excavated tunnel profile and local flaws in the sprayed concrete attaching to instrumentation equipments may also have caused uncertainties in the instrumentation results.

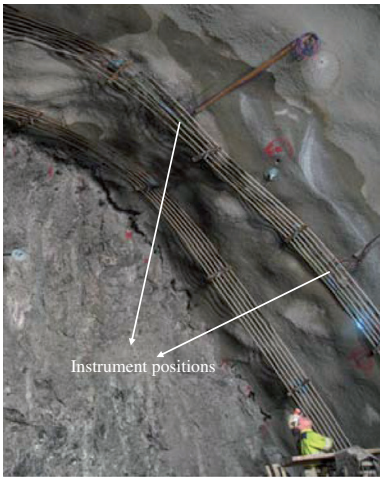

Fig. 7. Positions of two of the three sets of instruments (Grimstad et al., 2008).

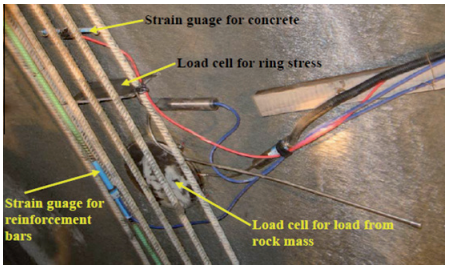

Fig. 8. Lay-out of one set of instruments in the weakness zone (Grimstad et al., 2008).

5. Numerical simulation

5.1. Description of numerical model

The finite difference code FLAC^{3D} (Itasca, 2005) was used in the numerical simulation. As shown in Fig. 12, only half of the tunnel needs to be generated due to symmetry. The inclined shadowed region is the location of weakness zone in the model. The left boundary of the model is the symmetry plane of the tunnel. The rest of boundaries are taken far away from the interested area (more than 40 m in the model). The mesh is denser near the instrumented location for higher simulation accuracy. Each boundary is fixed in the direction perpendicular to them, except the top boundary where the pressure caused by the gravity of rock overburden and 50 m sea water is applied. The model is considered as hydrostatic before tunnel excavation. The pore pressure is fixed at right and bottom boundaries where the pore pressure is expected to be not

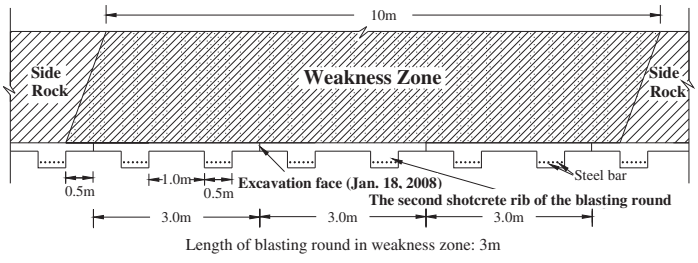

Fig. 6. Position of reinforced shotcrete ribs in weakness zone (longitudinal profile of tunnel roof).

Table 4
Instrumentation of rock support.

Instrumentation equipment	Type
Load cell for monitoring load from rockmass	Vibrating wire earth pressure cell with extra thick backplate, Model 4800 Height: 6 mm, diameter: 230 mm
Load cell for monitoring ring stress in sprayed concrete	Vibrating wire stress cell, NATM style, Model 4850-1 Height: 6 mm, length: 200 mm, width: 100 mm.
Strain gauge for monitoring reinforcement bar	Vibrating wire rebar strainmeter/sister bar, Model 4911 Diameter of rebar: 12 mm
Strain gauge for monitoring sprayed concrete	Vibrating wire strain gauge, concrete embedment, Model 4200 Active gauge length: 153 mm

much influenced by excavation, while it is allowed to change during simulation in the rest of the boundaries.

Based on communication with SINTEF (2010), who carried out the stress measurements at the site, the initial vertical stress can be assumed to be caused by gravity and considered as one of the principal stresses. Thus, it is estimated to be 2.9 MPa at the tunnel depth of 140 m below sea level. The maximum horizontal stress of 4.3 MPa according to SINTEF (2010) is in the direction of the tunnel alignment, while in the direction perpendicular to the tunnel alignment the horizontal stress is 2.5 MPa.

The weakness zone and side rock are simulated based on the Mohr–Coulomb model with elasto-perfectly plastic stress–strain law. Physical and mechanical properties of the weakness zone and the side rock used in the modeling are presented in Table 5. Dry density and porosity instead of total density are given for the weakness zone and side rock as required by the program for calculation of pore pressure distribution. The hydraulic conductivity of the weakness zone is estimated to 1×10^{-7} m/s, similar to that of side rock. The low permeability is considered due to the high clay content in the weakness zone and the clay filling of in the joints in the side rock.

The sprayed concrete is simulated with the same constitutive model as the weakness zone and side rock. Parameters of shotcrete required for simulation are given in Table 6. Since the next blasting round was 4 days after the installation of instrumentation in the weakness zone, final properties are assumed for the sprayed concrete due to the quick hardening when mixed with accelerator as used in the Finnfast Subsea Tunnel. Zero pore pressure is assumed within the shotcrete as all the rock supports in Norwegian subsea tunnels are drained (Blindheim et al., 2005).

The steel bars in the reinforced ribs of shotcrete are simulated as beam elements, the spiling bolts are simulated as pile elements (Trinh, 2006; Volkmann and Schubert, 2007), while the radial bolts and face bolts are simulated as cable elements due to different loading characteristics (Itasca, 2005). Parameters of these structural elements are listed in Tables 7 and 8. The geometrical parameters are calculated from geometrical dimensions. The section of the steel bar for strain gauge has a diameter of 12 mm, less than 16 mm of the diameter of other parts of reinforcement bars. The mechanical parameters are based on general data for rock support elements.

The excavation process is simulated by changing ground elements into null elements in sequence. Application of shotcrete after each excavation step is simulated by changing the corresponding layers of null elements into elements with corresponding properties of shotcrete. Effects of the swelling pressure on rock supports are simplified as uniformly distributed load from an engineering perspective.

5.2. Simulation results

5.2.1. Quantification of swelling pressure

In the simulation loading on rock supports is considered as the superimposed effects by tunnel excavation and swelling. As earlier discussed, the swelling pressure measured in laboratory is not directly comparable with the in situ swelling pressure. To quantify the swelling pressure on rock supports, numerical simulations have been carried out with different swelling pressures ranging from zero to 0.20 MPa at an interval of 0.04 MPa. This is realized in the model by applying the corresponding loads at the boundary between the weakness zone and shotcrete. A small portion of the loads may be shared by the weakness zone, and this is neglected in the analysis. For a simplified two dimensional model of a circular tunnel (tunnel radius: 6 m, total thickness of shotcrete: 45 cm), in a weakness zone with the same properties assumed, the weakness zone shares less than 6% of the loads under the elasticity condition. The actual loads shared by the weakness zone can be even less since the weakness zone close to the tunnel periphery has already yielded or has been close to yielding without accounting for the swelling effects.

The distribution of pore pressure during tunnel excavation may greatly affect rock behavior and the ground response. Fig. 13 illustrates the simulated pore pressure when passing through the weakness zone, which is consistent with the estimated pore pressure close to the tunnel periphery. The simulation results regarding the response of the rock support are of main interest here. The stabilized instrumented data for the situation when the tunnel has advanced far from the zone eliminate the influences from temperature variation due to concrete heat, and also represents the long term loading on rock supports. Therefore, the response of reinforced shotcrete rib at the equilibrium state when the tunnel has advanced far from the weakness zone is focused in simulation. Figs. 14 and 15 show the simulated results of strain in the reinforcement bar and ring stress in sprayed concrete with different

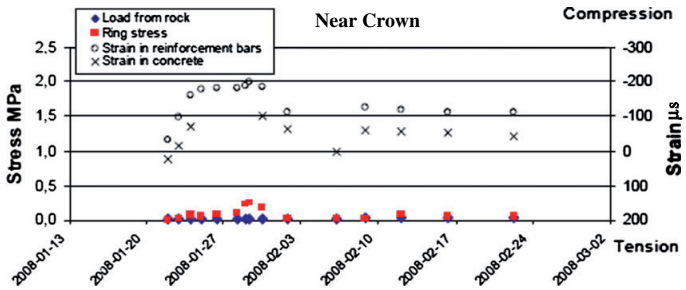

Fig. 9. Stress and strain at the crown (Grimstad et al., 2008).

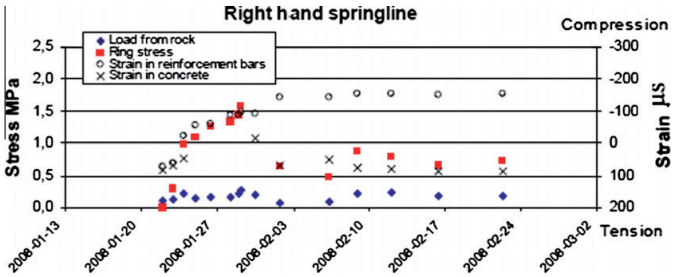

Fig. 10. Stress and strain at the right hand springline (Grimstad et al., 2008).

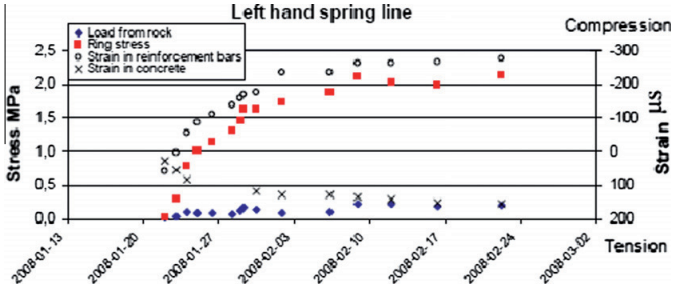

Fig. 11. Stress and strain at the left hand springline (Grimstad et al., 2008).

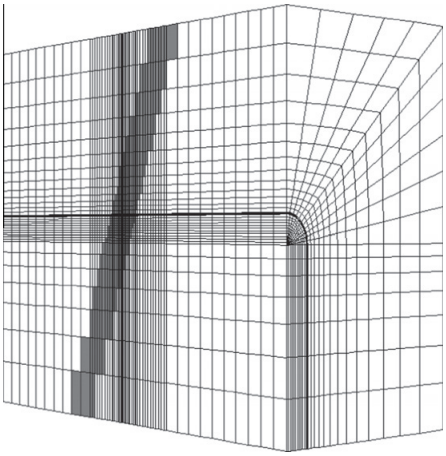

Fig. 12. FLAC3D model.

Table 5
Properties of weakness zone and side rock.

Properties	Weakness zone	Side rock
Dry density (kg/m^3)	2550	2680
Porosity (%)	15	2
Modulus of elasticity (E) (GPa)	2.68	43.5
Poisson's ratio (υ)	0.3	0.16
Bulk modulus[a] (K) (GPa)	2.2	21.3
Shear modulus[b] (G) (GPa)	1.0	18.8
Cohesion (MPa)	0.3	1.0
Friction	25°	35°
Dilation	–	10°

[a] $K = E/3(1 - 2\upsilon)$.
[b] $G = E/2(1 + \upsilon)$.

Table 6
Properties of shotcrete.

Properties	Value
Total density (kg/m^3)	2350
Modulus of elasticity (E) (GPa)	20
Poisson's ratio (υ)	0.2
Bulk modulus[a] (K) (GPa)	11.1
Shear modulus[b] (G) (GPa)	8.3
Cohesion (MPa)	7
Friction	45°
Dilation	12°
Tensile strength (MPa)	4

[a] $K = E/3(1 - 2\upsilon)$.
[b] $G = E/2(1 + \upsilon)$.

swelling pressures. It is found that even a small swelling pressure may considerably increase the ring stress in sprayed concrete and compression in the reinforcement bar. When swelling pressure increases to 0.16 MPa, the ring stress in sprayed concrete at the springline exceeds 2.1 MPa which is similar to the stabilized instrumented ring stress at the left hand springline. With the swelling pressure of 0.16 MPa, the simulated strain in the reinforcement bar near the crown is almost the same as the stabilized instrumented data. Comparing with the left hand springline, the instrumented strain in reinforcement bar at the right hand springline is much closer to the simulated one. The low instrumented loads from the rock mass at springlines are also verified by the simulation results. The strain in sprayed concrete along the tunnel alignment is much influenced by the fineness of the mesh. Since this parameter is not as important as the others in evaluating rock support response, this has not been fully considered in the model.

Table 7
Parameters of steel bars and spiling rockbolts.

Properties	Steel bars in reinforced ribs	Rebar section for strain gauge	Spiling rockbolts
Young's modulus (GPa)	200	200	200
Poisson's ratio	0.3	0.3	0.3
Cross-sectional area (m^2)	2.01×10^{-4}	1.13×10^{-4}	4.91×10^{-4}
Second moment respect to *y*-axis if the pile element (m^4)	1.6×10^{-9}	5.1×10^{-10}	0.96×10^{-8}
Second moment respect to *z*-axis if the pile element (m^4)	1.6×10^{-9}	5.1×10^{-10}	0.96×10^{-8}
Polar moment of inertia (m^4)	3.2×10^{-9}	1.02×10^{-9}	1.92×10^{-8}
Axial tensile yield strength (N)	–	–	0.55×10^{6}
Shear coupling spring cohesion per unit length (N/m)	–	–	0.6×10^{6}
Shear coupling spring stiffness per unit length (N/m^2)	–	–	1×10^{9}
Normal coupling spring cohesion per unit length (N/m)	–	–	0.6×10^{9}
Normal coupling spring stiffness per unit length (N/m^2)	–	–	1×10^{12}
Shear coupling spring friction angle	–	–	20°

Table 8
Parameters of radial rockbolts and facebolts.

Properties	Value
Young's modulus (GPa)	200
Grout exposed perimeter (m)	1.445×10^{-1}
Cross-sectional area (m^2)	3.14×10^{-4}
Grout cohesive strength per unit length (N/m)	0.6×10^{6}
Grout stiffness per unit length (N/m^2)	1×10^{9}
Grout friction angle	20°

Notes: Pretensioning of radial bolts 30 kN.

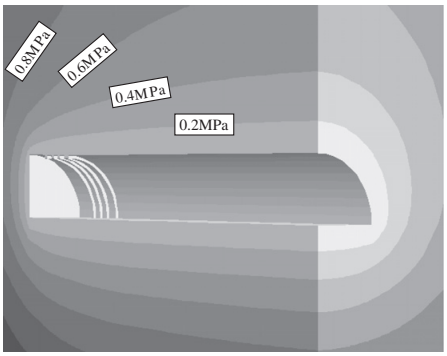

Fig. 13. Pore pressure distribution during tunnel excavation.

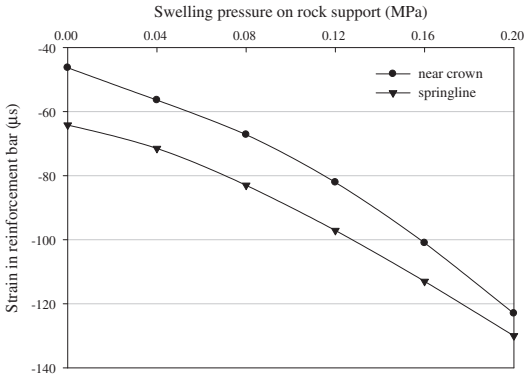

Fig. 14. Simulated strain in the reinforcement bar for different swelling pressures.

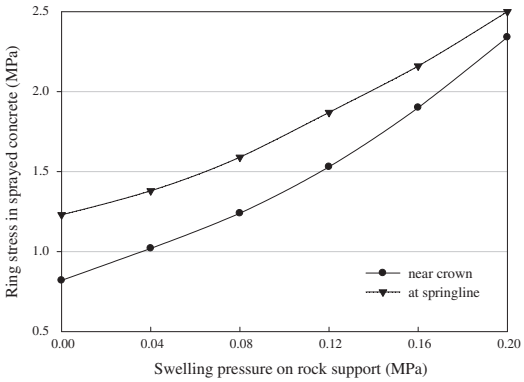

Fig. 15. Simulated ring stress in the sprayed concrete for different swelling pressures.

5.2.2. Comparison of support loading

The simulated results above are for the conditions where the instrumentation was conducted. The actual swelling pressure on rock supports can be different at other locations. It is expected to be higher close to the excavation face. Since there is no instrumentation to quantify the swelling pressure at other locations, the swelling pressure is taken the same of 0.16 MPa as the instru-

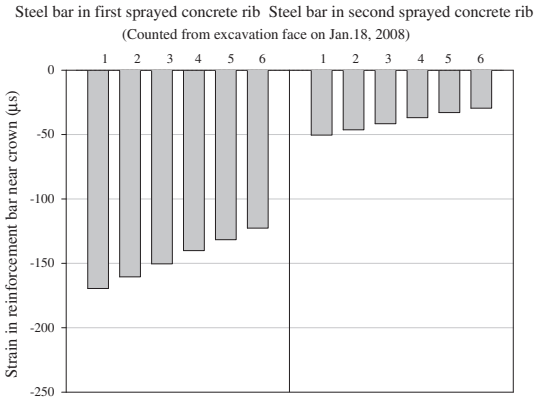

Fig. 16. Simulated strain in different reinforcement bars at crown for 0 swelling pressure.

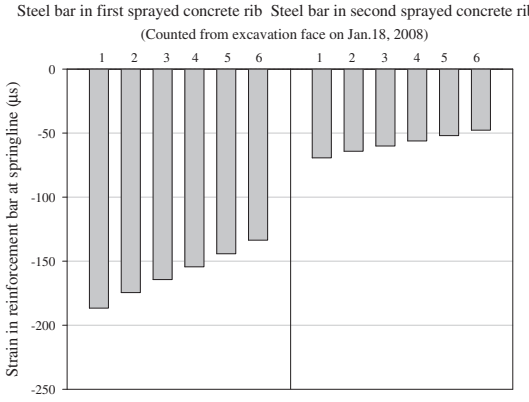

Fig. 17. Simulated strain in different reinforcement bars at springline for 0 swelling pressure.

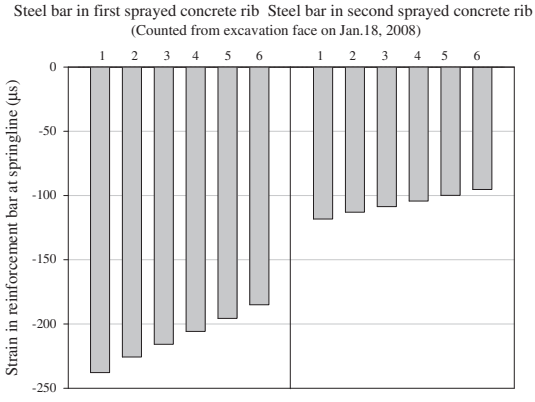

Fig. 19. Simulated strain in different reinforcement bars at springline for swelling pressure 0.16 MPa.

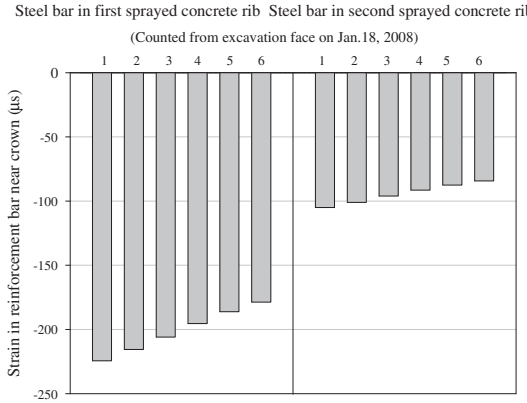

Fig. 18. Simulated strain in different reinforcement bars near crown for swelling pressure 0.16 MPa.

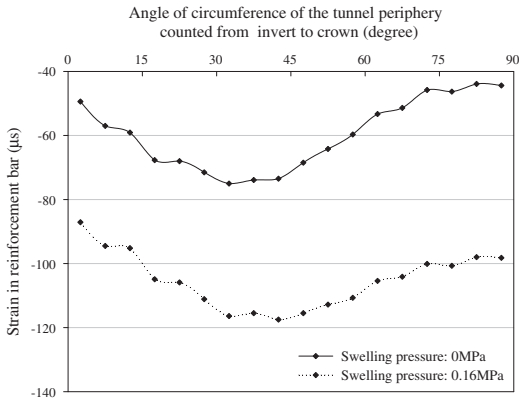

Fig. 20. Simulated strain in the second steel bar in the second shotcrete rib.

mented location in simulation. Figs. 16–19 show the strains in all reinforcement steel bars near the crown and at the springline in the sprayed concrete ribs for the blasting round on January 18th, 2008. It is found that the strains in steel bars in the first sprayed concrete rib are much higher than those in the second sprayed concrete rib. Even when the swelling effects on rock supports are not considered, the strains in the first steel bar in the first sprayed concrete rib are close to 170 μs near the crown and 190 μs at the springline. If the same swelling pressure of 0.16 MPa is assumed here, the strain in the first steel bar in the first sprayed concrete rib reaches over 220 μs near the crown and close to 240 μs at the springline.

Fig. 20 shows the strain in the second steel bar in the second sprayed concrete rib from invert to crown. It varies between approximately 45 μs and 75 μs without consideration of swelling effects. With the swelling pressure on rock supports of 0.16 MPa, the strain varies from around 85 μs to a little less than120 μs.

As an alternative support measure, the rock support without reinforced sprayed concrete ribs is simulated. When swelling effects are not included, the ring stress in the middle of the 15 cm sprayed concrete layer is 1.6 MPa near the crown and 2.1 MPa at the springline in the same tunnel cross section where instrumentation of ring stress was conducted. The ring stress increases to 3 MPa near the crown and over 3.3 MPa at springline if the swelling pressure of 0.16 MPa is applied on the 15 cm sprayed concrete layer, i.e. approximately 50% higher than for the alternative with shotcrete ribs. With the swelling pressure of 0.16 MPa on rock supports where the first steel bar in the first sprayed concrete rib was located, the ring stress increases to 6.2 MPa near the crown and 6.7 MPa at the springline.

6. Conclusion

The loading on rock supports in a major weakness zone containing swelling clay has been analysed based on a comparison between instrumentation results and numerical simulation. It has been found that swelling pressure may considerably increase the loading on rock supports. For a swelling pressure on rock supports at the instrumentation location of 0.16 MPa, many simulation results are comparable with the monitoring results.

Compared with the instrumented location, the loading on rock supports is much higher close to the excavation face and this area is more critical in terms of tunnel stability. Therefore, for reliable stability control through such zones the instrumentation should be installed as close to the excavation face as possible.

All instrumentation data and simulation results show that the loading on the sprayed concrete is far less than its compressive strength, even for the rock support without the reinforcement sprayed concrete rib. This suggests that such zones may often be excessively supported when swelling clay is not very active.

Most studies of weakness zones containing swelling clay are based on cases of failure, while those weakness zones without problems are often neglected. This may lead to unnecessary heavy rock support in such zones. The instrumented weakness zone provides the opportunity to quantitatively evaluate the loading effects on reinforced shotcrete ribs, which enriches the experiences of rock support in such weakness zones. It is to be hoped that further research in this field will lead to effective support design in weakness zones containing swelling clay.

Acknowledgements

The Norwegian Public Roads Administration is acknowledged for financing site visits to the Finnfast subsea tunnel, providing samples of gouge material and contributing economically to upgrading of the NTNU oedometer test equipment. Mr. Eystein Grimstad from the Norwegian Geotechnical Institute (NGI) is especially acknowledged for providing the instrumentation data to make the research possible, and Professor Stephen Lippard for having improved the language of the paper.

References

Aristorenas, G.V., 1992. Time-dependent behaviour of tunnels excavated in shale. Ph.D. Thesis. Massachusetts Institute of Technology, Boston, USA.

Barla, M., 2008. Numerical simulation of the swelling behaviour around tunnels based on special triaxial tests. Tunnelling and Underground Space Technology 23 (5), 508–521.

Bellwald, P., 1990. A contribution to the design of tunnels in argillaceous rock. Ph.D. Thesis. Massachusetts Institute of Technology, Boston, USA.

Blindheim, O.L., Grøv, E., Nilsen, B., 2005. Nordic sub sea tunnel projects. Tunnelling and Underground Space Technology 20 (6), 570–580.

Brekke, T.L., 1965. On the measurement of the relative potential swellability of hydrothermal montmorillonite clay from joints and faults in Precambrian and Paleozoic rocks in Norway. International Journal of Rock Mechanics and Mining Science 2, 155–165.

Brekke, T.L., Selmer-Olsen, R., 1965. Stability problems in underground constructions caused by montmorillonite-carrying joints and faults. Engineering Geology 1 (1), 3–19.

Geokon, 2008. Instructory Manual of Products. Geokon Inc., Lebanon, New Hampshire, USA. <http://www.geokon.com/products/>.

Grimstad, E., Tunbridge, L., Bhasin, R., Aarset, A., 2008. Measurements of forces in reinforced ribs of sprayed concrete. In: 5th International Symposium on Sprayed Concrete. Lillehammer, Norway.

ISRM Commission on Swelling Rocks, 1989. Suggested methods for laboratory testing of argillaceous swelling rock. International Journal of Rock Mechanics and Mining Science & Geomechanics Abstracts 26 (5), 415–426.

ISRM Commission on Swelling Rocks, 1999. Suggested methods for laboratory testing of swelling rocks. International Journal of Rock Mechanics and Mining Science & Geomechanics Abstracts 36 (3), 291–306.

Itasca, 2005. Fast Language Analysis of Continua in 3 Dimensions, Version 3.1, User's Manual. Consulting Group, Minneapolis, Minnesota, USA.

Norwegian Group for Rock Mechanics (NBG), 2000. Engineering Geology and Rock Engineering, Handbook No. 2. Oslo, Norway, p. 192.

Nilsen, B., Broch, E., 2009. Engineering Geology of Rocks, Basic Level Compendium. Department of Geology and Mineral Resources, NTNU, p. 76 (in Norwegian).

Nilsen, B., Palmstrøm, A., 2009. Engineering geological key factors for planning and constructing hard rock subsea tunnels. In: Proceedings of the Fifth Symposium on Strait Crossings, Trondheim, Norway, pp. 403–408.

Selmer-Olsen, R., Palmstrøm, A., Strømme, B., 1989. Tunnel collapses in swelling clay zones. Tunnels & Tunnelling 21, 49–51.

SINTEF, Rock Engineering Group, 2010. Personal communications.

Trinh, Q.N., 2006. Analysis of a cave-in problem in a hydropower tunnel in Vietnam. Ph.D. Thesis. NTNU, Trondheim, Norway.

Tyssekvam, I.O., 1996. Sampling and characterization of swelling material in weakness zones. Diploma Thesis. NTNU, Trondheim, Norway (in Norwegian).

Volkmann, G.M., Schubert, W., 2007. Geotechnical model for pipe roof supports in tunneling. In: Proceedings of the 33rd ITA-AITES World Tunneling Congress, Underground Space – The 4th Dimension of Metropolises, Prague, Czech, pp. 755–760.

Paper IV

Numerical analysis of rock fall at Hanekleiv road tunnel

Authors: Dawei Mao, Bjørn Nilsen and Ming Lu

The paper was accepted by Bulletin of Engineering Geology and the Environment in October 2011.

NUMERICAL ANALYSIS OF ROCK FALL AT HANEKLEIV ROAD TUNNEL

Dawei Mao[a], Bjørn Nilsen[a], Ming Lu[b]
[a]Norwegian University of Science and Technology, Trondheim, Norway
[b]SINTEF Rock Engieering, Trondheim, Norway

Dawei Mao, Bjørn Nilsen

Department of Geology and Mineral Resources Engineering, NTNU, NO-7491 Trondheim, Norway

Phone: +47 73590225

Fax: +47 73590898

E-mail: dawei.mao@ntnu.no

Ming Lu

SINTEF Rock Engineering, NO-7465, Trondheim, Norway

ABSTRACT

The twin tube, 1765 m long Hanekleiv road tunnel is located in Southeast Norway. Ten years after completion of the tunnel, a serious rock fall occurred approximately 1.1 km from the northern tunnel entrance at the southbound tube in a fault zone containing swelling clay. In addition to swelling, gravitational collapse due to the very low internal friction played an important role in the development of instability. Numerical analysis has been carried out for the rock slide. Based on modelling of the actually applied support, detected cracks during tunnel excavation as well as the tunnel collapse are verified. Simulation results show that even rock support of reinforced shotcrete ribs or 25 cm thick concrete lining as suggested based on the Q-system may not be sufficient for the fault zone.

Keywords: swelling clay; tunnel; rock fall; rock support; numerical analysis

Introduction

Instability has in some cases occurred in major faults/weakness zones with heavily crushed and altered rock mixed with gouge material, particularly when the gouge contains swelling clay minerals (Brekke and Selmer-Olsen, 1965; Selmer-Olsen and Palmstrøm, 1989; Nilsen and Dahlø, 1994; Nilsen and Palmstrøm, 2009; Nilsen, 2011). Such faults/weakness zones represent one of the most challenging conditions for Norwegian hard rock tunnelling. In most cases the instability has been encountered during construction. The rock slide at the Hanekleiv road tunnel, however, occurred ten years after the tunnel was completed and thus attracted wide attention (Bollingmo et al. 2007; Reynolds, 2007; Nilsen, 2011).

The location of the Hanekleiv road tunnel is shown in the simplified geological map of southeast Norway in Figure 1. The tunnel is 1765 m long and has two tubes. The net distance between the two tubes is approximately 15 m. Each tube has a theoretical cross section of excavation of about 65 m^2 (Norwegian Public Roads Administration, 2004). A simplified presentation of the topography and geology along the tunnel alignment is shown in Figure 2. The northern part of the tunnel passes through Silurian sandstone, which underlies a bed of Carboniferous slate/conglomerate overlain by Permian basalt. The southern half of the tunnel is in Permian syenite. The tunnels were both excavated from the north. The rock generally was fairly good, and the blasting round was normally 5 m. Only minor stability problems were experienced during tunnel excavation and break through was achieved after only 35 working weeks in November 1996. Steel fibre reinforced shotcrete and radial rock bolts were the major rock supports used (Bollingmo et al. 2007). The most difficult part was expected to be the northern part of tunnel due to the distinct, relatively flat bedding jointing of the sandstone. The rock fall however occurred in the syenite, approximately 1.1 km from the northern tunnel entrance of the southbound tube (Figure 2). A fault zone with swelling clay was identified during excavation, and this zone was sealed with 15 cm thick steel fibre reinforced shotcrete. During excavation of the tunnel, cracks in the shotcrete were detected at the fault zone, and 10 cm extra shotcrete was applied in this local area after

tunnel break through. Finally, the shield for water proofing and frost protection was installed. Details of this shielding are shown in Figure 3. Although the shielding may cope with minor pieces of falling rock, it is not designed to withstand major rock falls.

- Figure 1 -

- Figure 2 -

- Figure 3 -

Description of the Rock Fall

The rock fall at the Hanekleiv tunnel occurred in late December of 2006, ten years after completion of the tunnel. Figure 4 shows the section where the rock fall went through the frost and water shielding, where the rock overburden is approximately 75m. The section was generally dry and minor dripping was observed only at a few locations (Bollingmo et al. 2007).

- Figure 4 -

The caved in material was basically a mixture of small blocks, gravel and fragments of altered syenite, but included also a large block of syenite weighing several tons as shown in Figure 5. The total volume of the cave-in material was estimated to be 250 m^3. The fault zone causing the cave-in had an angle to the tunnel alignment of 10 – 15° (see Figure 4). It was bounded by two parallel joints striking approximately 030 - 040° and dipping 70 - 80° to the southeast. The joints were filled with clay gouge with a thickness of 5 to10 cm. The fault zone could be traced to a cross passage, where the width was only 20 to 50 cm (Bollingmo et al. 2007). Figure 6 shows longitudinal and cross sections of the rock slide area. The width of the fault zone at cross sections A and B in Figure 6 (17.5 m apart from each other) is 2.3 and 3.8 m respectively. The side rock near the fault zone was solid syenite with few cracks.

- Figure 5 -

- Figure 6 -

The rock mass quality of the fault zone based on site inspection after the rock fall was estimated to be extremely poor (Q = 0.01 - 0.02). Estimated individual parameters of the Q-system are given in Table 1. Heavy rock support like reinforced shotcrete rib or cast-in-place concrete lining should have been considered for the zone based on the support chart of Q–system (NGI, 2011). The cracks that developed in the sprayed concrete and the rock fall that ultimately occurred clearly demonstrated that the applied support consisting of rock bolts and shotcrete as insufficient for this fault zone.

- Table 1 -

Based on thorough investigation, it was concluded that, in addition to effect of the swelling process, gravitational collapse due to the very low internal friction played also an important role in the development of instability in the case (Bollingmo et al. 2007; Nilsen, 2011). The swelling process most likely was caused by both the water from joints and accumulation of moisture behind the water/frost shield, when ventilation has had little effect after tunnel completion. The strength of the material was also reduced with absorption of water during the swelling process. Swelling and strength reduction gradually developed till the collapse suddenly took place after ten years. The assumed combined effects will be focused upon in the numerical analysis.

Laboratory Testing of Swelling Clay

Clay samples were collected from the caved in material as well as from the clay fillings of the distinct joints at the cross passage. Swelling clay (smectite) was identified by the X-ray diffraction analysis. The mineral composition of the clay samples is shown in Table 2.

- Table 2 -

In Norway, a laboratory test method based on measuring the swelling pressure of remoulded specimens (Brekke, 1965) is commonly used for characterizing the swelling gouge materials. It is a standardized oedometer test where 20 g of dried clay powder with grain size less than 20 µm from the gouge material is precompressed at 2 MN/m^2 to constant volume and then unloaded until constant volume is reached again. The sample thickness is kept constant as water is accessed to the sample and the mobilized pressure is measured (SINTEF, 2005). The Norwegian National Group of ISRM, NBG, defines swelling pressure below 0.1 MPa as low, 0.1 - 0.3 MPa as moderate, 0.3 - 0.75 MPa as high and above 0.75 MPa as very high based on this type of test (NBG, 2000). For the collected samples, the clay fraction with grain size less than 20 µm accounted for only 14% of the weight and the tested swelling pressure was 0.18 MPa (Bollingmo et al. 2007; Nilsen, 2011).

Another common test to quantify the relative swelling potential is the free swelling test, in which the clay fraction with particle size less than 20 µm is also used. 10 ml of loosely packed dry clay powder is drizzled into a 50 ml measuring cylinder filled with distilled water. The volume occupied by the clay powder after sedimentation is recorded, and the free swelling is calculated as the percentage of the original powder volume. NBG defines free swelling below 100% as low, 100% - 140% as moderate, 140% - 200% as high and above 200% as very high (NBG, 2000). Based on this test, a free swelling of 150% was recorded for the Hanekleiv sample (Bollingmo et al. 2007; Nilsen, 2011).

Numerical Simulation

Description of Numerical Model

The finite difference code, FLAC3D (Itasca, 2009), has been used for numerical simulation of the Hanekleiv case. The generated model is shown in Figure 7, which represents the two-tube tunnel close to the area of rock fall. The X-axis and Y-axis are in the cross-section perpendicular to the tunnel alignment (Z-axis). The model size is $117m \times 78m \times 100m$ ($X \times Y \times Z$). Each boundary is fixed in the direction perpendicular to it, except the top boundary where the pressure caused by the gravity of rock overburden is applied. Simultaneous excavation of the two tubes is assumed in numerical simulation.

- Figure 7 -

Rock stress measurement has not been carried out at the Hanekleiv tunnel. The initial vertical stress, in accordance with general Norwegian experience, is however assumed to be caused by gravity and considered as one of the principal stresses. It is estimated to be 2 MPa at the tunnel depth. The direction and magnitude of horizontal principle stresses are estimated based on stress measurement for a tunnel at Drammen (Figure 1), which is only about 20 km North of Hanekleiv and in the same geological region as Hanekleiv (Hanssen, 1998). Stress measurements of high standard have been conducted here for a sewage tunnel. The orientation of the minimum horizontal stress at Drammen is approximately 020°. The ratio of the maximum horizontal stress to vertical stress is 2, and the ratio of the minimum horizontal stress to vertical stress is 0.6. The orientation of the alignment of the Hanekleiv tunnel (Figure 5) is very close to the direction of the minimum horizontal stress at Drammen. In the numerical simulation, for simplification, the minimum horizontal stress is taken as having the same direction as the tunnel alignment. Stress ratios, $k_H = 2$ and $k_h = 0.6$ as described above, are used.

A fault zone with geometry as illustrated in Figure 6 is considered in the model. The fault zone and side rock are simulated based on the Mohr-Coulomb model with an elasto-perfectly plastic stress-strain law. In consideration of the cracks detected during

excavation of the tunnel, a strain softening model is used for shotcrete in order to simulate its post-failure behaviour. Since the cracks in shotcrete were caused by tension, as demonstrated later by simulation results, the tensile strength of shotcrete is assumed to drop to zero when failure occurs. The shotcrete is in tensile failure in the simulation when the plastic tensile strain reaches 20 μs, which is calibrated based on the grid size of model. This indicates a brittle failure. The rate at which the tensile strength drops is controlled by the plastic tensile strain and the linear softening law for the tensile strength in FLAC3D (Itasca, 2009). Physical and mechanical properties of the original fault zone, the weakened fault zone (close to the tunnel periphery 10 years after excavation), the side rock and applied shotcrete used in the modelling are presented in Table 3. Since the strength reduction developed gradually inwards as previously mentioned, there was a variation of strength reduction in the weakened fault zone. In numerical simulation, the conservative simplification has been made that the properties of the weakest material from the cave-in rock mass are assumed for the whole weakened fault zone. The estimation of properties is based mainly on engineering experiences for these types of materials.

- Table 3 -

The suggested rock supports of reinforced shotcrete ribs and concrete lining based on the Q–system are also considered in simulation for comparison with the adopted support consisting of 25 cm shotcrete. Figure 8 shows the geometry of the simulated reinforced shotcrete ribs for one blasting round of 5 m. It is assumed that the distance between two shotcrete ribs is 2 m and the distance between the shotcrete rib and excavation face is 1m. The steel bars in the reinforced ribs of shotcrete are simulated as beam elements (Itasca, 2009). The geometrical parameters are calculated from geometrical dimensions and the mechanical parameters are based on general data for rock support elements as shown in Table 4.

- Figure 8 -

- Table 4 -

The thickness of concrete lining is assumed to be 25 cm supplementing the temporary rock support of 10 cm shotcrete. The concrete lining is modeled as being installed after break through of the whole tunnel. In numerical simulation, bulk modulus (16.7 GPa) and shear modulus (12.5 GPa) of the concrete are estimated based on the elasticity modulus of 30 GPa and Possion's ratio of 0.2. For simplicity, other parameters are assigned the same values as for shotcrete.

The ground water level above the caved in area is unknown and potential effects of the ground water have been neglected in the simulation. As earlier mentioned, the rock mass in the caved in area was relatively dry with dripping only at a few locations. Consequently, the water pressure on the shotcrete is assumed to have been very low. Rock bolts are not considered in the numerical simulation since very few bolts were installed and the detailed installation pattern is unknown.

Simulation results

The rock fall occurred 10 years after tunnel completion, indicating a long lasting, gradual process of mobilization of swelling pressure and strength weakening of the fault zone. This process is hard to define explicitly, and it has been focused in numerical simulation on three stages of mechanical states. The first stage represents tunnel excavation and detection of cracks in the shotcrete. The swelling pressure on the rock support of shotcrete is considered at the second stage. Combined effects of strength reduction of the fault zone and swelling are simulated at the last stage.

At the first stage, parameters of the original fault zone are used for the whole fault zone. The tunnel excavation with blasting round of 5 m is simulated by changing ground elements into null elements in sequence. Application of shotcrete after each excavation step is simulated by changing the corresponding layers of null elements into elements with corresponding properties of shotcrete. Simulation results show that the shotcrete

close to the blasting face at the fault zone was in tension failure. The yielded zones of shotcrete at the boundary of shotcrete and rock are shown to the left in Figure 9. Yielded zones were also found at the inner surface of shotcrete, and this verifies the detected cracks in the shotcrete. The area of simulated yielded zones of the fault, which is similar to the geometry of the slide area, is shown in the lower part of Figure 10. In the numerical simulation, the reduced strength of weakened fault zone is assumed for these yielded zones at the third stage.

- Figure 9 -

- Figure 10 -

Extra shotcrete was applied when cracks were detected in shotcrete. There is no detailed information on exactly where the extra shotcrete was applied. At the second stage of simulation, the extra shotcrete is however assumed to have been applied covering the whole area of the fault zone. Effects of the swelling pressure on rock support are considered from an engineering perspective as the uniformly distributed load. Swelling pressures up to 0.18 MPa have been assumed on the shotcrete support. This is realized in the simulation by applying the corresponding loads at the boundary between the fault zone and shotcrete (Mao et al. 2007). Yielded zones of shotcrete for swelling pressure 0.18 MPa are illustrated in the middle part of Figure 9. There is no essential difference of the areas of failed shotcrete by comparing the simulation results of yielded zones. This indicates that the relatively low swelling pressure had only a limited influence on the loading of shotcrete, and can not have been the only cause of the rock slide.

At the third stage, the properties of weakened fault zone are assumed for the simulated yielded zones of the fault. A previous study carried out at NTNU suggests that the in-situ swelling pressure is often lower than the laboratory value, in some cases only 50% (Tyssekvam, 1996). The right section of Figure 9 shows the yielded zones of shotcrete for weakened fault zone and a swelling pressure of 0.09 MPa (50% of the laboratory tested swelling pressure). The yielded area of shotcrete due to tension has been

greatly increased along the fault zone and continues to increase with more calculation steps. As a sign of misconvergence of the numerical simulation, the contiguous line of active plastic zones joining two surfaces indicates breakdown of the shotcrete and tunnel collapse (Itasca, 2009). This is also confirmed by the vector of velocity where the movement of the fault zone is much higher than for the other parts of the tunnel periphery. Figure 11 illustrates the vector of displacement close to the tunnel periphery at one instantaneous state.

Figure 12 shows the contour of shear strain increment of rock mass at cross sections A and B of the collapse area. The inclination of the contour lines is comparable to the dip of joints in the fault zone. The area within the contour line of strain increment of 45 μs has almost the same width as the slide area at both locations of cross section A and B.

- Figure 11 -

- Figure 12 -

Rock support consisting of shotcrete rib and concrete lining are simulated with the same swelling pressure (0.09 MPa) and strength reduction of the weakened fault zone. Simulated results show that the shotcrete ribs are not fully sufficient for the fault zone. Cracks are observed between reinforced shotcrete ribs as indicated by the fragmented yielded zones at the inner surface (upper part of left section in Figure 13). Figure 13 shows the area of yielded zones of shotcrete at the boundary of shotcrete and rock. The area is similar to the early case when only shotcrete is applied. For the cast-in-place concrete lining (25 cm) installed in addition to the temporary rock support of shotcrete (10 cm), the yielded area at the boundary of shotcrete and rock is considerably reduced as shown to the right part of Figure 13. The yielded zones at the inner surface of concrete lining indicate where cracks occur (upper part of right section in Figure 13). However, the numerical simulation may converge with the enhanced supports of shotcrete rib or concrete lining indicating that the tunnel fall could be prevented.

- Figure 13 -

Discussion and Conclusion

The gouge material in the collapse zone was not very active and the content of swelling clay (smectite and kaolinite) was quite low. Thus, it is logical to assume that the rock slide was not caused only by the swelling effects, but rather by the combined effects of swelling and strength reduction of the fault zone. It was a long process and took ten years until swelling and strength reduction finally resulted in the collapse.

Numerical analysis of the cave-in has been carried out with properties of the weakened fault zone estimated corresponding to the weakest material from the caved in rock mass. For modeling with support as actually used, both the detected cracks during tunnel excavation and the tunnel collapse are verified. The cracks were caused by tension. The swelling pressure has been found to have had a limited influence on the shotcrete, while the strength reduction played an important role in the development of instability. Rock support with reinforced shotcrete ribs could not have fully prevented the tunnel instability according to the numerical analysis. It could have prevented the rock fall, but cracks between the shotcrete ribs indicate potential instability. A 25cm thick concrete lining, in addition to the concrete, would have reduced the cracked area considerably. Special consideration is required for rock support under the combined effects of swelling and strength reduction of rock mass before such scenarios are included in the rock classification systems.

Acknowledgement

Professor Stephen Lippard is highly acknowledged for improving the language of the paper.

References

Bollingmo P, Nilsen B, Nordgulen Ø (2007) The cave-in at the Hanekleiv tunnel, 25 December 2006. Report from investigation panel established by the Norwegian Department of Transportation (in Norwegian), 14 February 2007

Brekke TL (1965) On the measurement of the relative potential swellability of hydrothermal montmorillonite clay from joints and faults in Precambrian and Paleozoic rocks in Norway. International Journal of Rock Mechanics and Mining Science 2:155-165

Brekke TL, Selmer-Olsen R (1965) Stability problems in underground constructions caused by montmorillonite-carrying joints and faults. Engineering Geology 1 (1):3-19

Hanssen TH (1998) Rock Stresses and tectonic activity. In: Proceedings of the Norwegian National Rock Mechanics Conference. Oslo, Norway, pp 29.1-29.24

Holmøy KH (2002) Significance of geological parameters for predicting water leakage in hard rock tunnels. PhD Thesis, NTNU, Trondheim, Norway, p 8

Itasca (2009) Fast Language Analysis of continua in 3 dimensions, version 3.1, user's manual. In: Itasca, I. (Ed.), Consulting Group, Minneapolis, Minnesota, USA

Mao D, Nilsen B, Lu M (2011) Analysis of loading effects on reinforced shotcrete ribs caused by weakness zone containing swelling clay. Tunnelling and Underground Space Technology 26:472–480

Nilsen B (2011) Cases of instability caused by weakness zones in Norwegian tunnels. Bulletin of Engineering Geology and the Environment 70:7–13

Nilsen B, Dahlø TS (1994) A study of cases of instability in hard rock tunnel. In: Proceedings of 7th IAEG Congress. Lisbon, Vol. VI, Balkema, pp 4233-4242

Nilsen B, Palmstrøm A (2009) Engineering geological key factors for planning and constructing hard rock subsea tunnels. In Proceedings of the 5th Symposium on Strait Crossings. Trondheim, Norway, pp 403-408

Norwegian Geotechnical Institute (NGI) (2011) http://www.ngi.no/en/Contentboxes-and-structures/Reference-Projects/Reference-projects/Q-method/

Norwegian Group for Rock Mechanics (NBG) (2000) Engineering Geology and Rock Engineering, Handbook No. 2. Oslo, Norway, p 192

Norwegian Public Roads Administration (2004) Manual of Road Tunnels, Handbook No. 021. Oslo, Norway, pp 31-38

Reynolds P (2007) Finding fault at Hanekleiv. Tunnels and Tunnelling International, March 2007, pp 14 – 16

Selmer-Olsen R, Palmstrøm A (1989) Tunnel collapses in swelling clay zones. Tunnels & Tunnelling 21: 49-51

SINTEF Rock Engineering Group (2005) Test procedure for swelling pressure measurement (In Norwegian). Internal Report, NTNU, Norway

Tyssekvam IO (1996) Sampling and characterization of swelling material in weakness zones (In Norwegian). Diploma Thesis, NTNU, Trondheim, Norway

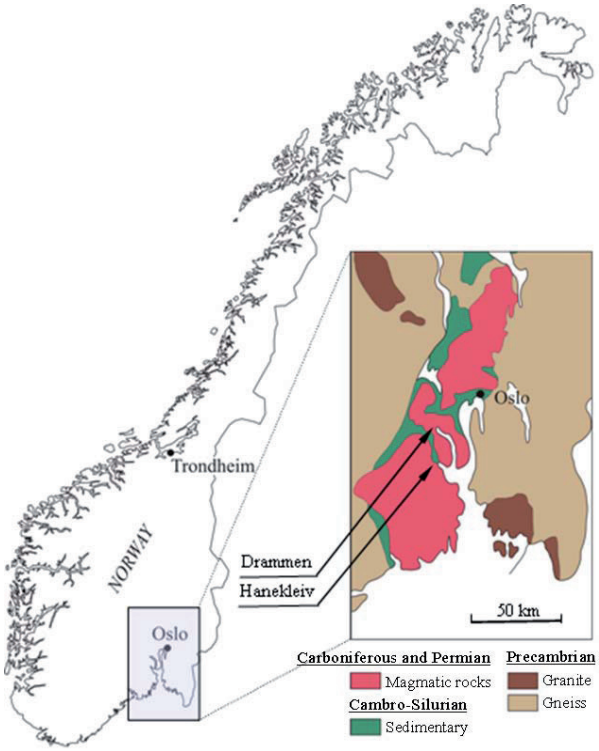

Figure 1. Simplified geological map of southeast Norway with the location of the Hanekleiv road tunnel and Drammen (modified after Holmøy, 2002).

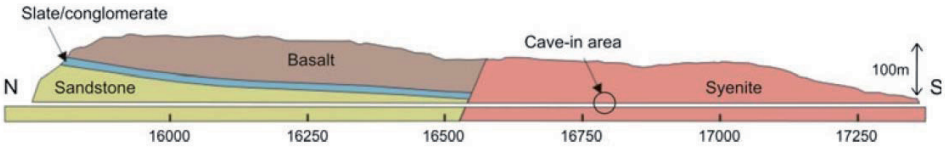

Figure 2. Simplified presentation of topography and geology along the tunnel alignment (Based on Bollingmo et al. 2007).

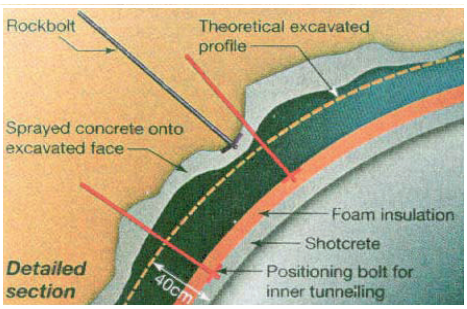

Figure 3. Principle sketch of shielding for water proofing and frost protection (Reynolds, 2007).

Figure 4. Cave-in section of the fault zone.

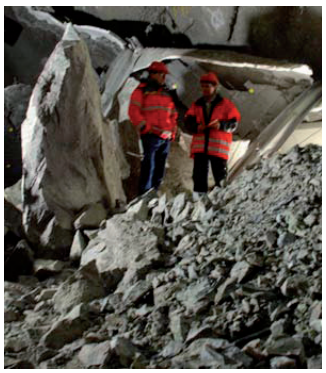

Figure 5. Caved in material.

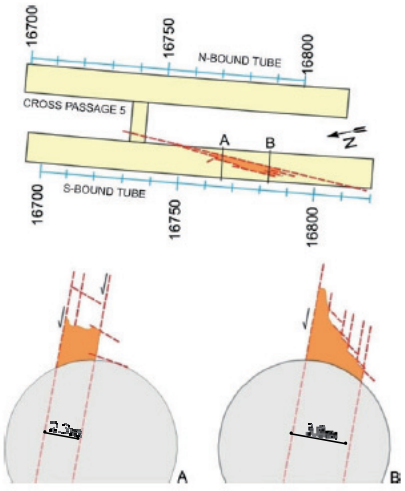

Figure 6. Longitudinal and cross sections of the rock slide area (modified after Bollingmo et al. 2007).

Table 1 Input parameters for estimation of Q-value for the fault zone

Parameter	fault zone
Rock quality designation (RQD)	10
Joint set number (J_n)	20
Joint roughness number (J_r)	1
Joint alteration number (J_a)	15
Joint water reduction factor (J_w)	1
Stress reduction factor (SRF)	2.5

Note: $Q = \frac{RQD}{J_n} \times \frac{J_r}{J_a} \times \frac{J_w}{SRF}$

Table 2 Mineral composition of the clay samples (Bollingmo et al. 2007)

Mineral	Content
Alkali feldspar	53%
Plagioclase	21%
Smectite	6%
Kaolinite	11%
Mica	9%

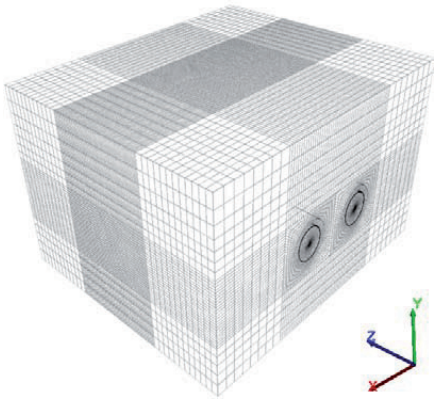

Figure 7. FLAC^{3D} model.

Table 3 Properties of fault zone, side rock and shotcrete

Properties	Original fault zone	Weakened fault zone	Side rock	Shotcrete
Density (kg/m^3)	2700	2700	2700	2350
Modulus of elasticity (E) (GPa)	3.1	2.0	45	20
Poisson's ratio (υ)	0.3	0.3	0.22	0.2
Bulk modulus[a] (*K*) (GPa)	2.6	1.7	26.8	11.1
Shear modulus[b] (G) (GPa)	1.2	0.8	18.4	8.3
Cohesion (MPa)	0.45	0.2	6	7
Friction	30^o	15^o	50	45^o
Dilation	-	-	15^o	12^o
Tensile strength (MPa)	-	-	1	0 – 4 [*]

[*] Tensile strength of shotcrete depends on the plastic tensile strain.

[a] $K=E/3(1-2\upsilon)$

[b] $G=E/2(1+\upsilon)$

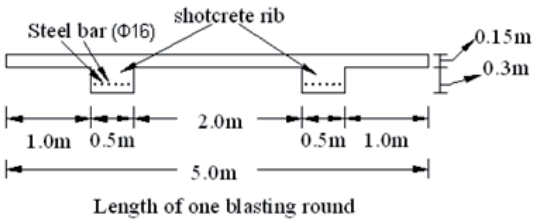

Figure 8. Geometry of the simulated reinforced shotcrete rib.

Table 4 Parameters of steel bars in shotcrete rib

Properties	Steel bar
Young's modulus (GPa)	200
Poisson's ratio	0.3
Cross-sectional area (m^2)	2.01×10^{-4}
Second moment respect to y-axis if the pile element(m^4)	1.6×10^{-9}
Second moment respect to z-axis if the pile element (m^4)	1.6×10^{-9}
Polar moment of inertia (m^4)	3.2×10^{-9}

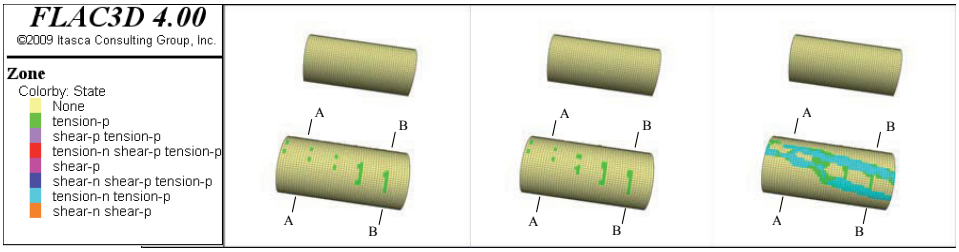

Figure 9. Yielded zones of shotcrete at three stages of the numerical simulation.
(Left: after excavation; Middle: swelling pressure considered; Right: Swelling pressure and weakened fault zone considered)

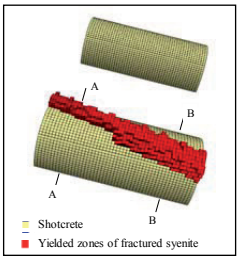

Figure 10. Yielded zones of fault based on numerical simulation.

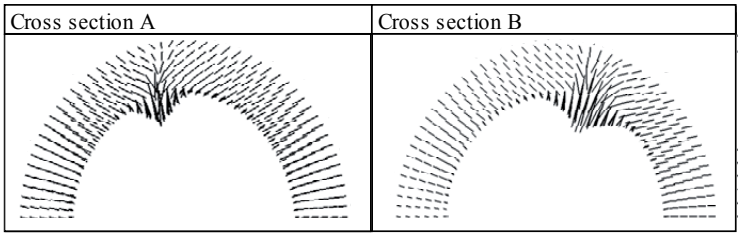

Figure 11. Displacement vector of cross sections A and B of rock fall area.

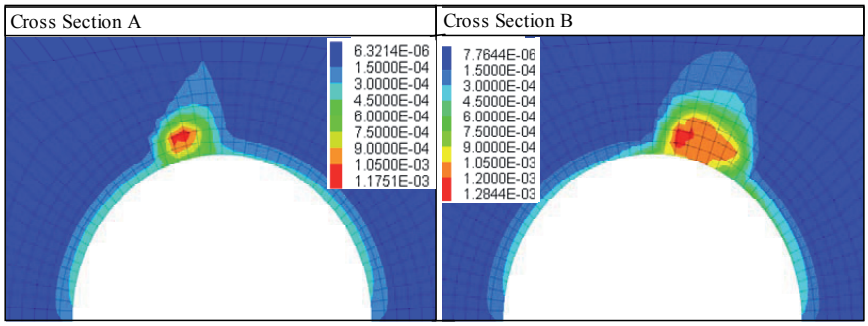

Figure 12. Contour of shear strain increment of cross sections A and B of rock fall area.

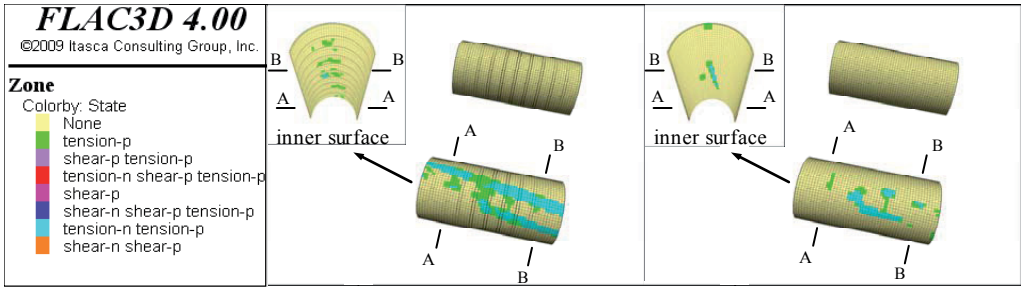

Figure 13. Yielded zones of shotcrete ribs (left) and concrete lining (right).
(swelling pressure and weakened fault zone considered)

Appendices

Is not included